

University of Groningen

Dynamics of Singlet and Triplet Excitons in Organic Semiconductors

Mikhnenko, Oleksandr Viktorovich

IMPORTANT NOTE: You are advised to consult the publisher's version (publisher's PDF) if you wish to cite from it. Please check the document version below.

Document Version

Publisher's PDF, also known as Version of record

Publication date:

2012

[Link to publication in University of Groningen/UMCG research database](#)

Citation for published version (APA):

Mikhnenko, O. V. (2012). *Dynamics of Singlet and Triplet Excitons in Organic Semiconductors*. s.n.

Copyright

Other than for strictly personal use, it is not permitted to download or to forward/distribute the text or part of it without the consent of the author(s) and/or copyright holder(s), unless the work is under an open content license (like Creative Commons).

The publication may also be distributed here under the terms of Article 25fa of the Dutch Copyright Act, indicated by the "Taverne" license. More information can be found on the University of Groningen website: <https://www.rug.nl/library/open-access/self-archiving-pure/taverne-amendment>.

Take-down policy

If you believe that this document breaches copyright please contact us providing details, and we will remove access to the work immediately and investigate your claim.

Downloaded from the University of Groningen/UMCG research database (Pure): <http://www.rug.nl/research/portal>. For technical reasons the number of authors shown on this cover page is limited to 10 maximum.

Singlet and Triplet Excitons in Organic Semiconductors

Oleksandr V. Mikhnenko



university of
 groningen

faculty of mathematics and
 natural sciences

zernike institute for
 advanced materials

Singlet and Triplet Excitons in Organic Semiconductors

Oleksandr V. Mikhnenko

PhD Thesis

University of Groningen, the Netherlands

Zernike Institute PhD Thesis Series 2012-02

ISSN: 1570-1530

ISBN: 978-90-367-5201-5 (print)

ISBN: 978-90-367-5202-2 (digital)

This research forms part of the research program of the Dutch Polymer Institute (DPI), Technology Area Functional Polymer Systems, DPI project #518.



Cover design by Oksana Pasishnychenko (www.oksancia.com).

Printed by Uitgeverij BOXPress (www.proefschriftmaken.nl).

Copyright © Oleksandr Mikhnenko, Groningen 2011.

RIJKSUNIVERSITEIT GRONINGEN

Dynamics of Singlet and Triplet Excitons in Organic Semiconductors

Proefschrift

ter verkrijging van het doctoraat in de
Wiskunde en Natuurwetenschappen
aan de Rijksuniversiteit Groningen
op gezag van de
Rector Magnificus, dr. E. Sterken,
in het openbaar te verdedigen op
vrijdag 13 januari 2012
om 14:30 uur

door

Oleksandr Viktorovich Mikhnenko

geboren op 24 februari 1983
te Brusyliv, Oekraïne

Promotores:

Prof. dr. M. A. Loi

Prof. dr. ir. P. W. M. Blom

Beoordelingscommissie:

Prof. dr. V. Dyakonov

Prof. dr. P. A. Bobbert

Prof. dr. J.C. Hummelen

dedicated to my parents

“there is no greater gift than education”

Contents

1. General Introduction	9
1.1 Organic Semiconductors	10
1.2 Excitons are Energy Chunks	11
1.3 Energy and Charge Transfer	13
1.4 The Physics of Exciton Diffusion	15
1.5 Exciton-exciton annihilation	17
1.6 Diffusion Limited Exciton Quenching	19
1.7 Measuring Singlet Exciton Diffusion Length	20
1.8 Do Triplets Diffuse Further?	23
1.9 Motivation and Scope	24
1.10 References	26
2. Exciton Quenching in Skin Layer of Spin-Coated Polymer Films	31
2.1 Introduction	32
2.2 Thickness Dependence of the PL Decay Times	34
2.3 Measurements of Exciton Diffusion Length	36
2.4 Skin Layer in Spin-Coated Films	38
2.5 Conclusions	42
2.6 Methods	42
2.7 References	44
3. Exciton Diffusion Length in Narrow Band Gap Polymers	47
3.1 Introduction	48
3.2 Modeling Photoluminescence Decays	50
3.3 Checking for PCBM Aggregation	52
3.4 Exciton Diffusion in Si-PCPDTBT	54
3.5 Discussion	55
3.6 Conclusions	56
3.7 Methods	57
3.8 References	58
4. Effect of Thermal Annealing on Exciton Diffusion	61
4.1 Introduction	62
4.2 Effect of Annealing on Crystallinity and Photophysical Properties	63
4.3 Exciton Diffusion Measurements	65
4.4 Using Different Exciton Quenching Molecule	67

4.5	Discussion	69
4.6	Conclusions.....	70
4.7	Methods	70
4.8	References	72
5.	Sensitive Triplet Exciton Detection	75
5.1	Introduction	76
5.2	Increase of Phosphorescence Intensity	77
5.3	Photoinduced Absorption	78
5.4	Dependence on Excitation Power	80
5.5	Discussion	81
5.6	Conclusions	82
5.7	Methods	82
5.8	References	84
6.	Direct Measurement of the Triplet Exciton Diffusion Length	87
6.1	Introduction	88
6.2	Sample Structure	89
6.3	Injection of Triplet Excitons	91
6.4	Detection of Triplet Excitons	93
6.5	Modeling the Triplet Penetration Profile	94
6.6	Discussion	95
6.7	Conclusions	95
6.8	Methods	96
6.9	References	97
	Summary	99
	Samenvatting	101
	Curriculum Vitae	105
	List of Publications	106
	Acknowledgments	109

Chapter 1

General Introduction

In this chapter basic concepts and definitions regarding the physical properties of organic semiconductors are introduced. The importance of exciton diffusion for the operation of optoelectronic devices is emphasized. By reviewing available experimental methods to study exciton diffusion we show that new techniques are needed to systematically measure singlet and triplet exciton diffusion length in organic semiconductors. The precise measurement of these physical quantities will have an important role in driving the design of new materials for high performing solar cells and light emitting diodes. Finally the scope of this thesis is summarized.

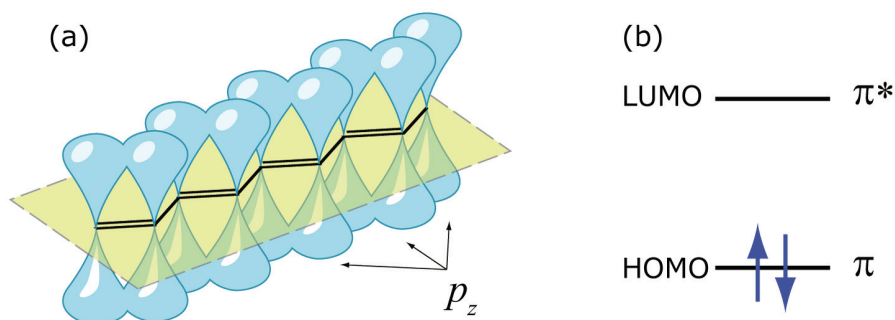


Figure 1.1: (a) A conjugated backbone with overlapping p_z orbitals that point out of the molecular plain. (b) Highest occupied and lowest unoccupied molecular orbitals (HOMO and LUMO). Arrows denote two electrons with different spins.

1.1 Organic Semiconductors

Organic semiconductors are carbon based compounds that show semiconducting properties. All kinds of optoelectronic devices including light emitting diodes (LED),^[1] solar cells,^[2] field effect transistors,^[3] memories,^[4] and sensors^[5] have been made using this class of semiconductors. Compared to the inorganic counterparts, the most important advantage of organic semiconductors is the possibility of tuning their properties by chemical modifications. Thus the efficiency of organic solar cells has been recently almost doubled up to 8.3% by synthesizing new polymers while keeping the device structure the same.^[6,7]

Organic electronics enables innovative thinking of applications. Imagine that to put a solar cell to the roof of a house one would only need to paint it, several times though. Illustrations and photographs in newspapers may become animated just like in the world of Harry Potter.^[8] Reality is not far from this technological world; organic displays and flexible solar cells are already for sale. Organic semiconductors will continue to find applications in new niche markets, in which flexible substrates, lightweight, biocompatibility, and low cost are more important factors than high performances. They, however, unlikely will substitute silicon in computer chips or similar devices since the charge carrier mobility and stability at ambient conditions are much better in inorganic semiconductors.

Alternation of single and double bonds between carbon atoms – conjugation – is a common structural property of all organic semiconductors. This zigzag backbone usually adopts planar conformation (**Figure 1.1a**). Covalent bonds between carbon atoms of such a backbone are formed by three sp^2 hybridized orbitals and one unhybridized orbital, which is commonly denoted as p_z .^[9] Unhybridized orbitals p_z provide electron clouds above and below the molecular plain. The adjacent p_z orbitals

overlap resulting in shared molecular orbitals that are often referred as extended π -system. Electrons on these orbitals are spatially delocalized meaning that they belong to the whole π -system, but not to specific carbon atoms. A π -system can be extended over the entire organic molecule or just over a part of it – conjugated segment.

In the ground state electrons fill orbitals of the lowest energies with maximum two electrons of opposite spins per each orbital. The energetically highest occupied (HOMO) and the lowest unoccupied (LUMO) molecular orbitals are very important for electrical conductivity and optical properties of organic semiconductors. They are often denoted as π and π^* orbitals in π -systems, respectively (**Figure 1.1b**). The energy difference between HOMO and LUMO is often referred as a band gap that typically values between 1.5 and 3.5 eV.

Electrical charges can be conducted in a thin film composed of conjugated molecules when, for instance, an electron is injected into LUMO of a molecule, followed by hopping to LUMO of a neighboring molecule and from that molecule to other molecules etc. The physical mechanism that determines conductivity of charges is hopping due to the weak interactions between molecules and to the significant degree of disorder, which is usually present in amorphous or polycrystalline thin films of organic semiconductors.^[10] Positive charges can be conducted by hopping among HOMOs of molecules.

1.2 Excitons are Energy Chunks

The ground state of the majority of organic molecules is electrically neutral and has net spin zero. A molecule can be excited when one electron from the HOMO is promoted to the LUMO, for instance by absorption of a photon. The Jablonski diagram in **Figure 1.2** presents possible transitions between electronic states of an isolated molecule. These states are positioned vertically by their energy and grouped horizontally by spin multiplicity. Electronic states with net spin zero or one are called singlets or triplets, respectively. The arrow **1** represents the absorption of a photon that brings a molecule from the ground state S_0 to the first singlet excited state S_1 ; transitions to higher singlet excited states are also possible (not shown in Figure 1.2). The transition **2** results in the emission of light and is called fluorescence. Triplet excited state T_1 can be created via the intersystem crossing **4**. The radiative transition **6** is called phosphorescence. Fluorescence and/or phosphorescence can be also referred as photoluminescence (PL) when these transitions are initiated by absorption of a photon. The non-radiative transitions **3** and **5** compete with fluorescence and phosphorescence. And finally transition **7** is the absorption of a photon that brings state T_1 to higher triplet excited states T_n . This process can be used to detect triplet excitons in photoinduced absorption experiments.^[11]

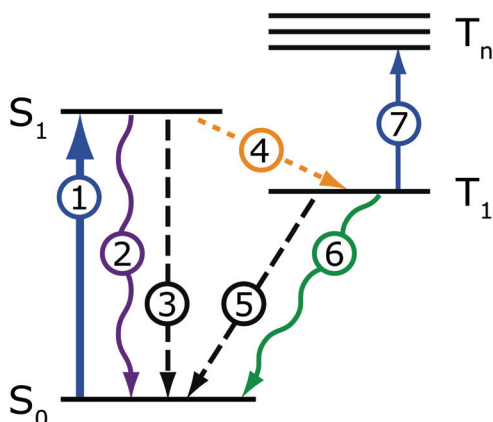


Figure 1.2: The Jablonski diagram of electronic transitions in organic semiconductors. The energies of singlet (S_0 and S_1) and triplet (T_1 and T_n) states are scaled vertically. Absorption (1) fluorescence (2), intersystem crossing (4), phosphorescence (6), nonradiative transitions (3 and 5), and photoinduced absorption (7) are presented as arrows.

In organic solids interactions of an excited molecule with neighbors impose reorganization of intermolecular distances and partial polarization of electronic configuration of the surrounding. This collective response to an excitation is called exciton or, in case of particularly strong interactions with surrounding, exciton-polaron.^[12] Because intermolecular interactions are usually weak in organic materials excitons are strongly localized; often the localization is limited mostly to a single conjugated segment. Excitons are electrically neutral and bear potential energy that can be released when the molecule returns to the ground state. Excitons with total spin of *zero* or *one* are called singlet or triplet, respectively. Although the Jablonski diagram in Figure 1.2 describes isolated molecules, transitions in organic solids are usually similar. Therefore singlet and triplet excitons are often denoted as S_1 and T_1 .

Two charged states – positive or negative polarons – can be created by subtraction from the HOMO or addition to the LUMO of an electron, respectively. Polaron entities include the charge and reorganization energy of the surrounding. Terms “hole” and “electron” are often used to denote positive and negative charges. An exciton can be described as a bound electron-hole pair, which is localized at a single conjugated segment. Such localization is due to relatively low dielectric constant of the organic medium resulting in the strong electrostatic attraction between the opposite charges. Furthermore, the excitonic wavefunction is usually localized at a single conjugated segment due to weak interactions between molecules in organic solids. The work needed to separate electron and hole of an exciton is called binding energy and is usually of the order of 0.3-0.5 eV for singlet excitons.^[13-15]

The binding energy of triplets is higher due to the attractive exchange interaction between electron and hole of the same spin orientation.^[11]

Triplet excitons cannot be directly generated by the absorption of a photon. Photons do not show strong coupling to electronic spins, because electromagnetic radiation does not carry any torque. The electron spin is an angular momentum that must be conserved. Thus the assistance of spin-orbit coupling and electron-phonon interaction are required to enable transitions such as the **4**, **5** and **6** in Figure 1.2. Organic semiconductors are composed of lightweight atoms such as carbon, hydrogen, oxygen, nitrogen and sulfur, which do not show strong spin-orbit coupling. Consequently, the transitions between excitonic states of different spin multiplicity are normally not efficient in this class of materials. Therefore triplet lifetime is about 6 orders of magnitude longer than that of singlets in organic semiconductors.

The working principle of light emitting diodes is based on the generation of excitons. Electrons and holes are injected into an organic semiconductor, which serves as active layer for the LED. Excitons are created when electron and hole meet each other in the active layer. According to the quantum mechanical rules of momentum addition, 25% of all excitons created in this way are singlets and 75% are triplets. The radiative recombination of triplet excitons is not very probable, thus only singlet excitons may contribute to the emitted light. That limits the internal quantum efficiency of an LED to 25%.^[11,16] In some materials with low charge carrier mobility the formation of singlet excitons may be somewhat more or less favorable due to the hyperfine fields.^[17–26] Nevertheless, in order to achieve highly performing LEDs triplet excitons should be manipulated toward radiative recombination.^[11,27–31] In this respect it is highly important to study the dynamics of both singlet and triplet excitons in order to improve the performance of organic LEDs.

1.3 Energy and Charge Transfer

An exciton can be relocated from an excited “donor” molecule to an “acceptor” molecule via a non-radiative process of energy transfer. At the end of this process the donor molecule is in the ground state and the acceptor molecule is in the excited state. Förster and Dexter mechanisms of energy transfer are distinguished (**Figure 1.3a** and **b**).^[32–34] Förster mechanism is based on a dipole-dipole electromagnetic interaction and occurs when the emission spectrum of donor has significant overlap with the absorption spectrum of acceptor. Therefore this type of energy transfer is called *resonant* energy transfer (FRET). The efficiency of FRET decreases with the distance r between donor and acceptor as r^{-6} . Significant FRET can be typically observed for donor-acceptor separations in the range of 2–5 nm.^[34–36] Usually, only singlet excitons can be transferred via the Förster mechanism; however, a triplet exciton that is located at a phosphorescent donor also can undergo FRET.^[37–42]

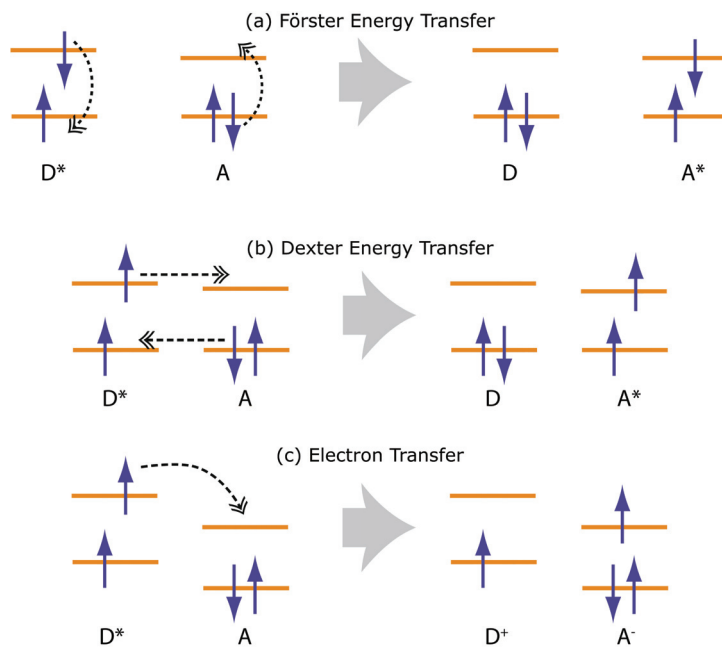


Figure 1.3: (a) Förster energy transfer. (b) Dexter energy transfer enables diffusion of triplet excitons. The horizontal lines are HOMO and LUMO energy levels of donor (D) and acceptor (A) molecules; the asterisk denotes excited state. The dashed arrows represent simultaneous rearrangement of the electronic configuration. (c) Electron transfer from an excited donor molecule (D^*) to a neutral acceptor (A).

Förster energy transfer is observed in photosynthesis when the energy of absorbed photons is channeled to the reaction center.

Actual exchange of electrons between donor and acceptor takes place during the Dexter energy transfer (Figure 1.3b).^[11,32,34] This may happen when donor and acceptor are only about 1 nm apart so there is a significant overlap of molecular orbitals. The probability of Dexter energy transfer exponentially decreases with the distance between donor and acceptor. Both singlet and triplet excitons may be transferred by this mechanism. FRET usually outperforms the efficiency of the Dexter energy transfer for singlet excitons, while triplets may be transferred between non-phosphorescent molecules only by the Dexter mechanism. In contrast to FRET, Dexter energy transfer does not require the overlap between emission and absorption spectra of the donor and acceptor molecules. However, the exciton energy of the acceptor should be lower than that of the donor molecule for efficient transfer.

Electron and hole, which are coulombically bound in an exciton, can be separated when their binding energy is overcome. Such a separation can be efficient at the interface with an electron accepting material. If the energy of LUMO of the acceptor is significantly lower than LUMO of the excited donor molecule, then electron transfer from donor may take place (see **Figure 1.3c**). This process is called

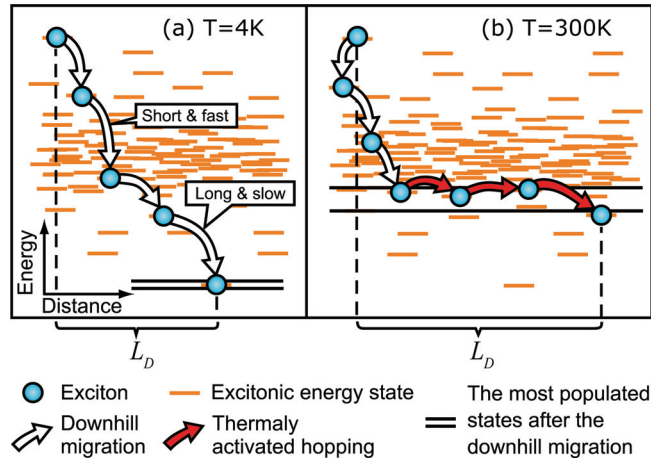


Figure 1.4: Exciton diffusion process at low and room temperatures. The excitonic Gaussian density of states is represented by the distribution of the excitonic energies. The exciton-phonon coupling determines the position of the energy level of the most populated states. **(a)** The downhill migration fully determines the exciton diffusion process at low temperatures. **(b)** At room temperature, the thermally activated hopping also contributes to the exciton diffusion length.

charge transfer; it is a short range interaction that takes place when there is a significant spatial overlap between wavefunctions of the donor and acceptor molecules. As a result of the electron transfer donor and acceptor are positively and negatively charged, respectively. Hole transfer is also possible when the energy levels of a donor and an acceptor are properly aligned. The physical mechanism of this process is the same as that of the electron transfer.

1.4 The Physics of Exciton Diffusion

Diffusion is a random motion of particles in space that leads to spreading from the areas of high concentration to the areas of low concentration. Diffusion is regarded to be normal when it can be described by the following equation:

$$\frac{\partial n}{\partial t} = D\nabla^2 n - \frac{n}{\tau}, \quad (1.1)$$

where n is the concentration of particles, D is a diffusion coefficient, ∇^2 is Laplace operator, and τ is the particle lifetime. The room mean square displacement of a particle from its initial position due to the diffusion process is called diffusion length, which is given by:

$$L_D = \sqrt{\frac{\sum dL_i^2}{N}} = \sqrt{2ZD\tau}, \quad (1.2)$$

where dL_i is the displacement of an exciton i from its original position, N is total number of excitons; and Z is equal to 1, 2 or 3 in case of one-, two- or three-dimensional diffusion, respectively.^[12] However, the factor of two is sometimes omitted in Equation (1.2):

$$L_D = \sqrt{ZD\tau} . \quad (1.3)$$

In this case the value L_D is approximately equal to the average displacement of a particle from its initial position. To be consistent with the literature we will refer to the diffusion length that is given by the expression (1.3).

Amorphous and polycrystalline films are characterized by a significant degree of disorder, in particular when they are cast from solution. Variation of molecular conformations and size of conjugated segments (especially in polymers), inhomogeneity of intermolecular interactions, chemical defects and impurities etc. lead to a Gaussian distribution of the HOMO-LUMO energy gaps – and excitonic energies. The half-width σ of the Gaussian is a measure for the disorder that is present in the bulk material. Excitons undergo migration among conjugated segments in solid organic material via energy transfer. Due to the disorder such a migration is a random walk and can be regarded as diffusion. The exciton diffusion length L_D is a very important parameter for operation of optoelectronic devices.

Figure 1.4 schematically shows the process of exciton diffusion in thin films of organic semiconductors at low and room temperatures.^[43] If excitons are created by absorption of a photon with energy that corresponds to the high energy tail of the DOS then exciton diffusion will be defined by the downhill migration toward lower energy sites. This relaxation ends typically after about 100 ps when the excitons reach the energy level of the most populated states. This energy level is proportional to $-\sigma^2 / KT$ under conditions of thermodynamic quasi-equilibrium and, more generally, is responsible for the o-o peak position of the steady state PL spectrum. At low temperatures (Figure 1.4a), such a level is situated deep in the tail of the Gaussian DOS, whereas at high temperatures excitons are distributed closer to the middle of the DOS (Figure 1.4b).

At low temperatures excitons are trapped after the downhill migration because there is no thermal energy to promote excitons to higher energy states and the density of lower energy states is not sufficient for hopping. As temperature increases, the probability of phonon absorption by excitons also increases. The level of the most populated energy sites climbs uphill on the DOS leading to the decrease of the energy difference between the occupied and neighboring conjugated segments (Figure 1.4a and b). If the temperature is high enough, the thermally activated hopping becomes favorable (Figure 1.4b), which does not lead to a significant change of the exciton energy but contributes to the exciton diffusion. Thus in the high temperature regime, the exciton diffusion consists of two steps, namely the downhill migration and the

thermally activated hopping, while at lower temperatures the downhill migration fully determines the exciton diffusion process.

Undoubtedly both the downhill migration and the temperature-activated hopping can be considered as random walks due to the disordered nature of organic semiconductor. However, not every random walk is a normal diffusion process that can be described by Equation (1.1). For a random walk, the diffusion coefficient is expressed by $D \propto l^2/dt$, where l^2 is the ensemble average of the hop length squared, and dt is the average hop time. Since the exciton hopping rate $1/dt$ depends^[44] on l stronger than l^{-2} , the necessary condition for the exciton migration to be a normal diffusion is that l to be constant in time. Because the temperature-activated hopping occurs among energy states of similar density, such a process can be considered as normal diffusion. In contrast, the downhill migration is anomalous diffusion because the average hopping length l is changing^[45] as moving downward in the DOS (Figure 1.4a).

At low temperature, where the downhill migration is the main contribution to the exciton diffusion, the diffusion coefficient D is expected to decrease with time. At room temperature, the exciton diffusion coefficient does not vanish after the downhill migration process but retains the value corresponding to the temperature-activated hopping; consequently, the overall process of exciton diffusion can be approximated as normal diffusion. It is important to note, that hopping of both singlet and triplet excitons can be regarded as normal diffusion at room temperature.^[43,46–51]

1.5 Exciton-exciton annihilation

High exciton densities and diffusion processes give rise to a high probability of two excitons meeting each other during their lifetimes. Exciton-exciton annihilation occurs when the interaction between these two excitons leads to a non-radiative recombination of at least one of them.^[11,52–56] For instance, annihilation of singlet (S_1) and triplet (T_1) excitons may result in a ground state (S_0) and a singlet exciton:



Other products of exciton annihilation are also possible.^[57] Efficient exciton annihilation (1.5) requires anti-parallel spins of triplet excitons due to the conservation law of angular momentum. Singlet excitons that are created as the result of exciton annihilation (1.5) may decay radiatively. Such emission is called delayed fluorescence because it can be observed after a pulsed laser excitation at times much longer than the PL decay time.

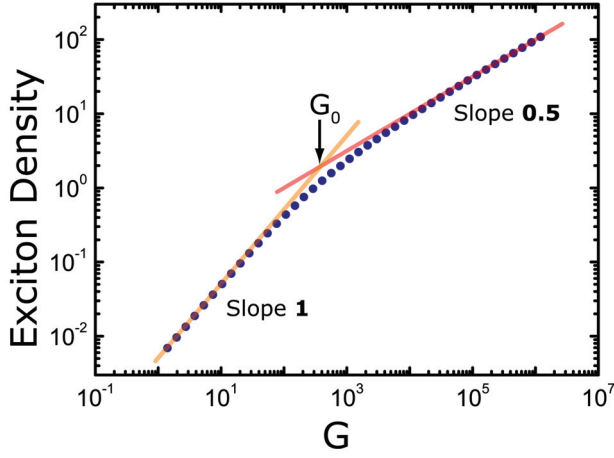


Figure 1.5: Simulated exciton density (circles) *versus* the exciton generation rate using Equation (1.9).

Exciton-exciton annihilation can be described mathematically by the following modification of the Equation (1.1):

$$\frac{\partial n}{\partial t} = D\nabla^2 n - \frac{n}{\tau} - \gamma n^2 + G, \quad (1.6)$$

$$\gamma = 4\pi R_a D; \quad (1.7)$$

where γ is the annihilation rate constant, R_a is the annihilation radius – the average distance between two excitons that undergo annihilation, and G is the exciton generation rate.

Under conditions of continuous and homogeneous generation $G = \text{const}$ we can set $\partial n / \partial t = 0$ and $\nabla^2 n = 0$ in Eq. (1.6):

$$\gamma n^2 + \frac{n}{\tau} - G = 0, \quad (1.8)$$

leading to the steady state solution:^[56]

$$n = \frac{1}{2\gamma\tau} \left(\sqrt{1 + 4\gamma\tau^2 G} - 1 \right). \quad (1.9)$$

Figure 1.5 shows an example plot of Equation (1.9) when $4\gamma\tau^2 = 0.01$ (circles). The dependence consists of two straight lines with slopes 1 and 0.5. In a log-log graph a straight line denotes function in a form of $y = cx^\alpha$, where α is the slope of that line. Slope 1 denotes linear dependence $n \propto G$ at generation intensities smaller than a certain threshold value G_0 . The square root dependence $n \propto \sqrt{G}$ at $G > G_0$ indicates the exciton-exciton annihilation. The threshold generation rate can be estimated from Eq. (1.9):

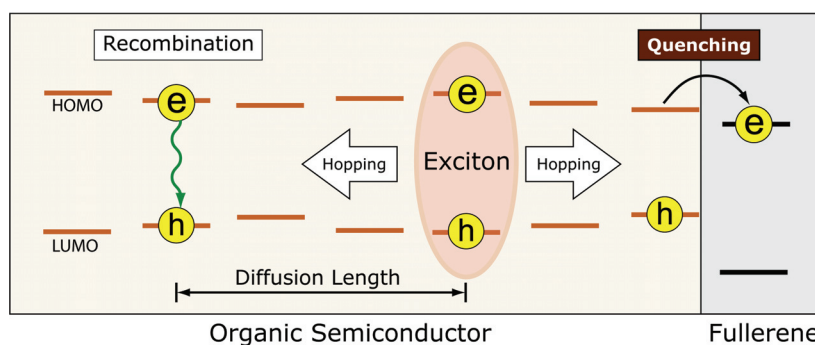


Figure 1.6: Exciton quenching due to charge transfer at semiconductor-fullerene interface. Electrons and holes are denoted as (e) and (h). Conjugated segments are schematically depicted as pairs of HOMO-LUMO levels.

$$G_0 \approx \frac{1}{\gamma\tau^2}. \quad (1.10)$$

The obtained expression shows that the exciton-exciton annihilation is a more important decay process for triplets than for singlets because of the long triplet lifetime τ . Triplet-triplet annihilation can be observed by recording the dependence of the photoinduced absorption intensity (transition 7 in Figure 1.2) on the generation rate G .^[58]

1.6 Diffusion Limited Exciton Quenching

Excitons can be quenched in several ways leading to the reduction of the exciton density, PL intensity and PL decay time. Exciton quenching is a very important process in operation of devices and for studying excitonic dynamics. The energy of excited state can be trapped during the diffusion process on non-radiative defect states that are always present in thin films of organic semiconductors. Strong quenching has been observed in the vicinity of metal interfaces.^[59] Exciton dissociation into non-radiative species such as free electrons and holes also leads to quenching. Furthermore, inhomogeneous regions of the amorphous films of higher density, as expressed in g/cm^3 etc., show higher rates of exciton quenching.^[60–63]

Figure 1.6 illustrates the dissociation of an exciton at the semiconductor-fullerene interface. In the most common situation the LUMO of fullerenes is significantly lower than LUMOs of organic semiconductors.^[36] Thus electron transfer to the fullerene is energetically favorable, which leads to exciton quenching. Exciton quenching due to charge transfer at the semiconductor-fullerene interface is reported to be at the time scale of 45 fs that is much shorter than typical exciton lifetime (~ 0.5

ns). Therefore fullerenes can be considered as perfect exciton quenchers for such donor semiconductors.^[64]

Semiconductor-fullerene heterojunctions are commonly used in organic solar cells to separate electrons and holes.^[2] In the simplest case the active layer of an organic solar cell consists of a bilayer semiconductor-fullerene heterojunction (Figure 1.6). The semiconductor plays the role of a light absorber in which singlet excitons are generated fairly homogeneously within the layer. The excitons undergo diffusion so that some of them will reach the interface with fullerene, where electron and hole are separated. These electrons and holes are then transported through layers of fullerene and organic semiconductor, respectively, and then extracted at the metallic electrodes of the solar cell resulting in photocurrent. Excitons that are capable of reaching the fullerene interface may undergo dissociation. Therefore the exciton diffusion length L_D sets the geometrical constraints on the useful thickness of the semiconductor layer. Excitons that are created at longer distance than L_D from the fullerene interface will not make a significant contribution to the photocurrent. Terao *et al.* showed almost linear correlation between the short circuit current of a solar cell and the exciton diffusion length.^[65] Thus for the design efficient solar cells it is important to measure and control the exciton diffusion length. Other parameters that influence the performance of solar cells include morphology of donor-acceptor interface and charge carrier mobility.

1.7 Measuring Singlet Exciton Diffusion Length

The singlet exciton diffusion length is typically reported in the range of 5-20 nm in amorphous and polycrystalline organic semiconductors.^[2,35,43,59,60,65-88] It is not entirely clear why the exciton diffusion length is so similar in such a broad selection of materials. What factors influence the exciton diffusion length? And finally how do these factors – and the exciton diffusion length itself – correlate with the performance of solar cells and LEDs? To answer these questions systematic measurements of exciton diffusion lengths are needed in materials with various chemical composition, morphology and performances in devices.^[65,69,78,89] However, most of the previously developed methods of measuring exciton diffusion length are not ideal for such studies. The reasons are the overall complexity of experimental methods and/or the theoretical model requiring several fitting parameters. In the following we summarize the available methods and discuss the advantages and pitfalls of each.

Fluorescence Quenching in Bilayers

Perhaps the most popular method to measure singlet exciton diffusion length is based on PL quenching in bilayers.^[35,43,65,68,72,73,75,77,80,85,86,90] In this method one of the interfaces of a thin film is brought into contact with an exciton quenching layer (**Figure 1.7**). Fullerenes or TiO₂ are commonly used as “quenching wall”. If the

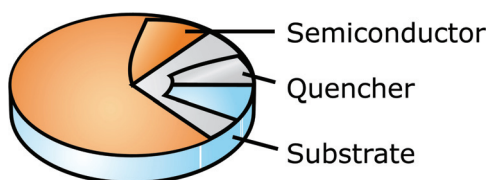


Figure 1.7: Bilayer structure for exciton diffusion measurement. Organic semiconductor is deposited on top of exciton quenching layer.

thickness of the organic layer is of the order of the exciton diffusion length, then large fraction of the excitons will be able to reach the “quenching wall” via diffusion. Consequently the PL decay time of such a sample will be shorter than in an isolated film. The measured PL decays are then fitted using a simple model that is based on Eq. (1.1) yielding the exciton diffusion length.

There are advantages and disadvantages of the bilayer method. On the positive side the modeling is straightforward with the exciton diffusion length as the only fitting parameter. The thickness of the semiconductor layer can be accurately measured using atomic force microscopy or ellipsometry. On the other hand the sample preparation is quite demanding. It may be challenging to prepare semiconductor layers as thin as 5 nm that are even in thickness and do not form pin-holes or other defects. Furthermore, all the interfaces should be sharp^[80] and ultra-flat; typically root mean square roughness of about 1 nm on the area of 100 μm^2 is required for accurate measurement. The effects of optical interference^[75,91] and variation of the exciton density due to optical absorption^[72] should be taken into account. Often PL decay times of isolated films also depend on the layer thickness even without the introduction of any quenchers,^[60,72] we address this effect in Chapter 2. All these factors set limits to use the bilayer structure for systematic measurements of the exciton diffusion length.

The problematic thickness-dependent effects can be avoided in an alternative bilayer method.^[69–71,87,92] A thick film, typically of the order of micrometers, is capped either with exciton blocking or exciton quenching layer. This heterostructure is excited with monochromatic light at various wavelengths. According to the absorption spectrum of the semiconductor the exciton generation profile is modulated. By comparing PL intensity of quenched and unquenched samples the exciton diffusion length can be extracted. The advantage of this method is that only two samples are needed for each material. However the mathematical model is complex and this method works the best when the variation of the generation profile is significant on the length scale of the exciton diffusion length. Therefore it is most applicable for single crystals, which show extremely long exciton diffusion length.^[87,92]

Exciton-Exciton Annihilation

The exciton diffusion coefficient can be estimated by measuring the efficiency of the exciton-exciton annihilation.^[70,72,74] The exciton diffusion coefficient is calculated from γ (Eq. 1.7), which can be measured experimentally by modeling the PL decays measured at various intensities of the incident light. Only one sample is needed for the measurements. However, the theoretical considerations are complex and there are two unknown parameters that are needed for the modeling, namely the annihilation radius R_a and initial exciton density n_0 . It is very difficult to set an independent experiment to measure these parameters and they are typically assumed to have a certain value. Only materials with exceptional photochemical stability can be investigated using this method because intense laser light is required for the exciton-exciton annihilation.

Microwave Conductivity

An interesting method to measure exciton diffusion length has been developed in Delft.^[82] Exciton quenching in semiconductor-TiO₂ bilayers has been estimated by observing enhancement in photoconductivity in the TiO₂ layer due to electron transfer from the semiconductor layer. The change in photoconductivity is estimated by measuring the change of the intensity of reflected microwave radiation upon optical excitation of the semiconductor. The microwave conductivity in TiO₂ is then modeled depending on the thickness of the organic layer. The important advantage of this method is that it is also sensitive for non-emissive excitons, such as triplets. However, this method has all the problems of the PL quenching methods in bilayers and therefore it is also not suitable for systematic studies.

Photocurrent Measurements

Exciton diffusion length can be estimated by modeling I-V characteristics of a solar cell or a similar device.^[2,83,84,88,93,94] The typical sample consists of at least one organic semiconductor layer and two electrodes. The theoretical model includes the electrical, optical, and exciton diffusion parts. It is a big challenge to describe the charge transport through a specific organic layer as well as to understand charge injection/extraction at the electrical contacts. The effect of metallic electrodes on the distribution of the excitation light – and generated excitons – within the device should be carefully calculated. Exciton quenching at metallic electrodes should be also included into the model. These photocurrent measurements are the most difficult way to extract the exciton diffusion length. It is reasonable to apply this method to a semiconductor with superior performance in devices, but not to systematic studies of many materials.

1.8 Do Triplets Diffuse Further?

Triplet excitons are expected to have longer diffusion length than singlets due to their much longer lifetime, see Eq. (1.3). However, values as short as 10-20 nm have been reported recently, similar to the singlet exciton diffusion length.^[71,95–101] On the other hand there are plenty of publications with triplet diffusion length of more than 100 nm.^[21,92,102,103] Moreover, different values in the range of 10-250 nm have been published for the same materials.^[30,96,97,102,104] Such a controversy probably stems from the fact that reliable measurements of the triplet exciton diffusion length is difficult. The available techniques are complex and it is hard to control the relevant processes that influence the exciton diffusion length. Moreover, simple PL quenching techniques can only be applied to phosphorescent materials.^[71,105] Here we summarize some of the methods used to measure the triplet exciton diffusion length.

Measurements in LED Configuration

A specially designed multilayer light emitting diode can be used to measure triplet exciton diffusion.^[21,30,95–97,106,107] In these structures the charge recombination region is spatially confined within a thin interfacial region between electron and hole transporting layers. A phosphorescent dopant is deployed in one of the transporting layers at certain distance L from the exciton generation region. The materials are selected such that triplet energy transfer from the host semiconductor to the dopant is favorable. Then the intensity of phosphorescent emission of the dopant molecules is correlated to the triplet density of the host material in the vicinity of the dopant layer, *i.e.* at distance L from the charge recombination region. The profile of triplet exciton density within the semiconductor layer is measured by recording the dependence of phosphorescence intensity of the dopant molecules *versus* distance L . This profile is theoretically modeled to extract the exciton diffusion length.

The emission intensity of the phosphorescent dopant is strongly affected by the outcoupling efficiency that must be carefully calculated and included into the model. In a working LED there is a significant amount of polarons that are efficient quenchers of triplet excitons. However polaron-triplet interactions have been always neglected in the LED-based methods.^[108] The thickness and position of the recombination region depends on the total electrical current that flows through the device. These effects set certain limits on the value of the working current. It is difficult to evaluate the effect of triplet-triplet annihilation in this method. Due to many complications and uncertainties in the LED methods, it is not surprising that very different values of the triplet diffusion length have been extracted in the same materials.

Phosphorescent Detection in Bilayers

Triplet exciton diffusion can be directly probed in a bilayer structure comprising a pure organic semiconductor layer and a layer that is heavily doped with phosphorescent molecules.^[104] Triplet excitons are created by intersystem crossing in the semiconductor, followed by their diffusion toward the doped layer, where their energy is transferred to the dopants and detected as phosphorescent emission. The phosphorescence decay and delayed fluorescence are then modeled using the diffusion equation, leading to the exciton diffusion length. The model used requires four fitting parameters including the exciton diffusion length, triplet-triplet annihilation rate, transfer rate from host material to the phosphorescent dopant, and the initial triplet density. In *4,4'-bis(N-carbazolyl)biphenyl* (CBP) the resulting exciton diffusion length was estimated to be 25 nm when triplet-triplet annihilation is efficient and 140 nm when the annihilation is absent.^[104] Disadvantages of this method are the large number of fitting parameters and the complex theoretical model.

Photocurrent and Microwave Conductivity

Triplet exciton diffusion length can be also measured using previously described methods such as the photocurrent modeling^[94,98,99,102,109] and the microwave conductivity measurements.^[100,110] In these methods it is important to distinguish contributions of triplet vs. singlet excitons to photocurrent or microwave conductivity leading to an additional complication. The effect of triplet-triplet annihilation also has been neglected when applying these methods. Values of triplet exciton diffusion lengths of 10-250 nm have been reported in several materials.

Other Techniques

There are only few reports describing other than the above mentioned methods of measuring the triplet exciton diffusion length. Extremely long triplet diffusion length of 2-4 μm has been measured in a ladder-type conjugated polymer using detection of triplet excitons with photoinduced absorption in polymer-fullerene blends.^[103] An ultra-long exciton diffusion length of 5 μm has been also measured in rubrene crystals using a combination of the photocurrent method with variation of the absorption of linearly polarized light relative to the crystallographic orientation.^[92] Far diffusing excitons in rubrene crystal are assumed to be triplets. The process of triplet-triplet annihilation has been left without attention in these studies though.

1.9 Motivation and Scope

Exciton diffusion is an important process in the operation of organic solar cells and light emitting diodes. In order to design new materials for efficient devices deep

understanding of excitonic processes in general is needed. In particular, the following questions should be answered. What is the relation between the exciton diffusion length and the performance of solar cells and LEDs? What is the influence of thermal annealing on the exciton diffusion length? Why is the singlet exciton diffusion length of the order of 10 nm in a very broad selection of materials, while triplet diffusion length has been reported in the wide range of 10-5000 nm? What is the impact of triplet-triplet annihilation on the triplet diffusion length? How do chemical composition and film morphology influence the exciton diffusion length? This thesis will answer many of these questions also with the development of new methods to measure singlet and triplet exciton diffusion length.

In **Chapter 2** we show why the PL decay time in spin-coated polymer thin films depends on the thickness of the films. We show that the semiconductor-vacuum interface introduces additional exciton quenching, which has to be accounted for modeling of the exciton diffusion. This effect creates additional complications in measurements of diffusion length using exciton quenching in bilayers.

In **Chapter 3** we present a new method to measure the exciton diffusion length which has numerous advantages compared to other techniques. The method is simple and fast, therefore it is suitable for systematic studies. It is based on a Monte Carlo simulation of the exciton diffusion, which enables modeling of exciton diffusion in complex morphologies of organic semiconductor-fullerene blends.

This new method is applied to the study of the influence of the thermal annealing on the exciton diffusion in **Chapter 4**. We show that exciton diffusion length becomes considerably shorter upon annealing in a small molecule organic semiconductor. An interesting approach to quantify quenching efficiency of new electron accepting molecules is also presented.

Chapter 5 presents an in-depth study of triplet exciton detection using phosphorescent Pd-coordinated porphyrin. We show that such detection does not influence the triplet lifetime in the host material. In this respect the triplet population is not perturbed. This detection method enables us to study processes such as triplet-triplet annihilation.

In **Chapter 6** we describe a new method to measure triplet exciton diffusion length in organic semiconductors. We record the penetration profile of triplet excitons, which were created at an interface of a thin film of organic semiconductor with a triplet injecting material. A layer of triplet detecting Pd-coordinated porphyrin is deployed at various distances from the injecting interface. The intensity of phosphorescent emission of the detecting layer is proportional to the local triplet density. The obtained penetration profile is then modeled to extract the triplet exciton diffusion length being the only fitting parameter. We show that triplet-triplet annihilation may lead to variation of the penetration depth in the range of 20-100 nm.

1.10 References

- [1] J. R. Sheats, *J. Mater. Res.* **2004**, *19*, 1974-1989.
- [2] P. Peumans, A. Yakimov, S. R. Forrest, *J. Appl. Phys.* **2003**, *93*, 3693-3723.
- [3] T. W. Kelley, P. F. Baude, C. Gerlach, D. E. Ender, D. Muyres, M. A. Haase, D. E. Vogel, S. D. Theiss, *Chem. Mater.* **2004**, *16*, 4413-4422.
- [4] R. C. G. Naber, K. Asadi, P. W. M. Blom, D. M. de Leeuw, B. de Boer, *Adv. Mater.* **2010**, *22*, 933-945.
- [5] U. Lange, N. V. Roznyatovskaya, V. M. Mirsky, *Anal. Chim. Acta* **2008**, *614*, 1-26.
- [6] M. Campoy-Quiles, T. Ferenczi, T. Agostinelli, P. G. Etchegoin, Y. Kim, T. D. Anthopoulos, P. N. Stavrinou, D. D. C. Bradley, J. Nelson, *Nat Mater* **2008**, *7*, 158-164.
- [7] M. A. Green, K. Emery, Y. Hishikawa, W. Warta, *Prog. Photovolt: Res. Appl.* **2011**, *19*, 84-92.
- [8] J. K. Rowling, *Harry Potter and the Sorcerer's Stone*, Scholastic Inc, **1997**.
- [9] K. P. C. Vollhardt, N. E. Schore, *Organic Chemistry*, W. H. Freeman, **2010**.
- [10] U. Rauscher, H. Bässler, D. D. C. Bradley, M. Hennecke, *Phys. Rev. B* **1990**, *42*, 9830.
- [11] A. Köhler, H. Bässler, *Mater. Sci. Eng., R* **2009**, *66*, 71-109.
- [12] M. Pope, C. E. Swenberg, *Electronic Processes in Organic Crystals and Polymers*, Oxford University Press, **1999**.
- [13] M. Scheidler, U. Lemmer, R. Kersting, S. Karg, W. Riess, B. Cleve, R. F. Mahrt, H. Kurz, H. Bässler, E. O. Göbel, P. Thomas, *Phys. Rev. B* **1996**, *54*, 5536.
- [14] A. Ruini, M. J. Caldas, G. Bussi, E. Molinari, *Phys. Rev. Lett.* **2002**, *88*, 206403.
- [15] J.-L. Brédas, D. Beljonne, V. Coropceanu, J. Cornil, *Chem. Rev.* **2004**, *104*, 4971-5004.
- [16] M. Carvelli, R. A. J. Janssen, R. Coehoorn, *Phys. Rev. B* **2011**, *83*, 075203.
- [17] P. A. Bobbert, *Nat Mater* **2010**, *9*, 288-290.
- [18] J. M. Lupton, D. R. McCamey, C. Boehme, *ChemPhysChem* **2010**, *11*, 3040-3058.
- [19] T. D. Nguyen, G. Hukic-Markosian, F. Wang, L. Wojcik, X.-G. Li, E. Ehrenfreund, Z. V. Vardeny, *Nat Mater* **2010**, *9*, 345-352.
- [20] A. P. Monkman, C. Rothe, S. M. King, *Proceedings of the IEEE* **2009**, *97*, 1597-1605.
- [21] M. A. Baldo, D. F. O'Brien, M. E. Thompson, S. R. Forrest, *Phys. Rev. B* **1999**, *60*, 14422.
- [22] J. S. Wilson, A. S. Dhoot, A. J. A. B. Seeley, M. S. Khan, A. Kohler, R. H. Friend, *Nature* **2001**, *413*, 828-831.
- [23] Y. Cao, I. D. Parker, G. Yu, C. Zhang, A. J. Heeger, *Nature* **1999**, *397*, 414-417.
- [24] C. Yang, Z. V. Vardeny, A. Köhler, M. Wohlgenannt, M. K. Al-Suti, M. S. Khan, *Phys. Rev. B* **2004**, *70*, 241202.
- [25] M. Wohlgenannt, K. Tandon, S. Mazumdar, S. Ramasesha, Z. V. Vardeny, *Nature* **2001**, *409*, 494-497.
- [26] S. P. Kersten, A. J. Schellekens, B. Koopmans, P. A. Bobbert, *Phys. Rev. Lett.* **2011**, *106*, 197402.
- [27] H. Kanno, Y. Sun, S. R. Forrest, *Appl. Phys. Lett.* **2006**, *89*, 143516-3.

- [28] Y. Sun, N. C. Giebink, H. Kanno, B. Ma, M. E. Thompson, S. R. Forrest, *Nature* **2006**, *440*, 908-912.
- [29] S. Reineke, F. Lindner, G. Schwartz, N. Seidler, K. Walzer, B. Lussem, K. Leo, *Nature* **2009**, *459*, 234-238.
- [30] G. Schwartz, S. Reineke, T. C. Rosenow, K. Walzer, K. Hügley, *Adv. Funct. Mater.* **2009**, *19*, 1319-1333.
- [31] Y. Chi, P.-T. Chou, *Chem. Soc. Rev.* **2010**, *39*, 638-655.
- [32] D. L. Dexter, *J. Chem. Phys.* **1953**, *21*, 836.
- [33] D. L. Dexter, R. S. Knox, T. Förster, *Phys. Status Solidi B* **1969**, *34*, K159-K162.
- [34] G. D. Scholes, *Annu. Rev. Phys. Chem.* **2003**, *54*, 57-87.
- [35] W. A. Luhman, R. J. Holmes, *Adv. Funct. Mater.* **2011**, *21*, 764-771.
- [36] R. Koeppel, N. S. Sariciftci, *Photochem. Photobiol. Sci.* **2006**, *5*, 1122-1131.
- [37] V. Cleave, G. Yahioglu, P. L. Barny, R. H. Friend, N. Tessler, *Adv. Mater.* **1999**, *11*, 285-288.
- [38] V. Cleave, G. Yahioglu, P. Le Barny, D. H. Hwang, A. B. Holmes, R. H. Friend, N. Tessler, *Adv. Mater.* **2001**, *13*, 44-47.
- [39] Y. Kawamura, S. Yanagida, S. R. Forrest, *J. Appl. Phys.* **2002**, *92*, 87-93.
- [40] X. Gong, S.-H. Lim, J. C. Ostrowski, D. Moses, C. J. Bardeen, G. C. Bazan, *J. Appl. Phys.* **2004**, *95*, 948-953.
- [41] J. Kalinowski, W. Stampor, M. Cocchi, D. Virgili, V. Fattori, P. Di Marco, *Chem. Phys.* **2004**, *297*, 39-48.
- [42] Y. Kawamura, J. Brooks, J. J. Brown, H. Sasabe, C. Adachi, *Phys. Rev. Lett.* **2006**, *96*, 017404-4.
- [43] O. V. Mikhenko, F. Cordella, A. B. Sieval, J. C. Hummelen, P. W. M. Blom, M. A. Loi, *J. Phys. Chem. B* **2008**, *112*, 11601-11604.
- [44] C. Madigan, V. Bulovic, *Phys. Rev. Lett.* **2006**, *96*, 046404-4.
- [45] L. M. Herz, C. Silva, A. C. Grimsdale, K. Müllen, R. T. Phillips, *Phys. Rev. B* **2004**, *70*, 165207.
- [46] S. T. Hoffmann, E. Scheler, J.-M. Koenen, M. Forster, U. Scherf, P. Strohriegel, H. Bässler, A. Köhler, *Phys. Rev. B* **2010**, *81*, 165208.
- [47] V. Jankus, C. Winscom, A. P. Monkman, *J. Phys.: Condens. Matter* **2010**, *22*, 185802.
- [48] I. I. Fishchuk, A. Kadashchuk, L. S. Devi, P. Heremans, H. Bassler, A. Kohler, *Phys. Rev. B* **2008**, *78*, 045211-8.
- [49] L. S. Devi, M. K. Al-Suti, C. Dosche, M. S. Khan, R. H. Friend, A. Kohler, *Phys. Rev. B* **2008**, *78*, 045210-8.
- [50] S. Athanasopoulos, E. V. Emelianova, A. B. Walker, D. Beljonne, *Phys. Rev. B* **2009**, *80*, 195209-7.
- [51] F. B. Dias, K. T. Kamtekar, T. Cazati, G. Williams, M. R. Bryce, A. P. Monkman, *ChemPhysChem* **2009**, *10*, 2096-2104.
- [52] R. G. Kepler, J. C. Caris, P. Avakian, E. Abramson, *Phys. Rev. Lett.* **1963**, *10*, 400-402.
- [53] C. E. Swenberg, *J. Chem. Phys.* **1969**, *51*, 1753.
- [54] A. Suna, *Phys. Rev. B* **1970**, *1*, 1716-1739.
- [55] J. Partee, E. L. Frankevich, B. Uhlhorn, J. Shinar, Y. Ding, T. J. Barton, *Phys. Rev. Lett.* **1999**, *82*, 3673-3676.
- [56] V. Dyakonov, G. Rösler, M. Schwoerer, E. L. Frankevich, *Phys. Rev. B* **1997**, *56*, 3852-3862.

- [57] R. E. Merrifield, *Pure Appl. Chem.* **1971**, *27*, 481-498.
- [58] O. V. Mikhnenko, P. W. M. Blom, M. A. Loi, *Phys. Chem. Chem. Phys.* **2011**, *13*, 14453-14456.
- [59] D. E. Markov, P. W. M. Blom, *Appl. Phys. Lett.* **2005**, *87*, 233511-3.
- [60] O. V. Mikhnenko, F. Cordella, A. B. Sieval, J. C. Hummelen, P. W. M. Blom, M. A. Loi, *J. Phys. Chem. B* **2009**, *113*, 9104-9109.
- [61] M. A. Loi, A. Mura, G. Bongiovanni, Q. Cai, C. Martin, H. R. Chandrasekhar, M. Chandrasekhar, W. Graupner, F. Garnier, *Phys. Rev. Lett.* **2001**, *86*, 732.
- [62] B. C. Hess, G. S. Kanner, Z. Vardeny, *Phys. Rev. B* **1993**, *47*, 1407.
- [63] R. K. Tikhoplav, B. C. Hess, *Synth. Met.* **1999**, *101*, 236-237.
- [64] C. J. Brabec, G. Zerza, G. Cerullo, S. De Silvestri, S. Luzzati, J. C. Hummelen, S. Sariciftci, *Chem. Phys. Lett.* **2001**, *340*, 232-236.
- [65] Y. Terao, H. Sasabe, C. Adachi, *Appl. Phys. Lett.* **2007**, *90*, 103515.
- [66] H. Wang, H.-Y. Wang, B.-R. Gao, L. Wang, Z.-Y. Yang, X.-B. Du, Q.-D. Chen, J.-F. Song, H.-B. Sun, *Nanoscale* **2011**, *3*, 2280.
- [67] S. Cook, H. Liyuan, A. Furube, R. Katoh, *J. Phys. Chem. C* **2010**, *114*, 10962-10968.
- [68] K. Masuda, Y. Ikeda, M. Ogawa, H. Benten, H. Ohkita, S. Ito, *ACS Appl. Mater. Interfaces* **2010**, *2*, 236-245.
- [69] R. R. Lunt, J. B. Benziger, S. R. Forrest, *Adv. Mater.* **2010**, *22*, 1233-1236.
- [70] S. Cook, A. Furube, R. Katoh, L. Han, *Chem. Phys. Lett.* **2009**, *478*, 33-36.
- [71] R. R. Lunt, N. C. Giebink, A. A. Belak, J. B. Benziger, S. R. Forrest, *J. Appl. Phys.* **2009**, *105*, 053711-7.
- [72] P. E. Shaw, A. Ruseckas, I. D. W. Samuel, *Adv. Mater.* **2008**, *20*, 3516-3520.
- [73] C. Goh, S. R. Scully, M. D. McGehee, *J. Appl. Phys.* **2007**, *101*, 114503.
- [74] A. J. Lewis, A. Ruseckas, O. P. M. Gaudin, G. R. Webster, P. L. Burn, I. D. W. Samuel, *Org. Electron.* **2006**, *7*, 452-456.
- [75] S. R. Scully, M. D. McGehee, *J. Appl. Phys.* **2006**, *100*, 034907-5.
- [76] D. E. Markov, P. W. M. Blom, *Phys. Rev. B* **2006**, *74*, 085206-5.
- [77] Y. Wu, Y. C. Zhou, H. R. Wu, Y. Q. Zhan, J. Zhou, S. T. Zhang, J. M. Zhao, Z. J. Wang, X. M. Ding, X. Y. Hou, *Appl. Phys. Lett.* **2005**, *87*, 044104-3.
- [78] D. E. Markov, C. Tanase, P. W. M. Blom, J. Wildeman, *Phys. Rev. B* **2005**, *72*, 045217-6.
- [79] D. E. Markov, J. C. Hummelen, P. W. M. Blom, A. B. Sieval, *Phys. Rev. B* **2005**, *72*, 045216-5.
- [80] D. E. Markov, E. Amsterdam, P. W. M. Blom, A. B. Sieval, J. C. Hummelen, *J. Phys. Chem. A* **2005**, *109*, 5266-5274.
- [81] L. Lüer, H.-J. Egelhaaf, D. Oelkrug, G. Cerullo, G. Lanzani, B.-H. Huisman, D. de Leeuw, *Org. Electron.* **2004**, *5*, 83-89.
- [82] J. E. Kroeze, T. J. Savenije, M. J. W. Vermeulen, J. M. Warman, *J. Phys. Chem. B* **2003**, *107*, 7696-7705.
- [83] C. L. Yang, Z. K. Tang, W. K. Ge, J. N. Wang, Z. L. Zhang, X. Y. Jian, *Appl. Phys. Lett.* **2003**, *83*, 1737-1739.
- [84] T. Stubinger, W. Brutting, *J. Appl. Phys.* **2001**, *90*, 3632-3641.
- [85] M. Theander, A. Yartsev, D. Zigmantas, V. Sundström, W. Mammo, M. R. Andersson, O. Inganäs, *Phys. Rev. B* **2000**, *61*, 12957.
- [86] A. Haugeneder, M. Neges, C. Kallinger, W. Spirkel, U. Lemmer, J. Feldmann, U. Scherf, E. Harth, A. Gügel, K. Müllen, *Phys. Rev. B* **1999**, *59*, 15346.

- [87] B. A. Gregg, J. Sprague, M. W. Peterson, *J. Phys. Chem. B* **1997**, *101*, 5362-5369.
- [88] J. J. M. Halls, K. Pichler, R. H. Friend, S. C. Moratti, A. B. Holmes, *Appl. Phys. Lett.* **1996**, *68*, 3120-3122.
- [89] L. D. A. Siebbeles, A. Huijser, T. J. Savenije, *J. Mater. Chem.* **2009**, *19*, 6067.
- [90] Y. C. Zhou, Y. Wu, L. L. Ma, J. Zhou, X. M. Ding, X. Y. Hou, *J. Appl. Phys.* **2006**, *100*, 023712-5.
- [91] C. Breyer, M. Vogel, M. Mohr, B. Johnev, K. Fostiropoulos, *Phys. Status Solidi B* **2006**, *243*, 3176 - 318.
- [92] H. Najafov, B. Lee, Q. Zhou, L. C. Feldman, V. Podzorov, *Nat. Mater.* **2010**, *9*, 938-943.
- [93] V. Bulovic, S. R. Forrest, *Chem. Phys. Lett.* **1995**, *238*, 88-92.
- [94] D. Qin, P. Gu, R. S. Dhar, S. G. Razavipour, D. Ban, *Phys. Status Solidi A* **2011**, *208*, 1967-1971.
- [95] W. Zhang, J. Yu, W. Wen, Y. Jiang, *J. Lumin.* **2011**, *131*, 1260-1263.
- [96] J. Wünsche, S. Reineke, B. Lüssem, K. Leo, *Phys. Rev. B* **2010**, *81*, 245201.
- [97] M. Lebental, H. Choukri, S. Chenais, S. Forget, A. Siove, B. Geffroy, E. Tutis, *Phys. Rev. B* **2009**, *79*, 165318-13.
- [98] W. A. Luhman, R. J. Holmes, *Appl. Phys. Lett.* **2009**, *94*, 153304-3.
- [99] B. P. Rand, S. Schols, D. Cheyuns, H. Gommans, C. Giroto, J. Genoe, P. Heremans, J. Poortmans, *Org. Electron.* **2009**, *10*, 1015-1019.
- [100] J. E. Kroeze, T. J. Savenije, L. P. Candeias, J. M. Warman, L. D. A. Siebbeles, *Sol. Energy Mater. Sol. Cells* **2005**, *85*, 189-203.
- [101] E. B. Namdas, A. Ruseckas, I. D. W. Samuel, S.-C. Lo, P. L. Burn, *Appl. Phys. Lett.* **2005**, *86*, 091104-3.
- [102] N. Matsusue, S. Ikame, Y. Suzuki, H. Naito, *J. Appl. Phys.* **2005**, *97*, 123512-5.
- [103] M. Samiullah, D. Moghe, U. Scherf, S. Guha, *Phys. Rev. B* **2010**, *82*, 205211.
- [104] N. C. Giebink, Y. Sun, S. R. Forrest, *Org. Electron.* **2006**, *7*, 375-386.
- [105] T. Fushimi, A. Oda, H. Ohkita, S. Ito, *J. Phys. Chem. B* **2004**, *108*, 18897-18902.
- [106] C. Wu, P. I. Djurovich, M. E. Thompson, *Adv. Funct. Mater.* **2009**, *19*, 3157-3164.
- [107] M. A. Baldo, C. Adachi, S. R. Forrest, *Phys. Rev. B* **2000**, *62*, 10967.
- [108] N. C. Giebink, S. R. Forrest, *Phys. Rev. B* **2008**, *77*, 235215-9.
- [109] Y. Shao, Y. Yang, *Adv. Mater.* **2005**, *17*, 2841-2844.
- [110] J. E. Kroeze, R. B. M. Koehorst, T. J. Savenije, *Adv. Funct. Mater.* **2004**, *14*, 992-998.

Chapter 2

Exciton Quenching in Skin Layer of Spin-Coated Polymer Films

Here we report about efficient exciton quenching close to the polymer-vacuum interface of spin-coated MDMO-PPV (poly[2-methoxy-5-(2'-ethyl-hexyloxy)-*p*-phenylenevinylene]) films. The quenching efficiency is estimated to be as high as that of the polymer-fullerene interface. This efficient quenching is consistent with enhanced intermolecular interactions close to the polymer-vacuum interface due to the formation of a “skin layer” during the spin-coating procedure. In the skin layer the polymer density is higher, i.e. the intermolecular distances are shorter than in the rest of the film. The effect of exciton quenching at the polymer-vacuum interface should be taken into account when the thickness of the polymer film is of the order of the exciton diffusion length; in particular, in the determination of the exciton diffusion length.*

*O. V. Mikhnenko, F. Cordella, A. B. Sieval, J. C. Hummelen, P. W. M. Blom, M. A. Loi, *J. Phys. Chem. B* **2009**, *113*, 9104-9109.

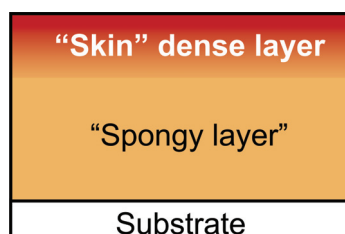


Figure 2.1: The bilayered structure of a spin-coated polymer film.

2.1 Introduction

Spin-coating or spin-casting is a thin film deposition technique from solution that is conducted by first wetting and then spinning a flat substrate. Depending on the rotation speed, the solution experiences centrifugal forces that, together with the solvent evaporation process, are responsible for the film formation. Spin-coating is a versatile deposition method that is used for various applications; for instance, to deposit photoresists or dielectric layers in microcircuit technology, to fabricate antireflection coatings for optical applications, or magnetic coatings in the data storage industry. Furthermore, spin-coating is used to deposit thin films of conjugated polymers to fabricate solar cells, field effect transistors, light-emitting diodes, etc.

Conjugated polymers show semiconducting properties and can be designed to be soluble in common organic solvents. For low-cost electronic devices, however, spin-coating is not as cost-effective as printing techniques, which are the most promising deposition methods for mass production.^[1] Nevertheless, in contrast to other techniques, spin-coating is simple, well understood,^[2,3] easy to control, and allows preparation of thin films of precise thicknesses. Therefore, it is an excellent deposition technique to investigate properties of conjugated polymers as well as to optimize devices based on them.

Over the past few decades the morphology of spin-coated polymer films has been studied extensively. It was predicted theoretically^[2,3] and shown experimentally^[4,5] that close to the polymer-vacuum interface, a "skin layer" is formed, which is characterized by a high density and in-plane ordering of molecular chains (**Figure 2.1**). The rest of the film has uniform density, which is shown to be 3 times less than the density of the skin layer in a typical conjugated polymer, such as poly[2-methoxy-5-(2'-ethyl-hexyloxy)-p-phenylenevinylene] (MEH-PPV).^[6] Because of such a density difference, the rest of the film is sometimes regarded as a "spongy layer".

The skin layer formation originates from the rapid solvent evaporation at the free surface, which leads to a local increase in the polymer concentration during spinning.

This rise in the concentration can be so abrupt that the polymer becomes almost solid close to the surface, which slows down the solvent evaporation rate from the rest of the forming film.^[3] Even when the film is fully formed, some of the solvent remains trapped below the skin layer. Usually, such solvent residuals are removed by vacuum baking. At this stage, the polymer viscosity is so high that the long chains cannot fill the space that was previously filled by the solvent residuals. Thus, a spongy layer is formed below the skin of the film.

The influence of the skin layer on the physical parameters, such as glass transition temperature^[6,7] and anisotropy of the refractive index,^[8,9] becomes apparent in relatively thin films, when the skin layer is a considerable part of the total film thickness. The relevant thickness range depends on the polymer properties, the solvent evaporation rate, and the spin conditions. In relatively thick films, the spongy layer dominates the total film volume, which results in thickness-independent film properties.

We report about the influence of the skin layer on the measurements of the exciton dynamics in conjugated polymers. In this class of materials, excitons can be considered as bound, localized electron-hole pairs. Once created, they tend to diffuse among conjugated segments by means of energy transfer. The average displacement of an exciton during its lifetime is called the exciton diffusion length. This parameter is very important in the design of organic solar cells because it determines the volume of the conjugated polymer from which excitons can reach the dissociation interface, where they can be separated into free electrons and holes to contribute to photocurrent.^[10] The measurement of the exciton diffusion length is therefore important both for the engineering of optoelectronic devices and for the fundamental knowledge about conjugated polymers.

The exciton diffusion length is often extracted from photoluminescence (PL) measurements by varying the thickness of the polymer film, which is deposited on top of an exciton quenching layer.^[10–17] When the polymer thickness is decreased to the order of the exciton diffusion length, the PL decay times in such a polymer-quencher heterostructure become shorter than those in the relatively thick films. The exciton diffusion length can then be estimated by modeling the thickness dependence of the PL decay process. The influence of the skin layer at the polymer-vacuum interface is usually neglected in such models.

Here, we study the exciton behavior in the skin layer of spin-coated MDMO-PPV films (for full name and chemical structure refer to **Figure 2.2**). We chose this soluble derivative of PPV because it has been widely used in solar cell research.^[18] For this class of materials, the exciton diffusion length is typically reported in the range of 5 – 7 nm.^[10,11,13–15,19–21] To extract the exciton diffusion length using polymer-quencher heterostructures, the polymer thickness should be varied in the range of 5 – 50 nm for MDMO-PPV. Absorption spectroscopy reveals that in this thickness range, the skin layer considerably contributes to the total film thickness and, thus, cannot be

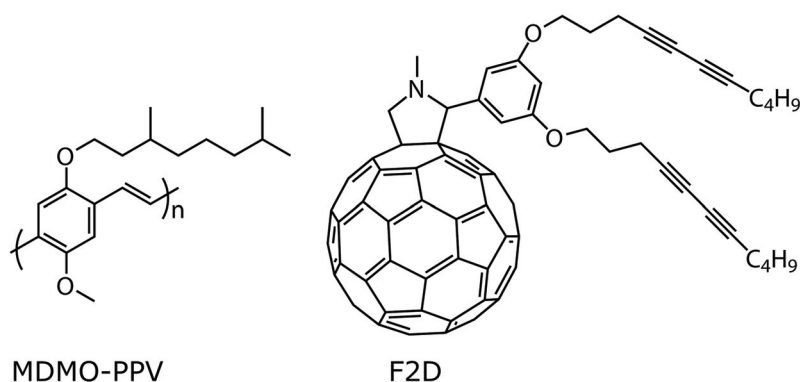


Figure 2.2: Chemical structures of poly[2-methyl-5-(3',7'-dimethyloctyloxy)-p-phenylenevinylene] (**MDMO-PPV**) and 1'-methyl-1',5'-dihydro-2'-(3,5-bis(undeca-4,6-diynyloxy)phenyl)-1*H*-pyrrolo[3',4':1,9](C₆₀-I_h)[5,6]fullerene (**F2D**).

neglected. We show that the PL decay times of the pristine MDMO-PPV films, spin-coated on quartz substrates, exhibit a thickness dependence similar to that of the polymer-quencher heterostructures. Such thickness dependence is caused by the efficient exciton quenching in the skin layer. The efficiency of this quenching can be estimated by measuring the exciton diffusion length both in the pristine films and in polymer-quencher heterostructures. The values of the exciton diffusion length, which are extracted from both kinds of samples, correspond to each other only if we assume that the exciton quenching in the skin layer is as efficient as the quenching at the polymer-fullerene interface, which is well-known for its high exciton quenching efficiency.^[10,22,23]

2.2 Thickness Dependence of the PL Decay Times

Figure 2.3 shows the PL decays of a 240-nm-thick polymer film serving as the reference sample (solid line). PL decays of 13 nm thick polymer film deposited on quartz substrate (pristine film, dotted line) and on insoluble fullerene layer of poly(F2D) (heterostructure, dashed line) are also shown. The chemical structure of F2D precursor is shown Figure 2.2. The PL decay times depend on polymer thickness for both heterostructures and pristine films, being faster for thinner samples. The dependence is monotonic and appears to be strongest in the polymer thickness range between 5 and 50 nm, whereas > 200 nm thick films are characterized by a thickness-independent PL decay. As stated above, excitons are efficiently quenched at the polymer-fullerene interface;^[10,22,23] the number of excitons that reach the interface is limited by the exciton diffusion length L_D .^[23] Consequently, for polymer thicknesses approaching L_D , the relative number of quenched excitons in the heterostructure is increased, leading to shorter PL decay times (Figure 2.3, dashed line).

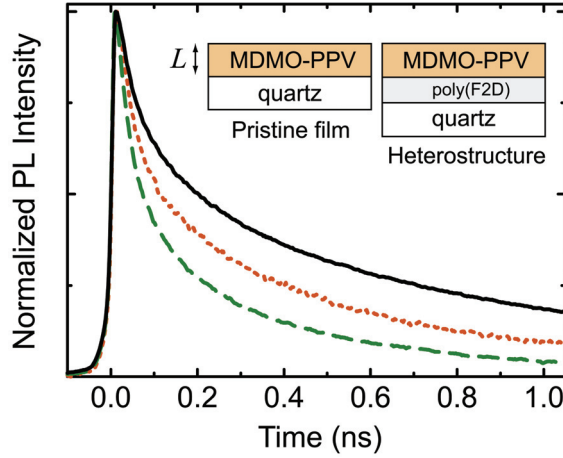


Figure 2.3: PL decays of pristine MDMO-PPV film (dotted line) and heterostructure (dashed line) of the same polymer thickness, 13 nm. The PL decay of 240-nm-thick reference pristine film is also shown (solid line). The PL decays are normalized to its maximum value. The inset shows the composition of the pristine films and the heterostructures.

The dotted line in Figure 2.3 shows that the PL decay times of pristine MDMO-PPV films depend on thickness in a manner similar to the heterostructures, being shorter for thinner films. Such thickness dependence can be ascribed to exciton quenching at one or both interfaces of the pristine polymer film. We will show that the skin layer of a spin-coated MDMO-PPV film quenches excitons with an efficiency similar to that of a polymer-fullerene interface.

To quantify the overall exciton quenching in a polymer film, we introduce the relative quenching efficiency $Q(L)$:

$$Q(L) = 1 - \frac{\text{Total PL of sample with polymer thickness } L}{\text{Total PL of thick reference sample}}, \quad (2.1)$$

where the total PL is the time integral of the PL decay normalized to its maximum value, and the reference sample is a > 200 nm thick MDMO-PPV film. The thickness dependencies of the relative quenching efficiency were measured for both pristine films and heterostructures. They are shown in **Figure 2.4** as circles and squares, respectively. In general, the overall quenching in the heterostructures was found to be more efficient than in pristine films. Hence, we can estimate that the quenching efficiency of the polymer-quartz interface is much smaller than that of the polymer-fullerene interface. On the other hand, if the exciton quenching efficiency is small or zero at the polymer-quartz interface, then the excitons should be quenched efficiently close to the polymer-vacuum interface (*i.e.* in the skin layer) to explain the pronounced thickness dependence $Q(L)$ for the pristine films (Figure 2.4).

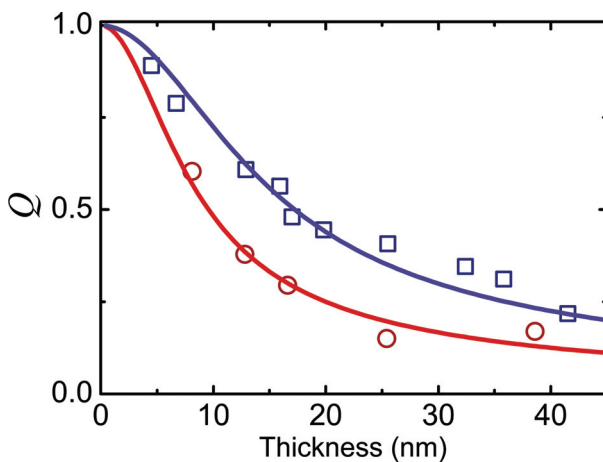


Figure 2.4: Measured relative quenching efficiency, Q , of the pristine films (circles) and the heterostructures (squares). The curves represent the best fits with Equations (2.8) and (2.7), respectively.

To independently quantify the exciton quenching at polymer-quartz interface and in the skin layer of a MDMO-PPV film, we will assume that the characteristics of the skin layer are essentially the same in the heterostructures and the pristine films.^[24,25] In the next section, we will quantify the quenching efficiency by following this hypothesis.

2.3 Measurements of Exciton Diffusion Length

The exciton diffusion length in polymer films is often measured using the diffusion-limited quenching at the interface with either fullerenes or fullerene derivatives,^[11,12,14,19–21] titania,^[13,15] or metals.^[16] The dependence of the relative quenching efficiency, Q , on the polymer thickness, L , is recorded experimentally, and it is fitted with a mathematical model based on a diffusion equation. Such a fitting results in a value of L_D typically in the range of 5 – 7 nm for PPV derivatives.^[10,11,13–15,19–21]

Here, we measure the exciton diffusion length to estimate the efficiency of the exciton quenching in the skin layer. For simplicity, we will neglect the finite thickness of the skin layer in the modeling. Then the quenching in this layer can be considered as an interface effect. Later, we will estimate the influence of a finite thickness of the skin layer on our results.

The exciton diffusion length is an intrinsic property of the conjugated polymer and should be the same in the heterostructures and the pristine films. Since in our sample geometry, the effect of interface quenching enters the diffusion model as

boundary conditions, we can estimate the efficiencies of such quenching simply by choosing the boundary conditions that lead to the proper value of L_D for both types of samples.

The exciton density, n , is modeled by the following diffusion equation:

$$\frac{\partial n(x,t)}{\partial t} = D \frac{\partial^2 n(x,t)}{\partial x^2} - \frac{n(x,t)}{\tau} + G(x,t) - S(x)n(x,t), \quad (2.2)$$

where τ denotes the exciton lifetime and D is the exciton diffusion coefficient that is related to the diffusion length by the equation $L_D = \sqrt{\tau D}$. Due to the sample symmetry, n depends only on one spatial coordinate x , which is the distance from the free interface. Because ultrafast photo excitation has been used, the generation term $G(x,t)$ can be represented as the initial exciton distribution, which is taken to be uniform due to the low absorption coefficient at the excitation wavelength.

The term $S(x)$ in Equation (2.2) denotes the interface quenching; it can be adjusted to mimic different boundary conditions. The polymer-vacuum interfaces of the heterostructures and the pristine films are assumed to be equal, implying common boundary conditions at this interface for both sorts of samples. As we noted in the previous section, the quenching efficiency of the polymer-vacuum interface is expected to be high. In our modeling, we assume it to be 100% efficient:

$$n(0,t) = 0. \quad (2.3)$$

The polymer-fullerene interface is known to be an efficient exciton quencher, which provides the second boundary condition for the heterostructures with polymer thickness L :

$$n(L,t) = 0. \quad (2.4)$$

The polymer-quartz interface is expected to be a weak exciton quencher; therefore, here, we assume that its quenching efficiency is negligible:

$$\frac{\partial n(L,t)}{\partial x} = 0. \quad (2.5)$$

With these boundary conditions, Equation (2.2) can be simplified to Cauchy problems and solved analytically for both types of samples. Then the relative quenching efficiency Q is simply

$$Q(L, L_D) = 1 - \frac{\int_0^L dx \int_0^\infty n_{quenched\ sample}(x,t) dt}{LN_0\tau}, \quad (2.6)$$

where $LN_0\tau$ is the total PL of a quencher free sample. Integration of Equation (2.6) leads to the analytical expressions Q_2 and Q_1 for the heterostructures and the pristine films, respectively:

$$Q_2(L, L_D) = \frac{2L_D}{L} \operatorname{Tanh} \frac{L}{2L_D}, \quad (2.7)$$

$$Q_1(L, L_D) = \frac{L_D}{L} \operatorname{Tanh} \frac{L}{L_D}. \quad (2.8)$$

Here, the exciton diffusion length, L_D , is the only fitting parameter, and the index near Q denotes the number of quenching interfaces.

The fitting of the experimental data for the heterostructures and the pristine films by Equations (2.7) and (2.8) is illustrated in Figure 2.4. The resulting values of the exciton diffusion length are 4.5 and 5 nm, respectively. These values are similar and were extracted from two different series of samples under the common assumption that the polymer-vacuum interface efficiently quenches excitons. It is important to note that the extracted values of the exciton diffusion length correspond to the one of the spongy layer.

These values would diverge when the boundary condition at the polymer-vacuum interface would be varied to reduce the quenching efficiency. In the limiting case, when the quenching efficiency of the polymer-vacuum interface approaches zero, the extracted exciton diffusion length from the heterostructures would be close to 9 nm, whereas that from the pristine films will virtually approach infinity. Thus, we can conclude that our assumption of efficient exciton quenching at the polymer-vacuum interface is correct because it leads to the similar values of the exciton diffusion length, extracted from either kind of sample.

2.4 Skin Layer in Spin-Coated Films

The theoretical prediction^[2,3] of a dense skin layer close to the free interface (Figure 2.1) was followed by the experimental confirmation of a bilayered film structure. On the basis of neutron reflection experiments on spin-coated MEH-PPV films, Webster *et al.*^[5] concluded that such films are composed of two well-defined and uniform layers of different densities. They reported a density ratio as high as 3 between a 24 nm, thin, dense layer and a 136 nm, thick, “spongy” layer. Lu and coauthors^[4] discovered the bilayered structure of spin-coated polyacrylamide films by reflection-absorption Fourier transform infrared spectroscopy. The molecules in the part of the layer closest to the substrate were found to be randomly oriented, whereas the skin layer showed spin-coating-induced in-plane chain orientation.^[4,8,26,27] Moreover, the idea of a bilayered structure of spin-coated films is also often used to explain the thickness dependence of the glass transition temperature in conjugated polymers.^[6,7] Here, we report spectroscopic evidence of the bilayered structure of a thin polymer film, which confirms the exciton quenching effect in the skin layer.

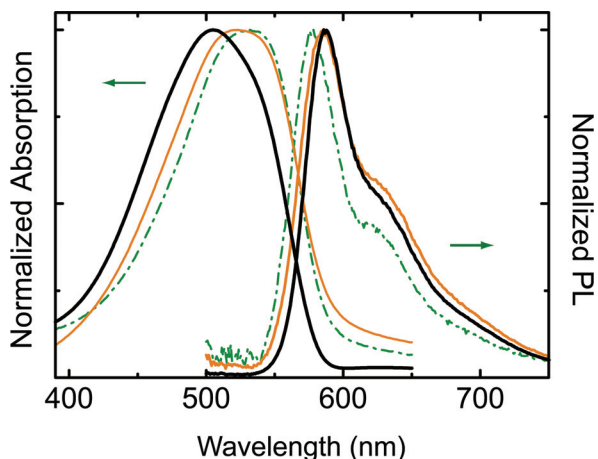


Figure 2.5: Normalized absorption and normalized photoluminescence spectra of polymer films with thicknesses 240 nm (solid, thick line), 42 nm (solid, thin line) and 7 nm (dashed-dotted line). The spectra are normalized to their maximum values.

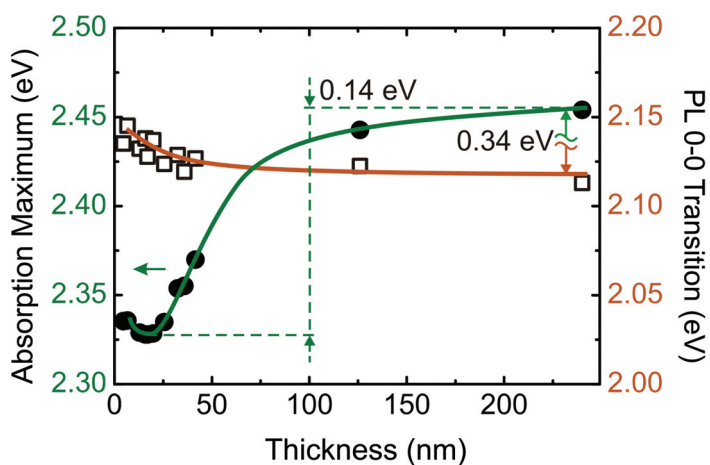


Figure 2.6: Measured thickness dependencies of the maximum position of the absorption spectrum (circles) and 0-0 PL transition (squares). The solid lines are shown as guides for eyes.

The absorption spectra of MDMO-PPV films of several polymer thicknesses are shown in **Figure 2.5**. It is important to note that the absorption spectra are equal for heterostructures and pristine films of the same polymer thickness. **Figure 2.6** displays the variation of the energy maximum of the absorption spectrum for films of different thicknesses. The absorption maximum shifts by 0.14 eV toward lower energies, when going from >200 nm to ~ 15 nm thickness. A further thickness decrease leads to the opposite trend; that is, to a blue shift. This thickness

dependence is relatively strong. For comparison, the Stokes shift for the 240 nm thick MDMO-PPV film is 0.34 eV (Figure 2.6), and the typical value for the half-width of the Gaussian excitonic density of states^[28] is ~ 0.1 eV.

The thickness dependence of the absorption spectrum can be explained in terms of the bilayered structure of spin-coated polymer films. As mentioned previously, the spin-coating procedure induces in-plane chain orientation in the skin layer of the film,^[4,8,26,27] whereas the polymer chains adopt random conformations in the spongy layer (Figure 2.1). Consequently, the skin layer is characterized by polymer chains with longer average conjugation length and by the red-shifted absorption,^[29] as compared to the spongy one. In > 200 nm thick films, the absorption spectrum is dominated by the spongy layer, whereas in thinner films, the skin layer becomes more important, leading to the red shift (Figure 2.6). For ultrathin films with thicknesses below 15 nm, the influence of the substrate dominates over the spin-coating-induced effects, resulting in the blue shift upon further thickness decrease.

One would expect that the exciton migration process is anisotropic at the interface between the two layers of the spin-coated polymer film. Indeed, due to the different degrees of ordering, a gradient of the conjugation length is formed between such layers. Since the excitons tend to migrate toward longer conjugated segments, one rather would expect a drift directed to the better-ordered skin layer than an isotropic diffusion process. Such a drift depletes the exciton population in the spongy layer and increases it in the skin layer. Since the density of states is considerably shifted toward lower energy in the skin layer, one would expect that any PL from the skin layer would be red-shifted. This would apply to samples in the thickness range of 5 – 50 nm.

Figure 2.5 shows the steady state PL spectra that correspond to the polymer films of thicknesses 7, 42, and 240 nm. Figure 2.6 summarizes the thickness dependence of the maximum position of the PL 0-0 transition. The dependence is weaker than that of the absorption spectrum; moreover, we can resolve a monotonic shift to higher energy with a thickness decrease in the range of 5 – 50 nm. It is important to note that we did not find substantial differences in the peak positions of the PL spectra between heterostructures and the corresponding pristine films.

We attribute the absence of the expected red shift of the PL spectrum to the exciton quenching in the skin layer of the spin-coated film. The observed photoluminescence is mostly coming from the spongy layer, which is not influenced by the spin-coating procedure, and thus, its degree of ordering does not depend on the sample thickness. In the thickness range of 5 – 20 nm, most of the excitons reach a quenching interface; thus, the observed photoluminescence is originated at the early stages of the exciton diffusion. During roughly the first 100 ps after the laser pulse, excitons undergo a thermalization process; that is, a downhill migration toward lower energy sites.^[30] The photons emitted during this process are blue-shifted as compared to the emission of thermalized excitons. In sufficiently thin films, excitons get

quenched before the completion of thermalization. Therefore, we observe a slight blue shift for films with thicknesses close to the exciton diffusion length (Figure 2.6).

One of the physical phenomena responsible for the exciton quenching in the skin dense layer can be the interchain coupling that leads to formation of nonradiative dark states. Ruini *et al.*^[31] performed *ab initio* calculations of PL intensity and real space exciton wave function for both PPV crystal and an isolated chain, showing that in the crystal, the lowest electronic excitation is an optically inactive exciton. They also noted that the PL efficiency would strongly depend on the local polymer density, being lower for more densely packed chains. Nguyen *et al.*,^[32] using scanning near-field optical microscopy, showed experimentally that the PL intensity is weaker from the denser clusters of an inhomogeneous MEH-PPV film. The concept of exciton quenching due to interchain interactions is supported by numerous reports on decrease of the PL quantum yield under application of hydrostatic pressure in various organic materials.^[33–35]

Our measurements show that the PL is quenched with high efficiency in the skin layer. Such a high quenching efficiency reflects the high number of excitons that decay nonradiatively close to the polymer-vacuum interface. It is energetically favorable for excitons to migrate into the region of higher density, which is characterized by longer average conjugation length. Since the film density increases when going from the spongy layer to the skin layer, excitons would rather drift into the latter than anisotropically diffuse between the layers. In this way, the exciton concentration increases in the skin dense layer, where the probability of nonradiative decay is high.^[31–35] As a result, the number of excitons that decay nonradiatively increases, and finally, the exciton quenching within the skin layer can be approximated as the 100% efficient quenching at the polymer-vacuum interface.

It is important to note that in the bilayered spin-coated film, the conformations of the polymer chains in the vicinity of the free surface are decoupled from the substrate and are fully determined by the spin-coating conditions. The detailed surface analyses of spin-coated poly(3-hexylthiophene) films by ultraviolet photoelectron spectroscopy, Penning ionization electron spectroscopy,^[25] and X-ray absorption fine structure spectroscopy^[24,25] show that the polymer chain conformation at the surface does not change upon thickness variation, obtained by changing the polymer concentration and keeping the spin speed constant. This supports our assumption that the skin layer is essentially the same for both the heterostructure and the pristine film of corresponding thickness.

Finally, we address the neglect of the skin layer thickness in our modeling of the relative quenching efficiency. Every exciton that passes from the spongy to the dense layer does not diffuse back due to the energy gradient, but subsequently decays nonradiatively due to the effect of enhanced density.^[31–35] The interface between the dense and the spongy layers is reported to be relatively sharp.^[5] Thus, this interface, not that of the polymer-vacuum, should be considered as the exciton quenching wall

in our modeling. Consequently, we should use the thickness of the spongy layer instead of the overall film thickness, L , in the modeling.

Although we had no opportunity to reliably estimate the thicknesses of the skin and spongy layers, the obtained results of the exciton diffusion length still allow us to draw our main conclusion. Suppose the thickness of the skin layer is about 10% of the overall film thickness, L . Then the thickness of the spongy layer is $0.9L$, which should be put into the modeling as a sample thickness. Since the relative quenching efficiencies (Equations 2.7 and 2.8) depend on the ratio L/L_D , the resulting values of the exciton diffusion length would be smaller than the obtained ones with a factor of 0.9 for both the heterostructures and the pristine films. This means that neglecting the skin layer thickness affects the *absolute values* of the measured exciton diffusion length, but not the *ratio* between them. Thus, we can still compare those values and conclude that the skin layer efficiently quenches excitons.

2.5 Conclusions

We showed that in the skin layer of spin-coated MDMO-PPV film excitons are quenched with high efficiency, comparable to that of a polymer-fullerene interface. One of the physical phenomena responsible for such a quenching is the formation of nonradiative states close to the polymer-vacuum interface due to higher polymer density. This effect should be taken into account for films in the thickness range of 5 – 50 nm, in particular when the exciton population is measured or estimated.

2.6 Methods

MDMO-PPV was spin-coated from chlorobenzene on top of clean quartz substrates and insoluble^[14] cross-linked fullerene films – poly(F2D) – to form the pristine films and heterostructures, respectively (inset to Figure 2.3). The spin speed of 2000 rpm was kept constant for all the samples, and the polymer thickness variation was ensured by changing the solution concentration. The sample preparation was done under nitrogen atmosphere.

The surfaces of the quartz substrates, of poly(F2D), and of MDMO-PPV were characterized by atomic force microscopy (AFM). The root-mean-square roughness was found to be <1 nm for all the surfaces on an area of $100 \mu\text{m}^2$. The thicknesses of organic layers were measured by AFM and nulling-zone ellipsometry. The thickness of poly(F2D) was kept to < 30 nm in all the heterostructures.

PL decays, continuous wave (cw) absorption, and PL spectra were measured for every sample. Time-resolved measurements were performed, exciting the samples with 100 fs laser pulses, produced by a Ti - sapphire laser and frequency-doubled at about 400 nm; the PL decays were recorded by a Hamamatsu streak camera. The

initial exciton density was estimated to be $\sim 10^{13} - 10^{14} \text{ cm}^{-3}$, being several orders of magnitude less than needed for exciton-exciton annihilation.^[36] The cw PL spectra were measured using a Hamamatsu CCD, and the absorption spectra were obtained with a Perkin-Elmer spectrometer. The samples were kept in a dynamic vacuum of $10^{-6} - 10^{-5}$ mbar during the photoluminescence measurements, and no degradation was observed. For the absorption measurements, the samples were sealed in a chamber under nitrogen atmosphere. For analysis, the decays were spectrally integrated and normalized to the maximum value. It was verified that optical interference and self-absorption effects can be safely ignored in the thickness range studied here.

2.7 References

- [1] C. J. Brabec, J. R. Durrant, *MRS Bull.* **2008**, *33*, 670.
- [2] C. J. Lawrence, *Phys. Fluids* **1988**, *31*, 2786.
- [3] D. E. Bornside, C. W. Macosko, L. E. Scriven, *J. Appl. Phys.* **1989**, *66*, 5185-5193.
- [4] X. Lu, I. Cheng, Y. Mi, *Polymer* **2007**, *48*, 682-686.
- [5] G. R. Webster, W. J. Mitchell, P. L. Burn, R. K. Thomas, G. Fragneto, J. P. J. Markham, I. D. W. Samuel, *J. Appl. Phys.* **2002**, *91*, 9066-9071.
- [6] M. Campoy-Quiles, M. Sims, P. G. Etchegoin, D. D. C. Bradley, *Macromolecules* **2006**, *39*, 7673-7680.
- [7] J. A. Forrest, K. Dalnoki-Veress, J. R. Stevens, J. R. Dutcher, *Phys. Rev. Lett.* **1996**, *77*, 2002.
- [8] M. Campoy-Quiles, P. G. Etchegoin, D. D. C. Bradley, *Phys. Rev. B* **2005**, *72*, 045209-16.
- [9] J. Sturm, S. Tasch, A. Niko, G. Leising, E. Toussaere, J. Zyss, T. C. Kowalczyk, K. D. Singer, U. Scherf, J. Huber, *Thin Solid Films* **1997**, *298*, 138-142.
- [10] P. Peumans, A. Yakimov, S. R. Forrest, *J. Appl. Phys.* **2003**, *93*, 3693-3723.
- [11] J. J. M. Halls, K. Pichler, R. H. Friend, S. C. Moratti, A. B. Holmes, *Appl. Phys. Lett.* **1996**, *68*, 3120-3122.
- [12] A. Haugeneder, M. Neges, C. Kallinger, W. Spirkl, U. Lemmer, J. Feldmann, U. Scherf, E. Harth, A. Gügel, K. Müllen, *Phys. Rev. B* **1999**, *59*, 15346.
- [13] J. E. Kroeze, T. J. Savenije, M. J. W. Vermeulen, J. M. Warman, *J. Phys. Chem. B* **2003**, *107*, 7696-7705.
- [14] D. E. Markov, E. Amsterdam, P. W. M. Blom, A. B. Sieval, J. C. Hummelen, *J. Phys. Chem. A* **2005**, *109*, 5266-5274.
- [15] S. R. Scully, M. D. McGehee, *J. Appl. Phys.* **2006**, *100*, 034907-5.
- [16] Y. Wu, Y. C. Zhou, H. R. Wu, Y. Q. Zhan, J. Zhou, S. T. Zhang, J. M. Zhao, Z. J. Wang, X. M. Ding, X. Y. Hou, *Appl. Phys. Lett.* **2005**, *87*, 044104-3.
- [17] Y. C. Zhou, Y. Wu, L. L. Ma, J. Zhou, X. M. Ding, X. Y. Hou, *J. Appl. Phys.* **2006**, *100*, 023712-5.
- [18] S. E. Shaheen, C. J. Brabec, N. S. Sariciftci, F. Padinger, T. Fromherz, J. C. Hummelen, *Appl. Phys. Lett.* **2001**, *78*, 841-843.
- [19] M. Theander, A. Yartsev, D. Zigmantas, V. Sundström, W. Mammo, M. R. Andersson, O. Inganäs, *Phys. Rev. B* **2000**, *61*, 12957.
- [20] D. E. Markov, J. C. Hummelen, P. W. M. Blom, A. B. Sieval, *Phys. Rev. B* **2005**, *72*, 045216-5.
- [21] D. E. Markov, C. Tanase, P. W. M. Blom, J. Wildeman, *Phys. Rev. B* **2005**, *72*, 045217-6.
- [22] L. W. Barbour, R. D. Pensack, M. Hegadorn, S. Arzhantsev, J. B. Asbury, *J. Phys. Chem. C* **2008**, *112*, 3926-3934.
- [23] C. J. Brabec, G. Zerza, G. Cerullo, S. De Silvestri, S. Luzzati, J. C. Hummelen, S. Sariciftci, *Chem. Phys. Lett.* **2001**, *340*, 232-236.
- [24] D. M. DeLongchamp, B. M. Vogel, Y. Jung, M. C. Gurau, C. A. Richter, O. A. Kirillov, J. Obrzut, D. A. Fischer, S. Sambasivan, L. J. Richter, E. K. Lin, *Chem. Mater.* **2005**, *17*, 5610-5612.

-
- [25] X. T. Hao, T. Hosokai, N. Mitsuo, S. Kera, K. K. Okudaira, K. Mase, N. Ueno, *J. Phys. Chem. B* **2007**, *111*, 10365-10372.
- [26] N. C. Ramsdale, Greenham C. M., *Adv. Mater.* **2002**, *14*, 212-215.
- [27] A. Boudrioua, P. A. Hobson, B. Matterson, I. D. W. Samuel, W. L. Barnes, *Synth. Met.* **2000**, *111-112*, 545-547.
- [28] R. Kersting, B. Mollay, M. Rusch, J. Wenisch, G. Leising, H. F. Kauffmann, *J. Chem. Phys.* **1997**, *106*, 2850-2864.
- [29] H. S. Woo, O. Lhost, S. C. Graham, D. D. C. Bradley, R. H. Friend, C. Quattrocchi, J. L. Brédas, R. Schenk, K. Müllen, *Synth. Met.* **1993**, *59*, 13-28.
- [30] O. V. Mikhnenko, F. Cordella, A. B. Sieval, J. C. Hummelen, P. W. M. Blom, M. A. Loi, *J. Phys. Chem. B* **2008**, *112*, 11601-11604.
- [31] A. Ruini, M. J. Caldas, G. Bussi, E. Molinari, *Phys. Rev. Lett.* **2002**, *88*, 206403.
- [32] T.-Q. Nguyen, B. J. Schwartz, R. D. Schaller, J. C. Johnson, L. F. Lee, L. H. Haber, R. J. Saykally, *J. Phys. Chem. B* **2001**, *105*, 5153-5160.
- [33] R. K. Tikhoplav, B. C. Hess, *Synth. Met.* **1999**, *101*, 236-237.
- [34] B. C. Hess, G. S. Kanner, Z. Vardeny, *Phys. Rev. B* **1993**, *47*, 1407.
- [35] M. A. Loi, A. Mura, G. Bongiovanni, Q. Cai, C. Martin, H. R. Chandrasekhar, M. Chandrasekhar, W. Graupner, F. Garnier, *Phys. Rev. Lett.* **2001**, *86*, 732.
- [36] A. J. Lewis, A. Ruseckas, O. P. M. Gaudin, G. R. Webster, P. L. Burn, I. D. W. Samuel, *Org. Electron.* **2006**, *7*, 452-456.

Chapter 3

Exciton Diffusion Length in Narrow Band Gap Polymers

We developed a new method to accurately extract the exciton diffusion length in organic semiconductors by blending them with a low concentration of methanofullerene[6,6]-phenyl C₆₁ butyric acid methyl ester (PCBM). The dependence of photoluminescence (PL) decay time on the fullerene concentration provides information on both exciton diffusion and the nanocomposition of the blend. Experimentally measured PL decays of blends based on two narrow band gap dithiophene-benzothiadizole polymers were modeled using a Monte Carlo simulation of 3D exciton diffusion in the blend. The extracted exciton diffusion length is 10.5±1 nm in both narrow band gap polymers, being considerably longer than the 5.4±0.7 nm that was measured with the same method in the model compound poly(3-hexylthiophene) as a reference. Our approach is simple, fast and allows to systematically measure and compare exciton diffusion length in a large number of compounds.*

*O. V. Mikhnenko, H. Azimi, M. Scharber, M. Morana, P.W.M. Blom, M. A. Loi, *Submitted for publication*

3.1 Introduction

Various techniques to measure the exciton diffusion length have been reported in the literature. The most popular method is the fluorescence quenching in thin films of organic semiconductors, in which one or both interfaces act as exciton quenching wall.^[1–10] In this approach the dependence of the exciton quenching efficiency on the semiconductor thickness is measured and modeled with 1D diffusion equation to extract the diffusion length. This is a direct measurement, however it is rather difficult to apply due to many experimental requirements and difficulties in modeling. A sharp boundary is necessary between the semiconductor and the quenching wall.^[3] The variation of the exciton density due to optical interference and absorption,^[5,11,12] the effect of the polymer-vacuum interface^[13] and Förster energy transfer^[5,10,14] should be carefully evaluated and taken into account in the modeling. Finally, high precision thickness measurements are needed to accurately determine the exciton diffusion length. Other measurement approaches include exciton density modulation due to light absorption;^[14–18] exciton-exciton annihilation;^[12,19,20] photocurrent modeling in solar cells^[21–23] and microwave conductivity.^[24] These methods have their advantages and also limitations that are related to the difficulties in sample preparation and/or sophisticated measurement technique, complicated modeling with many fitting parameters, etc.

Fluorescence quenching in thin films with randomly distributed quenchers is an interesting approach to measure the exciton diffusion length^[1,25–27] If the concentration of quencher sites is well controlled then the comparison of the photoluminescence (PL) decay of the blend with that of pristine semiconductor gives the value of the exciton diffusion length. On the experimental side, the sample preparation is very simple as well as the measurement of PL decays. However, the analytical model is rather tedious and can be applied only within certain limitations.^[1,26–28] Furthermore the knowledge about the nanocomposition of the blend is required for accurate measurements. Quenching molecules can form phase separated domains, leading to the reduction of the quenching efficiency and underestimation of the exciton diffusion length.

Here we developed a simple method to verify if quencher molecules are intimately mixed or form clusters in the blends with conjugated polymers and accurately evaluate the exciton diffusion length. The method is based on a Monte Carlo simulation that models PL decays in semiconductor-quencher mixtures. As interesting testing materials we have chosen PCPDTBT:PCBM blends (for full names and chemical structures refer to Figure 3.1). We measured for the first time the 3D exciton diffusion length of 10.6 ± 0.6 nm in PCPDTBT that is considerably longer than 5.4 ± 0.7 nm in P3HT. As an additional example we measured exciton diffusion length in other narrow band gap polymer – Si-PCPDTBT – with identical chemical structure to PCPDTBT, except for the substitution of the methylene bridge by the silylene

bridge. Interestingly, the resulting value of the exciton diffusion length is the same as for PCPDTBT. Our methodology has numerous advantages compared to other approaches, including simple sample preparation and easy experimental measurements, which allow to systematically study exciton diffusion length in a large number of materials.

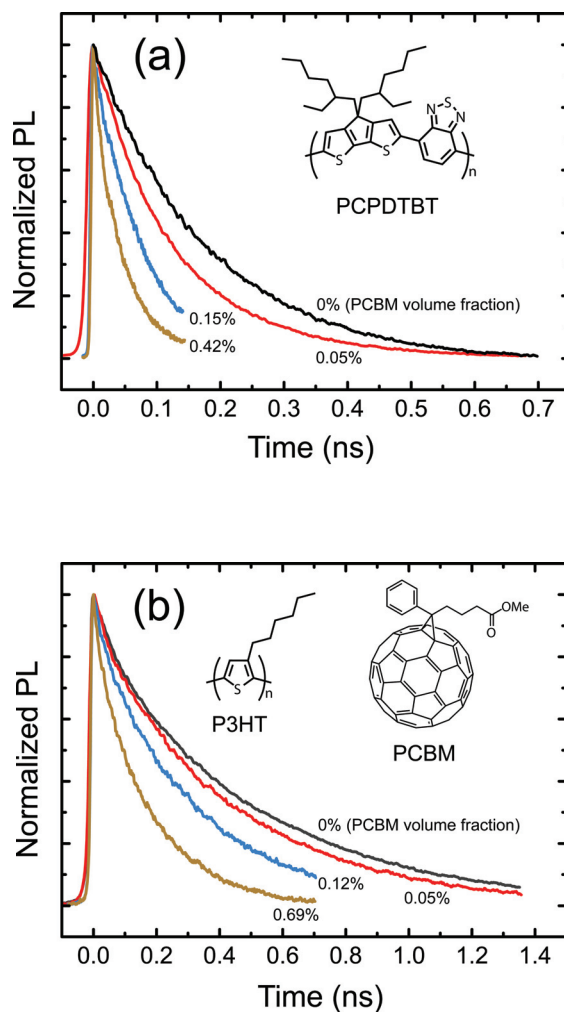


Figure 3.1: Measured photoluminescence decays in blends of PCPDTBT (a) or P3HT (b) with PCBM of various volume fractions. The data were normalized to the value at time zero. The insets show the chemical structures of poly[2,6-(4,4-bis-(2-ethylhexyl)-4H-cyclopenta[2,1-b;3,4-b']dithiophene)-*alt*-4,7-(2,1,3-benzothiadiazole)] (PCPDTBT), poly(3-hexylthiophene) (P3HT) and methanofullerene[6,6]-phenyl C₆₁ butyric acid methyl ester (PCBM).

3.2 Modeling Photoluminescence Decays

Figure 3.1 shows photoluminescence decays of polymer:PCBM blends of various PCBM volume fractions. Higher content of PCBM results in shorter PL decay times for both polymers PCPDTBT (Figure 3.1a) and P3HT (Figure 3.1b). The reduction of the PL decay time is a result of the diffusion limited exciton quenching at the polymer-PCBM interface. Considerable quenching is observed when the average distance between PCBM molecules is comparable to – or smaller than – the exciton diffusion length in the polymer phase. In this case the measured PL decay time represents the average diffusion time to quenchers, rather than the natural decay time.

The PL decay time strongly depends on the nanocomposition of the polymer:PCBM blends. For a certain volume fraction of PCBM, the largest quenching surface – consequently the shortest PL decay time – is achieved when PCBM molecules intimately mix with the polymer matrix and form a homogeneous spatial distribution. If the quencher molecules cluster together in phase separated domains, then the PL decay will show a slower dynamics due to the reduction of the quenching surface. To model exciton diffusion in the polymer:PCBM blends it is therefore very important to be aware of the nanocomposition in the blend.

We developed a Monte Carlo simulation of 3D exciton diffusion in a medium with morphology of arbitrary complexity, including intimate mixture and clustered quencher distribution. Non-interacting excitons undergo a random walk in this medium and decay non-radiatively when they contact a quenching site during their lifetime. The inputs of the simulation are the sample morphology, the natural PL decay time and the only fitting parameter is the exciton diffusion length. As output we get a PL decay that is the number of radiatively decayed excitons versus time. The simulation is repeated with the adjusted fitting parameter until the modeled and experimental data converge, resulting in the value of exciton diffusion length.

A cubic simulation box with the edge length of 50 nm and periodic boundary conditions is considered to be a continuous medium of polymer phase, in which PCBM quenchers are placed. PCBM molecules are approximated as balls of 1 nm in diameter. Two types of morphologies have been considered, intimate mixture and phase separated PCBM clusters of certain size. Intimate mixture is modeled by randomly placing PCBM molecules to the simulation box. A cluster of N molecules is modeled by a center molecule with $N-1$ nearest neighbors in the triclinic crystal structure of PCBM.^[29] The overlapping configurations are not accepted when randomly placing a new quencher or cluster to the box. A Boolean 3D grid of 0.05 nm pinch size is superimposed with the simulation box. Each 3D cell of the grid is given the value *true* or *false* if it overlaps or not with a PCBM molecule. Excitons are described as balls of 1 nm diameter in our Monte Carlo simulation. Since they interact only with quenchers, we can simplify the exciton representation to point particles by

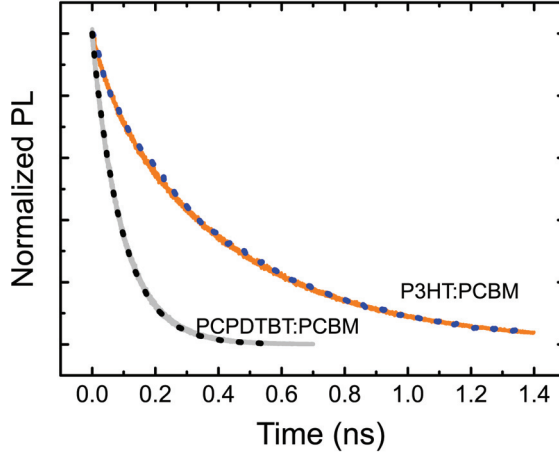


Figure 3.2: Fitting of experimentally measured PL decays (dotted lines) of polymer:PCBM blends with Monte Carlo simulation (solid lines). The volume fraction of PCBM was 0.05% in both blends. Data were normalized to their maximum value at time zero.

increasing the quencher size by the exciton radius. The spatial coordinates of the excitons are not restricted to the Boolean grid nodes.

At room temperature exciton hopping in conjugated polymers can be described by normal diffusion:^[8,30,31]

$$\frac{\partial n}{\partial t} = D \nabla^2 n - \frac{n}{\tau}, \quad (3.1)$$

where n is the exciton density, D is the diffusion coefficient, τ is the PL decay time in a pristine polymer film. According to the Einstein's theory of random walks normal diffusion can be modeled as a random walk with constant step size.^[6,32–35] Each time iteration δt every exciton is moved in a random 3D direction for a fixed distance δs , which is related to the diffusion coefficient D by a relationship:

$$D = \frac{\delta s^2}{6 \delta t}. \quad (3.2)$$

The time interval δt is chosen such that δs is several times smaller than the typical quencher size. The exciton diffusion length L_D is then given by the following expression:

$$L_D = \sqrt{3D\tau}. \quad (3.3)$$

The exciton is considered to be quenched if its new position overlaps with a grid cell, the value of which is *true*. Radiative recombination is assumed if an exciton has not been quenched after time Δt_i , which had been fixed at the beginning of the simulation by:

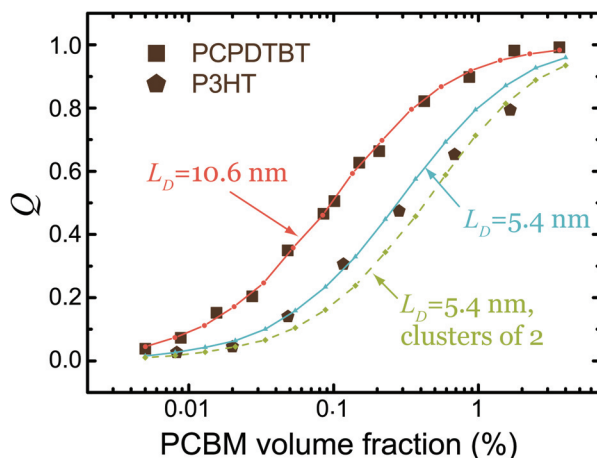


Figure 3.3: Measured dependencies of relative quenching efficiency versus volume fraction of PCBM in blends with PCPDPTBT (squares) and P3HT (pentagons). Curves represent modeled data for intimate mixture between polymer and PCBM (solid lines) and phase separated morphology of two PCBM molecules per cluster (dashed line).

$$\Delta t_i = -\tau \ln(w_i), \quad (3.4)$$

where w_i is a random number between 0 and 1.

Figure 3.2 illustrates the measured PL decays (dotted lines) of P3HT:PCBM and PCPDPTBT:PCBM blends with PCBM volume fraction of 0.05%. The PL decays, which were modeled with the Monte Carlo simulation, are depicted as solid lines. Our model fits the experimental data remarkably well and results in the values of the exciton diffusion coefficient of 2.2×10^{-4} and 27×10^{-4} cm²/s that correspond to the diffusion length of 5.5 and 10.8 nm in P3HT and PCPDPTBT, respectively. “intimate mixture” blend morphology was assumed when modeling these PL decays; we will verify this assumption below. PL decays of blends with other volume fractions were also modeled resulting in average values of exciton diffusion coefficients and lengths of $(2.2 \pm 0.3) \times 10^{-4}$ cm²/s and 5.4 ± 0.7 nm in P3HT; $(26 \pm 3) \times 10^{-4}$ cm²/s and 10.6 ± 0.6 nm in PCPDPTBT, respectively. The error is the standard deviation in the mean value.

3.3 Checking for PCBM Aggregation

PL decay times of samples of various PCBM fractions can be compared using the relative quenching efficiency Q that is defined as:

$$Q = 1 - \frac{\int PL_{blend} dt}{\int PL_{pristine} dt}, \quad (3.5)$$

where PL_{blend} and $PL_{pristine}$ are normalized to the value at time zero PL decays of a polymer:PCBM blend and pristine polymer, respectively. Nearly zero values of Q indicate that the exciton quenching is insignificant, which is typical for low concentrations of quenching molecules. At high PCBM concentrations most of the excitons are quenched, resulting in a short PL decay time and a close to unity values of Q .

The measured relative quenching efficiencies versus PCBM volume fraction are shown in **Figure 3.3** for PCPDTBT (squares) and P3HT (pentagons); the lines are modeled using the Monte Carlo simulation. Solid lines are for the intimate polymer:PCBM mixtures, while the dashed line represents the phase separated morphology with two PCBM molecules per cluster. The exciton diffusion length was set to the previously extracted values of 10.6 and 5.4 nm for PCPDTBT and P3HT respectively. The measured data for PCPDTBT is excellently described by the simulated curve in all the studied range of PCBM volume fractions. While the modeled curve of P3HT follows the experimental data points only up to a PCBM volume fraction of 0.3%; deviation from the measured values is observed for samples of higher PCBM content.

The deviation between modeled curve and experimental data points in Figure 3.3 can be explained by the cluster formation in the P3HT-PCBM blends. It is reasonable to assume that the formation of clusters during the solvent evaporation is more likely in blends of higher PCBM fractions. An increase of the cluster size results in the reduction of the interfacial area between polymer and PCBM. Consequently the relative quenching efficiency is smaller in the phase separated sample as compared to the intimately mixed blends of the same PCBM fraction. Indeed, the experimental data for volume fraction of 0.8% and higher is much better described by the simulation, in which PCBM molecules are set to form clusters of two molecules (dashed line in Figure 3.3).

Contrary, the MC simulation accurately describes the experimentally acquired data in PCPDTBT:PCBM blends assuming the formation of the intimate mixture (Figure 3.3). Therefore we conclude that PCBM molecules do not form clusters in the studied concentration range. Formation of clusters would be indicated by the deviation between the modeled and experimental dependencies at higher PCBM concentrations.

Regio-regular P3HT is known to form polycrystalline domains.^[36] Therefore it is not surprising that PCBM tend to phase separate in the blends. PCPDTBT does not form crystalline domains if processed without additives,^[37-41] which is in accordance with the intimate mixture morphology deduced in this work. The exciton diffusion length in P3HT has been previously reported in the range of 3 and 8.5 nm.^[7,12,24,27] Our measurements result in 5.4 nm, which is in agreement with the literature and further confirms the validity of our method. The fact that the exciton diffusion length

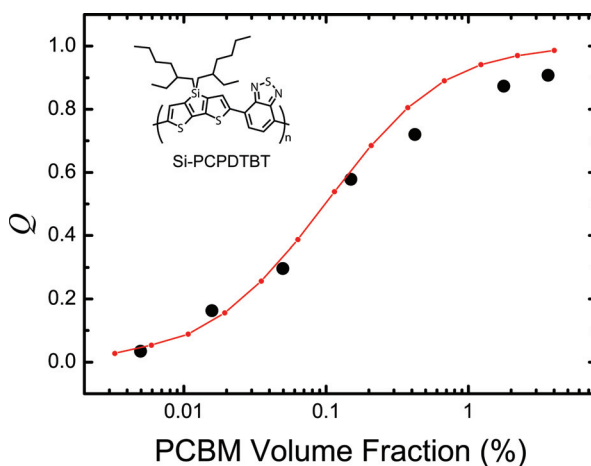


Figure 3.4: Measured (circles) relative quenching efficiency versus PCBM volume fraction in poly[(4,4'-bis(2-ethylhexyl)dithieno[3,2-*b*:2',3'-*d*]silole)-2,6-diyl-*alt*-(2,1,3-benzothiadiazole)-4,7-diyl] (**Si-PCPDTBT**). The curve is the fitting of the measured data with the Monte Carlo simulation assuming the intimate mixture morphology of Si-PCPDTBT:PCBM blends. The inset shows the chemical structure of Si-PCPDTBT.

of 10.6 nm in PCPDTBT is longer than that in P₃HT is consistent with the superior solar cell performance of the former material.^[37,42]

3.4 Exciton Diffusion in Si-PCPDTBT

The developed methodology for measuring exciton diffusion length can be easily applied to various materials. As an additional example we investigated another narrow band gap material, namely Si-PCPDTBT, for full name and chemical structure refer to **Figure 3.4**. The chemical structure of this polymer is identical to PCPDTBT, except the substitution of the methylene bridge by a silylene bridge (see Figures 3.4 and 3.1a). Si-PCPDTBT is a promising material for applications in solar cells as it does not require processing additives or post annealing steps in order to reach power conversion efficiency above 5%.^[40]

Figure 3.4 shows the dependence of the measured relative quenching efficiency on the PCBM volume fraction in Si-PCPDTBT:PCBM blends (circles). The fitting of the PL decays of the blends with PCBM volume fraction below 0.3% using the Monte Carlo simulation results in the average exciton diffusion coefficient of $(11 \pm 2.2) \times 10^{-4}$ cm²/s that corresponds to the diffusion length of 10.5 ± 1 nm. The error is the standard deviation in the mean value.

The solid line in Figure 3.4 is modeled using the mean value of the exciton diffusion coefficient and assuming intimate mixture of Si-PCPDTBT:PCBM blends.

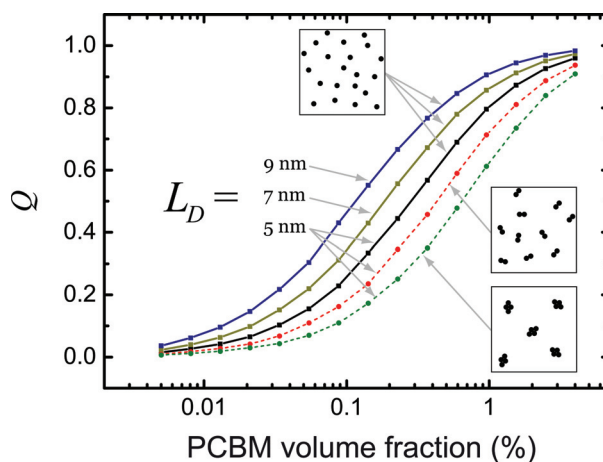


Figure 3.5: Modeled relative quenching efficiency versus volume fraction of PCBM in P3HT setting various exciton diffusion length (solid lines) and clustering (dashed lines). The insets schematically show the morphology of intimate mixture (top) and phase separated blends of two and four molecules per cluster (right). The total number of PCBM molecules (black dots) is the same in each inset.

The modeled curve deviates from the experimental data points at higher volume fractions than 0.3%. Such a deviation indicates the phase separation of the polymer:PCBM blends. Formation of PCBM clusters at higher PCBM concentration is consistent with the fact that Si-PCPDTBT shows higher crystallinity than the carbon bridged polymer in as-cast films.^[40] High degree of crystallinity, which is expected to enhance the phase separation, is the common feature of Si-PCPDTBT and P3HT films.

Interestingly, the silicon bridged polymer shows the same exciton diffusion length as the carbon bridged material, while the exciton diffusion coefficient is about two times smaller in Si-PCPDTBT. Mathematically such a contrast is possible due to the fact that PL decay time of the silicon-bridged polymer in pristine film is about two times longer than PL decay time of the carbon bridged one (see Eq. 3.3). Similar result has been shown by Markov et. al. in a family of poly(*p*-phenylene vinylene)-derivatives, in which increase of the exciton diffusion coefficient was compensated by the decrease of the PL decay time leading to the same values of the exciton diffusion length.^[43]

3.5 Discussion

Figure 3.5 shows the family of modeled dependencies of relative quenching efficiency on the volume fraction of PCBM in P3HT; PCBM-PCPDTBT blends give

similar results (not shown in Figure 3.5). The solid lines are calculated by setting the exciton diffusion length – from left to right – to 9, 7 and 5 nm. The dashed lines represent samples with phase separated domains of 2 and 4 PCBM molecules per cluster, setting the exciton diffusion length to 5 nm. In the intermediate concentration range the relative quenching efficiency is very sensitive for the exciton diffusion length and the blend morphology. As expected, the highest quenching efficiency is achieved for the longest exciton diffusion length and homogeneous distribution of the quenching molecules. While the lowest values of Q are obtained when PCBM molecules are set to form clusters of the largest size.

Remarkably the curves in Figure 3.5 do not cross in the intermediate concentration range, but rather replicate each other by a translation along the horizontal axis. Therefore we can summarize our methodology as follows: if the experimental data can be described by one of the curves then the quencher molecules form either an intimate mixture with the polymer or clusters of fixed size in the whole concentration range. The latter option is unlikely because the cluster formation probability is increasing with the concentration of quenchers. If the measured relative quenching efficiency grows with the PCBM volume fraction more slowly than a typical modeled curve, then quenchers form larger phase separated domains in that concentration range.

The developed methodology of exciton diffusion measurement has numerous advantages as compared to other approaches. The only fitting parameter is the exciton diffusion length; the model does not require assumptions, for instance, about the exciton-exciton annihilation cross-section.^[12,19,20] The measured exciton diffusion length corresponds to the diffusion in three dimensions, which is the case in the bulk heterojunction solar cells. The effects at interfaces can be safely neglected because the samples are much thicker than the exciton diffusion length. The exciton density variations due to optical interference and light absorption do not influence the PL decay in the blends because samples are isotropic and low excitation densities have been used, which are insufficient for the considerable exciton-exciton annihilation. The simplicity of sample preparation and experimental methods makes it practical to systematically measure and compare exciton diffusion length in large number of materials. Finally, we can access the polymer-quencher morphology of low quencher concentrations using the MC simulation. To the best of our knowledge, this question has not been addressed before in the PCBM concentration range of 0.01-5 wt%.

3.6 Conclusions

Using a newly developed method we found that PCBM molecules form intimate mixtures with PCPDTBT in blends with PCBM concentration ranging from 0.01 to 5 wt%. Phase separated domains have been detected in Si-PCPDTBT and P3HT at concentrations above 0.9 wt% and 1.8 wt%, respectively. The knowledge about the

blend morphology allows us to model 3D diffusion and accurately determine the exciton diffusion coefficients of $(2.2 \pm 0.5) \times 10^{-4}$, $(26 \pm 3) \times 10^{-4}$ and $(11 \pm 2) \times 10^{-4}$ cm²/s that correspond to the diffusion lengths of 5.4 ± 0.7 , 10.6 ± 0.6 , and 10.5 ± 1 nm in P3HT, PCPDTBT and Si-PCPDTBT, respectively. Remarkably the exciton diffusion length is the same in both narrow band gap polymers. Compared to other approaches, the proposed method for exciton diffusion measurement has numerous advantages and is suitable for systematic studies in a large number of materials.

3.7 Methods

PCPDTBT and Si-PCPDTBT were synthesized by Konarka Technologies; PCBM and regio-regular P3HT were purchased from Solene BV and Sigma-Aldrich, respectively. Polymer solutions in chlorobenzene were mixed with various fractions of PCBM dilute solution, and spin-coated on glass substrates to produce ~100 nm thick films of polymer:PCBM blends. Samples were prepared under inert nitrogen atmosphere and encapsulated with a glass substrate to further protect films from air during the optical measurements. No annealing steps have been applied to the blends. The PCPDTBT- and Si-PCPDTBT-based blends were excited at 760 nm by the principal harmonics of a 100 fs pulsed Ti-Sapphire laser. P3HT-based blends were excited 380 nm by frequency doubled pulses of the same laser. The initial exciton density was kept well below 10^{15} cm⁻³. PL decays were measured by two Streak cameras sensitive in the near infrared and the visible spectral parts, respectively. The PL decays of PCPDTBT were deconvoluted with the instrument response function and fitted as mono- or bi-exponential decays for further analysis. Software for Monte Carlo simulations has been specifically developed to model exciton diffusion in polymer:PCBM blends. Mersenne twister algorithm^[44] has been used as a pseudo random number generator, implemented by A. Fog.^[45]

The PCBM volume fraction is the volume occupied by PCBM molecules, which are assumed to be balls with diameter of 1 nm, divided by the total volume of the blend. The polymer density is an important parameter for determination of the PCBM volume ratio. In our simulation we took a P3HT density of 1.1 g/cm³ (Ref. ^[46,47]). The density of PCPDTBT and Si-PCPDTBT has not been reported yet, however conjugated polymers typically have densities in the range of 0.9 – 1.4 g/cm³ (Ref. ^[46–48]). We found it reasonable to set the density to 1.3 g/cm³ in our simulations, resulting in the exciton diffusion length of ~10.5 nm. Generally, the fitting results depend only weakly on the polymer density. Thus settings of 1.2 or 1.4 g/cm³ in the simulation lead to an exciton diffusion length of 11.1 and 10.2 nm, respectively, resulting in a change of approximately 0.5 nm per 0.1 g/cm³.

3.8 References

- [1] A. Haugeneder, M. Neges, C. Kallinger, W. Spirkl, U. Lemmer, J. Feldmann, U. Scherf, E. Harth, A. Gügel, K. Müllen, *Phys. Rev. B* **1999**, *59*, 15346.
- [2] M. Theander, A. Yartsev, D. Zigmantas, V. Sundström, W. Mammo, M. R. Andersson, O. Inganäs, *Phys. Rev. B* **2000**, *61*, 12957.
- [3] D. E. Markov, E. Amsterdam, P. W. M. Blom, A. B. Sieval, J. C. Hummelen, *J. Phys. Chem. A* **2005**, *109*, 5266-5274.
- [4] Y. Wu, Y. C. Zhou, H. R. Wu, Y. Q. Zhan, J. Zhou, S. T. Zhang, J. M. Zhao, Z. J. Wang, X. M. Ding, X. Y. Hou, *Appl. Phys. Lett.* **2005**, *87*, 044104-3.
- [5] S. R. Scully, M. D. McGehee, *J. Appl. Phys.* **2006**, *100*, 034907-5.
- [6] Y. C. Zhou, Y. Wu, L. L. Ma, J. Zhou, X. M. Ding, X. Y. Hou, *J. Appl. Phys.* **2006**, *100*, 023712-5.
- [7] C. Goh, S. R. Scully, M. D. McGehee, *J. Appl. Phys.* **2007**, *101*, 114503.
- [8] O. V. Mikhnenko, F. Cordella, A. B. Sieval, J. C. Hummelen, P. W. M. Blom, M. A. Loi, *J. Phys. Chem. B* **2008**, *112*, 11601-11604.
- [9] K. Masuda, Y. Ikeda, M. Ogawa, H. Benten, H. Ohkita, S. Ito, *ACS Appl. Mater. Interfaces* **2010**, *2*, 236-245.
- [10] W. A. Luhman, R. J. Holmes, *Adv. Funct. Mater.* **2011**, *21*, 764-771.
- [11] C. Breyer, M. Vogel, M. Mohr, B. Johnev, K. Fostiropoulos, *Phys. Status Solidi B* **2006**, *243*, 3176 - 318.
- [12] P. E. Shaw, A. Ruseckas, I. D. W. Samuel, *Adv. Mater.* **2008**, *20*, 3516-3520.
- [13] O. V. Mikhnenko, F. Cordella, A. B. Sieval, J. C. Hummelen, P. W. M. Blom, M. A. Loi, *J. Phys. Chem. B* **2009**, *113*, 9104-9109.
- [14] R. R. Lunt, N. C. Giebink, A. A. Belak, J. B. Benziger, S. R. Forrest, *J. Appl. Phys.* **2009**, *105*, 053711-7.
- [15] H. Najafov, B. Lee, Q. Zhou, L. C. Feldman, V. Podzorov, *Nat. Mater.* **2010**, *9*, 938-943.
- [16] R. R. Lunt, J. B. Benziger, S. R. Forrest, *Adv. Mater.* **2010**, *22*, 1233-1236.
- [17] S. Cook, A. Furube, R. Katoh, L. Han, *Chem. Phys. Lett.* **2009**, *478*, 33-36.
- [18] B. A. Gregg, J. Sprague, M. W. Peterson, *J. Phys. Chem. B* **1997**, *101*, 5362-5369.
- [19] S. Cook, H. Liyuan, A. Furube, R. Katoh, *J. Phys. Chem. C* **2010**, *114*, 10962-10968.
- [20] A. J. Lewis, A. Ruseckas, O. P. M. Gaudin, G. R. Webster, P. L. Burn, I. D. W. Samuel, *Org. Electron.* **2006**, *7*, 452-456.
- [21] C. L. Yang, Z. K. Tang, W. K. Ge, J. N. Wang, Z. L. Zhang, X. Y. Jian, *Appl. Phys. Lett.* **2003**, *83*, 1737-1739.
- [22] T. Stubinger, W. Brutting, *J. Appl. Phys.* **2001**, *90*, 3632-3641.
- [23] J. J. M. Halls, K. Pichler, R. H. Friend, S. C. Moratti, A. B. Holmes, *Appl. Phys. Lett.* **1996**, *68*, 3120-3122.
- [24] J. E. Kroeze, T. J. Savenije, M. J. W. Vermeulen, J. M. Warman, *J. Phys. Chem. B* **2003**, *107*, 7696-7705.
- [25] H. Wang, H.-Y. Wang, B.-R. Gao, L. Wang, Z.-Y. Yang, X.-B. Du, Q.-D. Chen, J.-F. Song, H.-B. Sun, *Nanoscale* **2011**, *3*, 2280.
- [26] D. E. Markov, P. W. M. Blom, *Phys. Rev. B* **2006**, *74*, 085206-5.
- [27] L. Lüer, H.-J. Egelhaaf, D. Oelkrug, G. Cerullo, G. Lanzani, B.-H. Huisman, D. de Leeuw, *Org. Electron.* **2004**, *5*, 83-89.

- [28] B. Y. Balagurov, V. G. Vaks, *JETP* **1973**, 65, 1939-1946.
- [29] M. T. Rispens, A. Meetsma, R. Rittberger, C. J. Brabec, N. S. Sariciftci, J. C. Hummelen, *Chem. Commun.* **2003**, 2116.
- [30] F. B. Dias, K. T. Kamtekar, T. Cazati, G. Williams, M. R. Bryce, A. P. Monkman, *ChemPhysChem* **2009**, 10, 2096-2104.
- [31] M. Anni, M. E. Caruso, S. Lattante, R. Cingolani, *J. Chem. Phys.* **2006**, 124, 134707.
- [32] S. B. Lee, I. C. Kim, C. A. Miller, S. Torquato, *Phys. Rev. B* **1989**, 39, 11833.
- [33] M. R. Riley, F. J. Muzzio, H. M. Buettner, S. C. Reyes, *Phys. Rev. E* **1994**, 49, 3500.
- [34] M. R. Riley, H. M. Buettner, F. J. Muzzio, S. C. Reyes, *Biophys J* **1995**, 68, 1716-1726.
- [35] J. A. Anta, *Energy Environ. Sci.* **2009**, 2, 387.
- [36] X. Yang, J. Loos, S. C. Veenstra, W. J. H. Verhees, M. M. Wienk, J. M. Kroon, M. A. J. Michels, R. A. J. Janssen, *Nano Lett.* **2005**, 5, 579-583.
- [37] J. Peet, J. Y. Kim, N. E. Coates, W. L. Ma, D. Moses, A. J. Heeger, G. C. Bazan, *Nat Mater* **2007**, 6, 497-500.
- [38] D. Di Nuzzo, A. Aguirre, M. Shahid, V. S. Gevaerts, S. C. J. Meskers, R. A. J. Janssen, *Adv. Mater.* **2010**, 22, 4321-4324.
- [39] M. Morana, H. Azimi, G. Dennler, H.-J. Egelhaaf, M. Scharber, K. Forberich, J. Hauch, R. Gaudiana, D. Waller, Z. Zhu, K. Hingerl, S. S. van Bavel, J. Loos, C. J. Brabec, *Adv. Funct. Mater.* **2010**, 20, 1180-1188.
- [40] M. C. Scharber, M. Koppe, J. Gao, F. Cordella, M. A. Loi, P. Denk, M. Morana, H.-J. Egelhaaf, K. Forberich, G. Dennler, R. Gaudiana, D. Waller, Z. Zhu, X. Shi, C. J. Brabec, *Adv. Mater.* **2010**, 22, 367-370.
- [41] M. Morana, M. Wegscheider, A. Bonanni, N. Kopidakis, S. Shaheen, M. Scharber, Z. Zhu, D. Waller, R. Gaudiana, C. Brabec, *Adv. Funct. Mater.* **2008**, 18, 1757-1766.
- [42] M. Reyes-Reyes, K. Kim, D. L. Carroll, *Appl. Phys. Lett.* **2005**, 87, 083506.
- [43] D. E. Markov, C. Tanase, P. W. M. Blom, J. Wildeman, *Phys. Rev. B* **2005**, 72, 045217-6.
- [44] M. Matsumoto, T. Nishimura, *ACM Trans. Model. Comput. Simul.* **1998**, 8, 3-30.
- [45] "Pseudo random number generators," can be found under <http://www.agner.org/random/>, **n.d.**
- [46] T. J. Prosa, M. J. Winokur, J. Moulton, P. Smith, A. J. Heeger, *Macromolecules* **1992**, 25, 4364-4372.
- [47] J. Mårdalen, E. J. Samuelsen, O. R. Gautun, P. H. Carlsen, *Solid State Communications* **1991**, 77, 337-339.
- [48] C. W. T. Bulle-Lieuwma, W. J. H. van Gennip, J. K. J. van Duren, P. Jonkheijm, R. A. J. Janssen, J. W. Niemantsverdriet, *Applied Surface Science* **2003**, 203-204, 547-550.

Chapter 4

Effect of Thermal Annealing on Exciton Diffusion

In this chapter we show that the method we have developed for measuring the singlet exciton diffusion length in blends with [6,6]-phenyl-C₆₁-butyric acid methyl ester (PCBM) can be applied not only to polymeric materials, but also to small molecule organic semiconductors. Small organic molecules have a large potential for molecular re-organization upon thermal annealing. Here we show that the exciton diffusion length is decreased upon annealing from 9 to 3 nm in a thin film of a diketopyrrolopyrrole derivative. Such a variation is attributed to exciton delocalization effects in the crystalline domains that are formed during the annealing process as well as to the exciton quenching at grain boundaries.*

*O.V. Mikhnenko, J. Lin, Y. Shu, J. E. Anthony, P. W. M. Blom, T.-Q. Nguyen, M. A. Loi, *Submitted for publication*

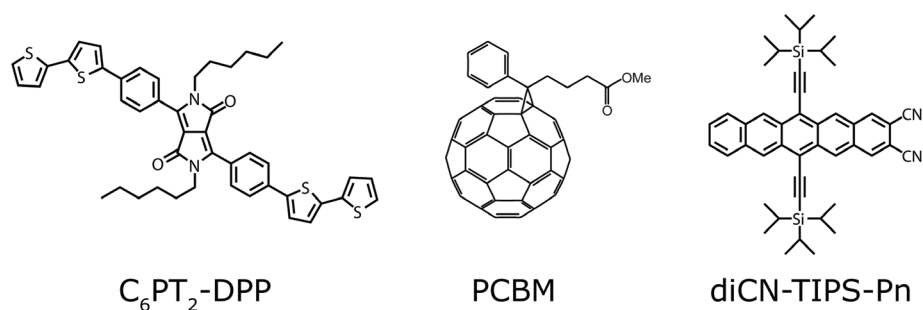


Figure 4.1: Chemical structures of 2,5-dihexyl-3,6-bis[4-(2,2'-bithiophene-5-yl)phenyl]pyrrolo[3,4-c]pyrrole-1,4-dione (**C₆PT₂-DPP**), [6,6]-phenyl-C₆₁-butyric acid methyl ester (**PCBM**) and 2,3-dicyano-6,13-bis-(triisopropylsilylethynyl)pentacene (**diCN-TIPS-Pn**).

4.1 Introduction

An interpenetrating network of electron donating and electron accepting materials – a bulk heterojunction – is an efficient structure to be used as active layer of thin film solar cells.^[1,2] Thermal annealing is often applied to bulk heterojunctions in order to improve their morphology for more efficient charge extraction.^[3–7] Typically annealing enhances the phase separation of donor and acceptor materials and promotes the formation of polycrystalline phases resulting in higher charge carrier mobility. The power conversion efficiency of annealed solar cells is sometimes increased by orders of magnitude as compared to untreated devices.^[7] Despite the strong interest for the exciton diffusion processes in as-cast films,^[8] thermally annealed thin films only received little attention in the literature. Several experiments show that the exciton diffusion length is longer in phases with stronger molecular interactions.^[9–16] Since thermal annealing usually improves the local crystallinity of phase separated domains, the exciton diffusion length is expected to be longer in annealed films.

Here we show that in contrast to expectations, the exciton diffusion length decreases upon annealing from 9 to 3 nm in C₆PT₂-DPP (for full name and chemical structure see **Figure 4.1**). C₆PT₂-DPP is a small molecule organic semiconductor that belongs to the family of diketopyrrolopyrrole derivatives.^[7,17–23] Compared to polymers, small molecules have numerous advantages including easier synthetic procedures, higher purity, monodispersity, and higher possibility of supramolecular organization. Therefore small molecules are potentially suited for devices that require high charge carrier mobilities.^[24,25] Currently the power conversion efficiency of

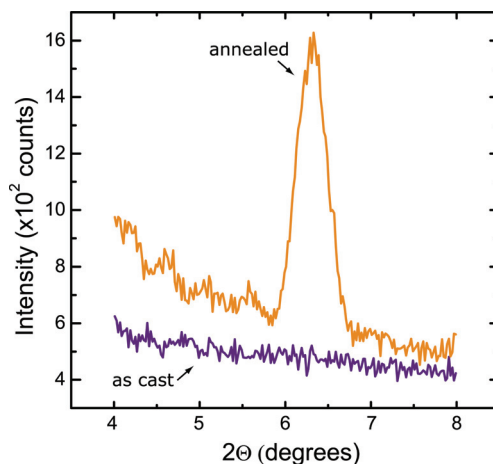


Figure 4.2: X-ray diffraction pattern of pristine C_6PT_2 -DPP film before and after thermal annealing at 75 °C.

solution processed solar cells based on small molecules up to 6.7% (Ref. [7,26–32]), approaching the efficiencies of polymer-based devices.[33]

4.2 Effect of Annealing on Crystallinity and Photophysical Properties

Figure 4.2 shows the x-ray diffraction pattern of thin film of C_6PT_2 -DPP before and after thermal annealing at 75 °C. Before annealing there are no features in the diffraction pattern, indicating the isotropic amorphous structure of the film. After annealing at 80 °C a strong peak is appearing at 6.3° due to the emergence of a polycrystalline arrangement.

Figure 4.3a presents the photoluminescence (PL) spectra of C_6PT_2 -DPP in chloroform solution and in film before and after annealing. The PL spectrum undergoes a gradual red shift going from solution to as-cast thin films; followed by a further red shift as a result of annealing. Such a red shift is due to intermolecular interactions in the thin film, which are enhanced upon annealing-induced crystallization. Excitons undergo delocalization among adjacent molecules in thin films resulting in the observed red shift. The delocalization is most pronounced in the annealed films due to the polycrystalline ordering (Figure 4.2).[34–37]

Thermal annealing has also a strong effect on the PL decay time of the C_6PT_2 -DPP films. **Figure 4.3b** illustrates that the PL decay time of the annealed C_6PT_2 -DPP film is significantly shorter than that of the as-cast film. For data analysis we describe PL decays in thin films of C_6PT_2 -DPP with a bi-exponential function:

Table I. Bi-exponential decay constants of as cast and annealed films of C₆PT₂-DPP. The decays were normalized to the value at time zero such that $a_1 + a_2 = 1$. The integral over time is given by $a_1\tau_1 + a_2\tau_2$, see Eq. (4.1).

	a_1	τ_1 (ns)	a_2	τ_2 (ns)	Integral (ns)
As-cast film	0.765	2.514	0.235	0.248	1.981
Annealed film	0.820	1.094	0.180	0.149	0.923

$$PL(t) = a_1 e^{-t/\tau_1} + a_2 e^{-t/\tau_2}. \quad (4.1)$$

The values of a_1 , a_2 , τ_1 , and τ_2 of both as-cast and annealed films of C₆PT₂-DPP are listed in **Table I** for reference. There are several reasons that may be responsible for the faster PL decay in the annealed films. The enhanced delocalization of excitons in polycrystalline films may lead to an increase in the efficiency of exciton dissociation to non-emissive species – such as free charges – resulting in shorter PL decay times.^[34–39] Lunt *et al.* showed that photoluminescence can be quenched at the boundaries of the polycrystalline domains,^[40] which also may lead to shorter PL decay times.

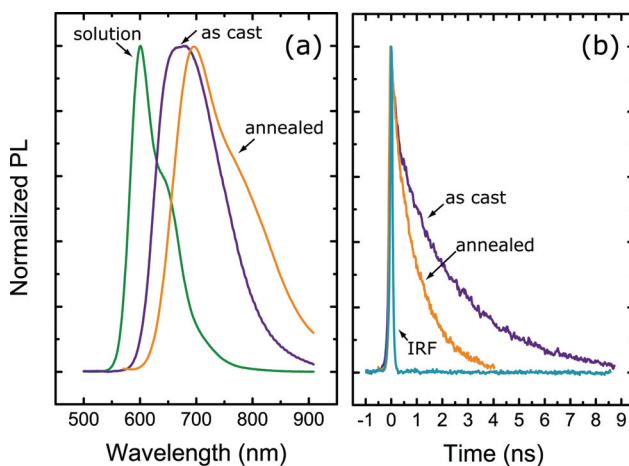


Figure 4.3: (a) Photoluminescence spectra of C₆PT₂-DPP in chloroform solution, and thin film before and after annealing. The data were normalized to the maximum intensity value. (b) PL decays of as-cast and annealed pristine C₆PT₂-DPP films. The instrument response function (IRF) to 100 fs laser pulse is also presented. Normalization was made to the value at time zero.

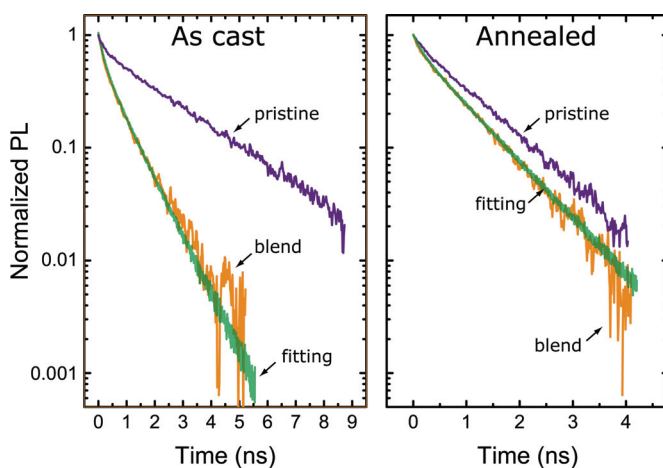


Figure 4.4: PL decays of C_6PT_2 -DPP thin film and blend with 0.82wt% PCBM before (left) and after annealing (right). PL decays were normalized to the value at time zero. The result of the fitting of the PL decays of the blend with Monte Carlo simulation is also presented.

4.3 Exciton Diffusion Measurements

To measure the exciton diffusion length in C_6PT_2 -DPP we apply the method that was described in detail in Chapter 3. We model the PL decays of C_6PT_2 -DPP:PCBM blends with various PCBM concentrations using Monte Carlo simulation. This simulation takes as inputs the concentration of PCBM molecules, the morphology of the blend, the parameters of the bi-exponential PL decay in the pristine film, and the only fitting parameter – the exciton diffusion coefficient. As output we get a simulated PL decay, which is then compared to the experimentally measured data.

At the beginning of a simulation run, non-interacting excitons – balls of 1 nm in diameter – are randomly placed into the simulation box of $50 \times 50 \times 50$ nm, which corresponds to the input morphology of the blend C_6PT_2 -DPP:PCBM. Typical morphology is the homogeneous random distribution of non-overlapping PCBM molecules that are modeled as balls of 0.5 nm radius.^[41] Periodic boundary conditions are imposed to the simulation box to mimic an infinitely large medium. Excitons are moved in a random 3D direction by the fixed distance δs during each iteration time δt . According to the Einstein theory of random walks the exciton diffusion coefficient D is related to δs and δt as:

$$D = \frac{\delta s^2}{6 \delta t}. \quad (4.2)$$

An exciton is considered to decay radiatively at time t_i , which is defined at the beginning of the simulation run in order to reflect the bi-exponential PL decay in the pristine film:

$$t_i = -\tau_k \ln(w_i), \quad (4.3)$$

$$\text{if } \left(\rho_i < \frac{a_1}{a_1 + a_2} \right) \text{ then } k = 1; \text{ otherwise } k = 2, \quad (4.4)$$

where w_i and ρ_i are independent random numbers between 0 and 1; index k distinguishes between the components of the bi-exponential decay. If an exciton touches a PCBM molecule before time t_i then it is considered to be quenched and does not undergo radiative recombination. At least 2×10^5 excitons are modeled during each simulation run. The modeled PL decay is the number of radiatively decayed excitons *versus* time. The simulation is repeated with adjusted exciton hopping distance δs until the modeled PL decay coincides with the experimentally measured one for the specific concentration of PCBM molecules in the modeled sample.

Figure 4.4 shows an example of the fitting of the experimentally measured PL decays before and after annealing at 80 °C of the C₆PT₂-DPP:PCBM blend. The PCBM concentration in this specific sample was $6.5 \times 10^{18} \text{ cm}^{-3}$ that corresponds to 0.82 wt% or the PCBM volume fraction of 0.3%. The fitting results in an exciton diffusion coefficient of $1 \times 10^{-4} \text{ cm}^2/\text{s}$ and $2.5 \times 10^{-5} \text{ cm}^2/\text{s}$, which correspond to an exciton diffusion length of 8.7 nm and 2.8 nm for the as-cast and annealed samples, respectively. The 3D exciton diffusion length is calculated using the following expression:

$$L_D = \sqrt{3D\tau}, \quad (4.5)$$

where τ is the average PL decay time of the pristine film of C₆PT₂-DPP (see Eq. 4.1 and Ref. [42]):

$$\tau = \frac{a_1\tau_1^2 + a_2\tau_2^2}{a_1\tau_1 + a_2\tau_2}. \quad (4.6)$$

The exciton diffusion coefficients and diffusion lengths were extracted for each sample resulting in the average values of $(1.1 \pm 0.1) \times 10^{-4}$ and $(2.5 \pm 0.4) \times 10^{-5} \text{ cm}^2/\text{s}$; 8.8 ± 0.3 and 2.8 ± 0.2 nm for the as-cast and annealed samples, respectively. The error is the standard deviation of the mean value. To compare samples with different PCBM concentrations we introduce the relative quenching efficiency:

$$Q = 1 - \frac{\int dt PL_{\text{blend}}}{\int dt PL_{\text{reference}}}, \quad (4.7)$$

where PL_{blend} and $PL_{\text{reference}}$ are normalized to the value at time zero PL decays of the blend and pristine C₆PT₂-DPP film, respectively.

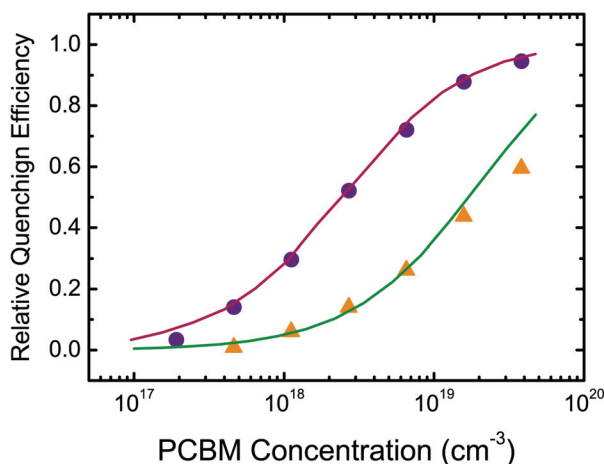


Figure 4.5: Dependence of the relative quenching efficiency on the PCBM content in as-cast (circles) and annealed (triangles) samples. The lines are the result of the Monte Carlo simulation, see text.

Figure 4.5 shows the dependence of the relative quenching efficiency on the PCBM concentration in the as-cast and annealed blends. The solid lines in Figure 4.5 are calculated by setting in the simulation the extracted average values of the exciton diffusion coefficients. The simulated curve accurately describes the relative quenching efficiency of as-cast films in all the concentration range using a single value of the diffusion coefficient. Consequently, we conclude that the PCBM molecules do not form phase separated domains in the as-cast blends. Deviation from the experimental data is expected at higher concentrations of PCBM if clusters were formed (see Chapter 3).

The relative quenching efficiency of annealed blends is also accurately described by the simulated curve in Figure 4.5. Only at PCBM concentration of $3.8 \times 10^{19} \text{ cm}^{-3}$ the modeled curve deviates from the experimental data point, suggesting the formation of small clusters of PCBM molecules at that concentration.

4.4 Using Different Exciton Quenching Molecule

Upon annealing we found a significant decrease of the exciton diffusion length from 9 to 3 nm in C₆PT₂-DPP. When modeling the PL decays we assumed that PCBM forms an intimate mixture with C₆PT₂-DPP. This assumption should be additionally verified because thermal annealing could induce phase separation in the blend. In order to check if such a phase separation indeed occurred we compare PCBM:C₆PT₂-DPP blends with diCN-TIPS-Pn:C₆PT₂-DPP blends. diCN-TIPS-Pn is an efficient exciton quencher that has quite different chemical structure as compared to PCBM.^[43]

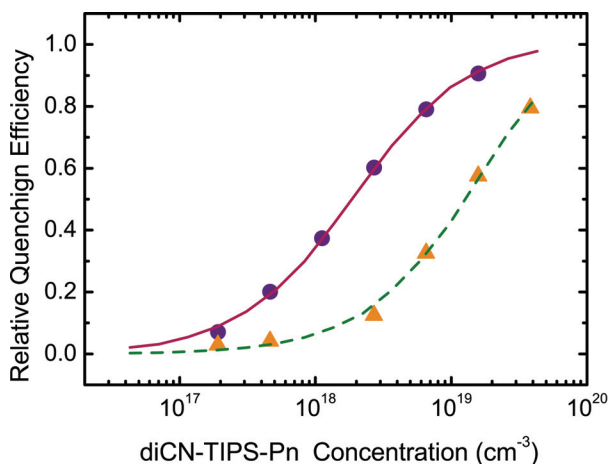


Figure 4.6: Relative quenching efficiency *versus* quencher concentration in diCN-TIPS-Pn:C₆PT₂-DPP blends in as cast (circles) and annealed (triangles) samples. The lines are modeled with Monte Carlo simulation by setting the quenching radius of diCN-TIPS-Pn to 0.81 nm, see text.

First we quantify the exciton quenching efficiency of diCN-TIPS-Pn in the blends with C₆PT₂-DPP by modeling the PL decays of as-cast films. For simplicity, the molecular shape of diCN-TIPS-Pn is approximated in our simulations as an isotropic ball. An exciton is considered to be quenched upon contact with the surface of this ball. The measured PL decays are modeled by setting the exciton diffusion coefficient to the value that was previously found using PCBM:C₆PT₂-DPP blends, and varying only the exciton quenching radius of diCN-TIPS-Pn. In this way we found a value for the exciton quenching radius of 0.81 ± 0.03 nm. The error is the standard deviation of mean value among 5 samples with different concentrations of diCN-TIPS-Pn. Interestingly, the quenching radius of diCN-TIPS-Pn is larger than the quenching radius of fullerenes – 0.5 nm – this is possibly due to the Förster energy transfer from C₆PT₂-DPP to diCN-TIPS-Pn.

Figure 4.6 shows the dependence of the relative quenching efficiency on the concentration of quenching molecules in diCN-TIPS-Pn:C₆PT₂-DPP blends before (circles) and after (triangles) annealing. The solid line was calculated by setting the exciton diffusion coefficient to 1.1×10^{-4} cm²/s and the quenching radius of diCN-TIPS-Pn to 0.81 nm. This simulated curve excellently fits the experimental data confirming that (i) we accurately determined the quenching radius of diCN-TIPS-Pn and (ii) there are no phase separated domains in the as-cast blends.

The dashed line in Figure 4.6 was back-calculated using the exciton diffusion coefficient of 2.5×10^{-5} cm²/s, which was extracted in the annealed PCBM:C₆PT₂-DPP blends; and the quenching radius of 0.81 nm that we determined for as-cast diCN-TIPS-Pn containing blends. This curve predicts the experimental data points of the

annealed blends (triangles) remarkably well in the whole range of studied concentrations.

The measured relative quenching efficiency in PCBM and diCN-TIPS-Pn containing blends can be described with a single diffusion coefficient indicating that the morphology of PCBM and diCN-TIPS-Pn containing blends are the same. It is unlikely that both PCBM and diCN-TIPS-Pn form phase separate domains of the same size because these acceptor molecules have very different chemical structure and thus different intermolecular interactions. Therefore we conclude that both PCBM and diCN-TIPS-Pn indeed form an intimate mixture with C₆PT₂-DPP in the annealed films and show that we correctly assumed the blend morphology when modeling the PL decays. Thus the extracted value of 2.5×10^{-5} cm²/s is an accurate exciton diffusion coefficient for the annealed films of C₆PT₂-DPP.

4.5 Discussion

Generally, enhanced intermolecular interactions such as in molecular crystals were shown to result in longer exciton diffusion length than in the amorphous phases of various materials.^[9–14,16] Lunt *et al.* showed that the exciton diffusion length in 3,4,9,10-perylenetetracarboxylic dianhydride (PTCDA) increases from 6 to 20 nm with increasing the grain size of molecular crystals in a poly-crystalline thin film.^[40] The exciton diffusion length in PTCDA appeared to be limited by defects at grain boundaries, which showed efficient exciton quenching. Other studies show that enhanced delocalization of excitons leads to higher probability of exciton dissociation to non-emissive species such as free charges.^[34–39] Consequently, PL decay time becomes shorter upon exciton delocalization. In this case stronger intermolecular interactions due to a higher degree of crystalline ordering^[34] and/or higher local density of the material^[35–39] may limit the exciton diffusion length.

In our experiments we found that the exciton diffusion length in the annealed polycrystalline films of C₆PT₂-DPP is much shorter than in the as-cast amorphous material. Significant red shift of PL spectrum suggests that excitons are more delocalized in the annealed films. Such delocalization may be responsible for the reduction of the PL decay time upon annealing^[34–38] (Figure 4.3) leading to shorter exciton diffusion length. Moreover, the measured exciton diffusion coefficient is about five times smaller in the annealed films resulting in further decrease of the exciton diffusion length.

It is important to note that in our model we considered the annealed polycrystalline films as a continuous medium. In reality the boundaries of polycrystalline domains may contribute to the exciton scattering and even quenching.^[40] Therefore the measured exciton diffusion coefficient in the annealed films is the effective value within complex polycrystalline morphology. The exciton

diffusion coefficient within a single crystalline domain may be different, for instance higher than the value reported here. Nevertheless our result is useful for modeling the operation of bulk heterojunction solar cells.

Despite the fact that exciton diffusion length is relatively short in the annealed films of C₆PT₂-DPP, the power conversion efficiency of bulk heterojunction solar cells based on this material and a C₇₀ fullerene derivative is as high as 1.1%.^[18] This efficiency has been achieved upon annealing of the active layer, while as-cast devices showed poorer performance (0.89%). Thus it appears that there is no a simple direct correlation between the exciton diffusion length and the final performances of C₆PT₂-DPP:PC₇₀BM bulk heterojunction solar cell. Thermal annealing induces significant improvements on the blend morphology and charge mobility in C₆PT₂-DPP films.^[18] These improvements presumably compensate the reduction of the exciton diffusion length resulting in higher performance of the annealed devices.

Finally, the reduction of the exciton diffusion length upon annealing may be compensated by the effect of exciton delocalization, which promotes generation of free charges. Wang *et al.* showed that measured exciton diffusion length of 3.5 nm in poly(3-hexylthiophene) (P3HT) cannot explain high performance of bulk heterojunction solar cell based on that polymer.^[44] Exciton delocalization in the range of 4.8-9 nm is needed to describe the experimental data in Ref. ^[44].

4.6 Conclusions

We have accurately measured the exciton diffusion coefficients and diffusion lengths of $(1.1 \pm 0.1) \times 10^{-4}$ and $(2.5 \pm 0.4) \times 10^{-5}$ cm²/s; 8.8 ± 0.3 and 2.8 ± 0.2 nm in as-cast and annealed thin films of C₆PT₂-DPP. The exciton diffusion appears to be limited in the annealed samples presumably due to the delocalization effects and exciton quenching on the grain boundaries of the polycrystalline film. It appears that there is no a simple direct correlation between the measured exciton diffusion length and the performance of bulk heterojunction solar cells that are based on the studied material. Thermal annealing leads to simultaneous increase of the solar cell performance and decrease of the exciton diffusion length in C₆PT₂-DPP.

4.7 Methods

C₆PT₂-DPP was synthesized in group of Prof. Thuc-Quyen Nguyen, diCN-TIPS pentacene was provided by Prof. John Anthony, PCBM was purchased from Solenne BV. No additional purification steps have been applied to any of the materials used. X-ray diffraction patterns were measured with a X'Pert Phillips Material Research Diffractometer using Cu K α radiation with emission wavelength of $\lambda = 1.54 \text{ \AA}$. Thin films were spin-coated from chloroform in a glove box under nitrogen atmosphere

and encapsulated with a clean glass prior to optical measurements. Thermal annealing of the encapsulated films was performed on a hotplate at 80 °C for 10 minutes. The thicknesses of all thin films were about 100 nm, as measured with Dektak profilometer.

For photoluminescence measurements samples were excited at 380 nm with frequency doubled 100 fs laser pulses of a Ti-sapphire laser. The cw-spectra were collected with a Hamamatsu CCD detector. Time resolved photoluminescence was measured with a Hamamatsu streak camera. PL decays of diCN-TIPS-Pn:C₆PT₂-DPP blends were spectrally integrated from 620 to 660 nm in order to exclude emission of diCN-TIPS-Pn that is centered at 730 nm. PL decays of PCBM:C₆PT₂-DPP were integrated within the whole emission spectrum.

A density of 1.2 g/cm³ was estimated from the crystal structure of C₆PT₂-DPP and was used to calculate the concentration of exciton quenching molecules. Thermal annealing may influence the material density due to molecular reorganization. However, the resulting values of exciton diffusion length depend only weakly on the material density. For example, for the annealed films the modeled exciton diffusion length is changed only by approximately 0.2 nm per 0.1 g/cm³. The software for Monte Carlo simulation relies on Mersenne-twister algorithm of pseudo random number generation.^[45,46]

4.8 References

- [1] G. Yu, J. Gao, J. C. Hummelen, F. Wudl, A. J. Heeger, *Science* **1995**, *270*, 1789 - 1791.
- [2] S. E. Shaheen, C. J. Brabec, N. S. Sariciftci, F. Padinger, T. Fromherz, J. C. Hummelen, *Appl. Phys. Lett.* **2001**, *78*, 841-843.
- [3] V. D. Mihailetschi, H. X. Xie, B. de Boer, L. J. A. Koster, P. W. M. Blom, *Adv. Funct. Mater.* **2006**, *16*, 699-708.
- [4] M. Reyes-Reyes, K. Kim, D. L. Carroll, *Appl. Phys. Lett.* **2005**, *87*, 083506.
- [5] X. Yang, J. Loos, S. C. Veenstra, W. J. H. Verhees, M. M. Wienk, J. M. Kroon, M. A. J. Michels, R. A. J. Janssen, *Nano Lett.* **2005**, *5*, 579-583.
- [6] M. Morana, H. Azimi, G. Dennler, H.-J. Egelhaaf, M. Scharber, K. Forberich, J. Hauch, R. Gaudiana, D. Waller, Z. Zhu, K. Hingerl, S. S. van Bavel, J. Loos, C. J. Brabec, *Adv. Funct. Mater.* **2010**, *20*, 1180-1188.
- [7] B. Walker, A. B. Tamayo, X.-D. Dang, P. Zalar, J. H. Seo, A. Garcia, M. Tantiwiwat, T.-Q. Nguyen, *Adv. Funct. Mater.* **2009**, *19*, 3063-3069.
- [8] P. Peumans, A. Yakimov, S. R. Forrest, *J. Appl. Phys.* **2003**, *93*, 3693-3723.
- [9] S.-B. Rim, R. F. Fink, J. C. Schöneboom, P. Erk, P. Peumans, *Appl. Phys. Lett.* **2007**, *91*, 173504.
- [10] L. D. A. Siebbeles, A. Huijser, T. J. Savenije, *J. Mater. Chem.* **2009**, *19*, 6067.
- [11] Y. Terao, H. Sasabe, C. Adachi, *Appl. Phys. Lett.* **2007**, *90*, 103515.
- [12] H. Marciniak, X.-Q. Li, F. Würthner, S. Lochbrunner, *J. Phys. Chem. A* **2011**, *115*, 648-654.
- [13] V. Bulovic, S. R. Forrest, *Chem. Phys. Lett.* **1995**, *238*, 88-92.
- [14] J. E. Kroeze, R. B. M. Koehorst, T. J. Savenije, *Adv. Funct. Mater.* **2004**, *14*, 992-998.
- [15] H. Najafzadeh, B. Lee, Q. Zhou, L. C. Feldman, V. Podzorov, *Nat. Mater.* **2010**, *9*, 938-943.
- [16] G. Wei, R. R. Lunt, K. Sun, S. Wang, M. E. Thompson, S. R. Forrest, *Nano Lett.* **2010**, *10*, 3555-3559.
- [17] A. B. Tamayo, B. Walker, T.-Q. Nguyen, *J. Phys. Chem. C* **2008**, *112*, 11545-11551.
- [18] J. Lin, C. Kim, A. B. Tamayo, T.-Q. Nguyen, *in preparation* **2011**.
- [19] B. Walker, C. Kim, T.-Q. Nguyen, *Chem. Mater.* **2011**, *23*, 470-482.
- [20] B. Walker, A. Tamayo, D. T. Duong, X. Dang, C. Kim, J. Granstrom, T. Nguyen, *Adv. Energy Mater.* **2011**, *1*, 221-229.
- [21] A. B. Tamayo, M. Tantiwiwat, B. Walker, T.-Q. Nguyen, *J. Phys. Chem. C* **2008**, *112*, 15543-15552.
- [22] A. B. Tamayo, X.-D. Dang, B. Walker, J. Seo, T. Kent, T.-Q. Nguyen, *Appl. Phys. Lett.* **2009**, *94*, 103301.
- [23] C. Kim, J. Sherman, A. Tamayo, B. Walker, S. Parkin, G. Wu, T.-Q. Nguyen, *submitted to Chem. Mater.* **2011**.
- [24] B. P. Rand, J. Genoe, P. Heremans, J. Poortmans, *Prog. Photovoltaics Res. Appl.* **2007**, *15*, 659-676.
- [25] M. T. Lloyd, J. E. Anthony, G. G. Malliaras, *Mater. Today* **2007**, *10*, 34-41.
- [26] Y. Sun, G. C. Welch, W. L. Leong, C. J. Takacs, G. C. Bazan, A. J. Heeger, *Nat. Mater.* **2011**.

- [27] N. M. Kronenberg, V. Steinmann, H. Bürkstümmer, J. Hwang, D. Hertel, F. Würthner, K. Meerholz, *Adv. Mater.* **2010**, *22*, 4193-4197.
- [28] R. Fitzner, E. Reinold, A. Mishra, E. Mena-Osteritz, H. Ziehlke, C. Körner, K. Leo, M. Riede, M. Weil, O. Tsaryova, A. Weiß, C. Urich, M. Pfeiffer, P. Bäuerle, *Adv. Funct. Mater.* **2011**, *21*, 897-910.
- [29] G. Wei, S. Wang, K. Sun, M. E. Thompson, S. R. Forrest, *Adv. Energy Mater.* **2011**, *1*, 184-187.
- [30] Y. Liu, X. Wan, F. Wang, J. Zhou, G. Long, J. Tian, Y. Chen, *Adv. Mater.* **2011**, DOI 10.1002/adma.201102790.
- [31] M. Hirade, C. Adachi, *Appl. Phys. Lett.* **2011**, *99*, 153302.
- [32] Y. Liu, X. Wan, F. Wang, J. Zhou, G. Long, J. Tian, J. You, Y. Yang, Y. Chen, *Adv. Energy Mater.* **2011**, *1*, 771-775.
- [33] M. A. Green, K. Emery, Y. Hishikawa, W. Warta, *Prog. Photovolt: Res. Appl.* **2011**, *19*, 84-92.
- [34] A. Ruini, M. J. Caldas, G. Bussi, E. Molinari, *Phys. Rev. Lett.* **2002**, *88*, 206403.
- [35] M. A. Loi, A. Mura, G. Bongiovanni, Q. Cai, C. Martin, H. R. Chandrasekhar, M. Chandrasekhar, W. Graupner, F. Garnier, *Phys. Rev. Lett.* **2001**, *86*, 732.
- [36] R. K. Tikhoplav, B. C. Hess, *Synth. Met.* **1999**, *101*, 236-237.
- [37] T.-Q. Nguyen, B. J. Schwartz, R. D. Schaller, J. C. Johnson, L. F. Lee, L. H. Haber, R. J. Saykally, *J. Phys. Chem. B* **2001**, *105*, 5153-5160.
- [38] B. C. Hess, G. S. Kanner, Z. Vardeny, *Phys. Rev. B* **1993**, *47*, 1407.
- [39] O. V. Mikhnenko, F. Cordella, A. B. Sieval, J. C. Hummelen, P. W. M. Blom, M. A. Loi, *J. Phys. Chem. B* **2009**, *113*, 9104-9109.
- [40] R. R. Lunt, J. B. Benziger, S. R. Forrest, *Adv. Mater.* **2010**, *22*, 1233-1236.
- [41] M. T. Rispens, A. Meetsma, R. Rittberger, C. J. Brabec, N. S. Sariciftci, J. C. Hummelen, *Chem. Commun.* **2003**, 2116.
- [42] D. E. Markov, J. C. Hummelen, P. W. M. Blom, A. B. Sieval, *Phys. Rev. B* **2005**, *72*, 045216-5.
- [43] Y.-F. Lim, Y. Shu, S. R. Parkin, J. E. Anthony, G. G. Malliaras, *J. Mater. Chem.* **2009**, *19*, 3049.
- [44] H. Wang, H.-Y. Wang, B.-R. Gao, L. Wang, Z.-Y. Yang, X.-B. Du, Q.-D. Chen, J.-F. Song, H.-B. Sun, *Nanoscale* **2011**, *3*, 2280.
- [45] M. Matsumoto, T. Nishimura, *ACM Trans. Model. Comput. Simul.* **1998**, *8*, 3-30.
- [46] "Pseudo random number generators," can be found under <http://www.agner.org/random/>, **n.d.**

Chapter 5

Sensitive Triplet Exciton Detection

We developed a sensitive spectroscopic method to probe triplet concentration in thin films of polyfluorene (PF) at room temperature. The energy of photoexcited triplet excitons is transferred to the guest metal-organic complex, meso-tetratolylporphyrin-Pd (PdTPP), and detected as phosphorescent emission. The phosphorescence intensity of PdTPP-PF blends is proportional to the independently measured triplet concentration using photoinduced absorption experiments. The high sensitivity of this method allows room temperature detection of triplet excitons in spin-coated polymer films as thin as 10 nm. We found that the triplet lifetime is independent on PdTPP concentration and therefore this method is nearly *non-perturbing* for the triplet population.*

*O. V. Mikhnenko, P. W. M. Blom, M. A. Loi,
Phys. Chem. Chem. Phys. **2011**, *13*, 14453-14456

5.1 Introduction

To design highly efficient optoelectronic devices, a thorough understanding of the physics of triplet excitons in organic semiconductors is required. According to spin statistics, 75% of all electron-hole pairs form triplet excitons in an organic light emitting diode (OLED). Since organic materials consist of rather light atoms with weak spin-orbit interactions, the radiative transitions of triplets – phosphorescence – is usually inefficient. To extract the energy of triplet excitons as light output, the triplets should be manipulated toward phosphorescent emitting systems^[1–4] or extracted as delayed fluorescence.^[5] Recently, it been pointed out that also in solar cells the transformation of singlet to triplet excitons can significantly enhance the power conversion efficiency^[6–9] Furthermore, the reverse to triplet-triplet annihilation process, singlet fission, shows great potential for further optimization of solar cells.^[10,11] The physical processes that influence the device performances include diffusion, triplet-triplet annihilation, singlet fission, and triplet-polaron interactions. Experimental approaches to study these processes rely on the detection of triplet excitons. In particular, it is very important to detect triplet excitons at low densities, below the triplet-triplet annihilation threshold, to access the intrinsic properties of triplets such as triplet exciton diffusion.

However, detection of low triplet concentrations is very challenging at room temperature in ultrathin films using the conventional methods such as phosphorescence spectroscopy or photoinduced absorption. At room temperature triplet lifetime is usually one order of magnitude shorter than at liquid nitrogen temperatures.^[1,12–15] Consequently both phosphorescence and photoinduced absorption signals are difficult to detect. Furthermore, the phosphorescence intensity and absorption of the triplet excited state are proportional to the film thickness. Generally, if the sample thickness is of the order of 100 nm, which is a typical active layer thickness for OLEDs and organic solar cells, the application of these methods at room temperature requires high laser intensities and high triplet densities, usually well above the triplet-triplet annihilation threshold. Thus it is important to develop alternative sensitive methods to detect low concentrations of triplet excitons in device configurations.

Doping organic semiconductors with metal-organic complexes can allow the phosphorescent detection of the triplet excitons. A triplet that is initially generated in the organic semiconductor can be transferred to the dopant complex.^[16–21] Owing to high atomic number of the metal, such as Palladium, Iridium etc., the spin-orbit coupling of the complex is relatively large enabling the efficient radiative recombination of the transferred triplet exciton. However, the triplet harvesting by metal-organic complexes is capable to strongly perturb^[22] the triplet population of the host material and influence processes such as triplet-triplet annihilation.^[3]

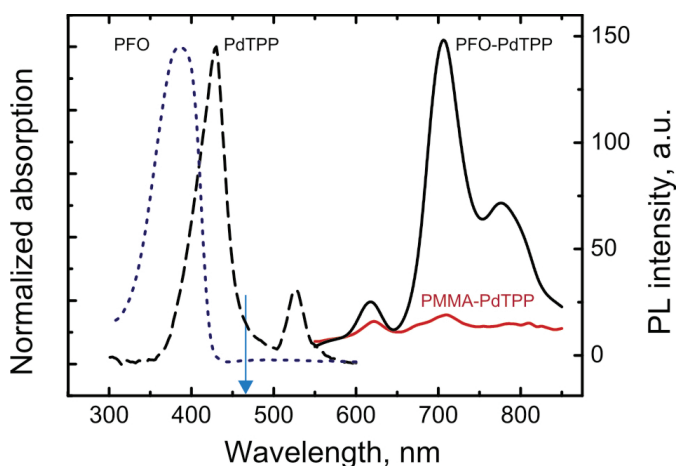


Figure 5.1: Absorption spectra of PFO (dotted) and PdTPP (dashed). Photoluminescence spectra of two layer heterostructures PFO-PdTPP and PMMA-PdTPP are plotted as solid lines. The excitation wavelength at 466 nm is marked with the arrow.

Here we present a nearly *non-perturbing* sensitive detection of low triplet densities in ultrathin films of a conjugated polymer at room temperature. We have chosen poly(9,9-di-n-octylfluorene) (PFO) as a model polymer with high potential for applications in optoelectronic devices such as light emitting diodes and lasers.^[23] We show that the Palladium-coordinated porphyrin, meso-tetratolylporphyrin-Pd (PdTPP), can be used as non-perturbing phosphorescent sensor of triplet excitons in PFO. This porphyrin molecule is photochemically stable, has sharp absorption bands, long phosphorescence decay time and appropriate energy level alignment with PFO.

5.2 Increase of Phosphorescence Intensity

Figure 5.1 shows the photoluminescence/phosphorescence spectrum of PdTPP film deposited by vacuum sublimation on top of a spin-coated layer of PMMA. The PdTPP thickness was controlled by the quartz thickness monitor during the sublimation and was set to 1 nm. The PMMA is a wide band gap material and plays the role of an inert flat substrate. The excitation wavelength of 466 nm was detuned from the absorption maxima of PdTPP. Three weak peaks at 620 nm, 670 nm and 700 nm are resolved in the emission spectrum of PdTPP. Only the peak at 700 nm is attributed to phosphorescence with a decay time of the order of a millisecond; the other peaks appear to be the prompt photoluminescence of PdTPP. It is important to note that the intensity of phosphorescent emission was as weak as that of photoluminescence also when PdTPP was deposited on clean quartz substrates regardless of the film thickness, which was varied in a wide range up to 1 μm .

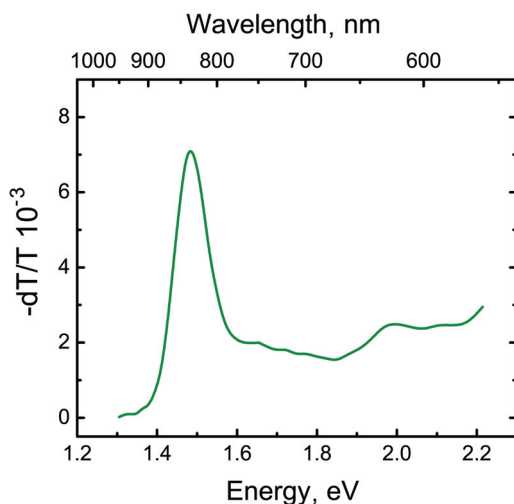


Figure 5.2: Photoinduced absorption spectrum of PFO thin film.

The PL spectrum of PdTPP film, sublimed under the same conditions on top of a 10 nm thick spin-coated PFO film, is also plotted in Figure 5.1. Remarkably, the phosphorescent intensity of the PdTPP layer is one order of magnitude higher when deposited on top of PFO as compared to PMMA-PdTPP heterostructure. The increase in phosphorescent intensity indicates that PFO acts as an antenna to collect optical excitations for PdTPP. Below we will show that the enhanced phosphorescence of PdTPP is mainly due to optically generated triplet excitons in PFO layer that are transferred to PdTPP.

5.3 Photoinduced Absorption

Figure 5.2 shows the photoinduced absorption spectrum of a 2.5 μm thick drop-casted PFO film. The spectrum was acquired at room temperature and consists of a distinct peak at ~ 1.45 eV with a shoulder on the higher energy side. The detected feature is typical^[12,24] for the T₁-T_n transition in PFO and its intensity is proportional to the product of the sample thickness, the concentration and the absorption cross-section of the triplet excited states.^[1] The triplet exciton concentration is proportional to their lifetime that is relatively short at room temperature (0.1 μs), as compared with liquid nitrogen temperatures (1-7 μs , Ref. ^[12]). Consequently thick PFO film and high laser excitation power (500 mW/mm²) are necessary to record the photoinduced absorption spectrum.

It is noteworthy that the laser excitation at 466 nm is able to generate triplet excitons in ample concentration to have triplet-triplet annihilation in PFO. The corresponding photon energy of 2.66 eV is just above the triplet energy

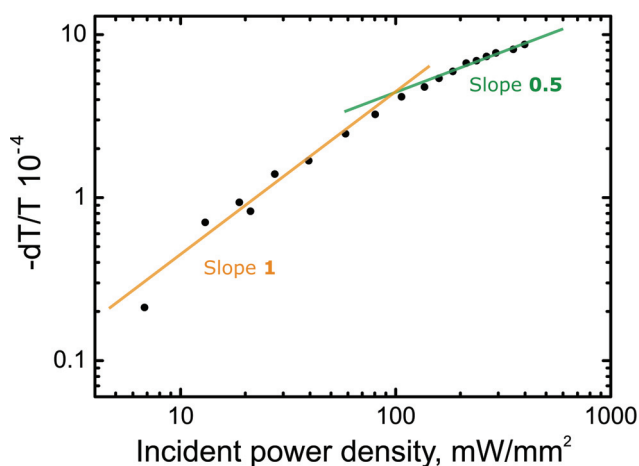


Figure 5.3: Dependence of the maximum of the T1-Tn transition on the incident power density in PFO; sample was excited at 466 nm.

of 2.3 eV.^[1,13,25] On the other hand, the polymer's optical gap is about 3-3.2 eV. The mechanism of triplet exciton generation under such conditions can be understood from considerations of the density of states (DOS). Due to the disordered nature of the polymer, excitonic density of states is rather broad and can be described with a Gaussian distribution. Singlet excitons can be generated at the low energy tail of the DOS in our experiments. Those excitons can undergo intersystem crossing to generate triplets.

Figure 5.3 illustrates the dependence of the T1-Tn transition peak intensity on the incident power density. At low excitation densities the triplet peak increases linearly with the incident laser power. Above ~ 100 mW/mm² its intensity scales as square root of the supplied power. On the log-log graph these two regimes appear as branches with slopes 1 and 0.5, respectively.

The non-linear dependence of the triplet peak intensity on the incident power density is determined by the triplet-triplet annihilation (TTA) phenomenon.^[1,26-31] The probability that two triplet excitons meet each other during their lifetime is significant when their concentration is high. Once brought together two triplets (T^*) can undergo annihilation, which results in one singlet excited state (S^*) and one singlet ground state (S):



The TTA process introduces an additional decay path for triplet excitons that is responsible^[14] for the slope of 0.5 on the log-log plot in Figure 5.3.

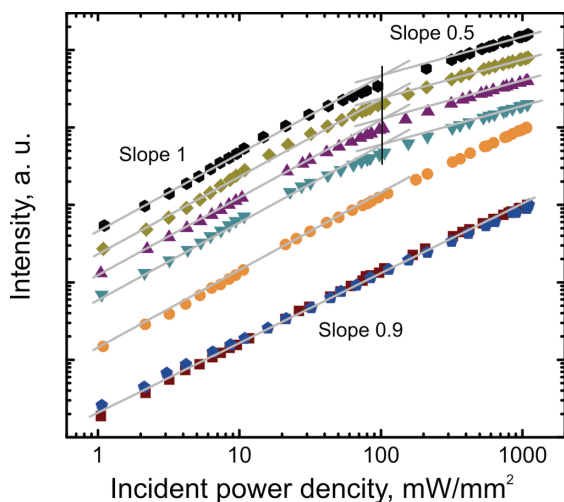


Figure 5.4: The dependence of the phosphorescence intensity at 700 nm on the incident power density of PdTPP blended in PFO with the following concentrations, from top to bottom: 0.05 wt% (hexagons), 0.5 wt% (diamonds), 5 wt% (triangles), 25 wt% (triangles) and 60 wt% (circles). Laser excitation was at 466 nm. The data were first normalized to the value at the maximum incident power of 1000 mW/mm² and then displaced vertically for clarity. The two dependencies with slope 0.9 correspond to PdTPP imbedded in inert matrix of PMMA (pentagons) and PS blend (squares).

5.4 Dependence on Excitation Power

Figure 5.4 shows the dependences of the phosphorescent emission intensity of PdTPP at 700 nm under different power excitation in various sample configurations. All the data were first normalized to their maximum value and then displaced vertically for clarity. The upper five curves correspond to drop-casted samples of PdTPP blended with PFO in concentrations ranging from 0.05 wt% (top) to 60 wt%. The two lowest curves with slope 0.9 correspond to PdTPP blended into PMMA (pentagons) and PS (squares) with concentration of 0.03 wt% and 0.1 wt%, respectively.

PFO acts differently as host material for PdTPP in comparison to PMMA or PS. A small amount of PdTPP blended into PMMA or PS reveals nearly linear dependence of the phosphorescent intensity on the incident power in the whole studied power range. On log-log scale these dependences appear with a slope of ~ 0.9 (Figure 5.4). In contrast, similar concentrations of PdTPP blended with PFO show two distinct regimes on the log-log plot, with slopes of 1 and 0.5 respectively. It is important to note that the photoluminescence intensity of the PdTPP measured at 620 nm

depends linearly on the incident power density in each blend, as does the PFO emission above 550 nm in the PdTPP-PFO sample (not shown here).

The comparison of Figures 5.3 and 5.4 reveals that the phosphorescence intensity of PdTPP-PFO blends is proportional to the intensity of the independently measured triplet T1-Tn PIA band, which is proportional to the triplet concentration. In this way we demonstrate that PdTPP acts as a sensor of triplet excitons in PFO. The non-linearity of the phosphorescence intensity at high incident power densities is then governed by the triplet-triplet annihilation process within the PFO matrix. Triplet energy transfer is possible from PFO to PdTPP since the triplet level of PdTPP (1.8 eV) is below that of PFO (2.3 eV), the back transfer is energetically unfavorable.

5.5 Discussion

To understand the impact of the PdTPP guest molecules on the triplet lifetime of PFO, blends of various PdTPP concentrations have been examined. Samples with PdTPP concentration of 25 wt% and lower show identical non-linearity at high excitation powers, which is represented by the slope of 0.5 on the log-log scale (Figure 5.4). Only the sample with concentration of 60 wt% deviates from the general trend and resembles the dependency of the porphyrins in the inert matrix.

Figure 5.4 demonstrates that the threshold laser power at which the dependence changes from linear to non-linear regime is identical in wide range of concentrations from 0.05 to 25 wt%. This threshold power corresponds to the triplet density $[T_{th}]$, above which the TTA is efficient. Furthermore $[T_{th}]$ is determined by the triplet lifetime τ , see Eq. (1.10) and Ref. [1]:

$$[T_{th}] \propto 1/\tau^2 . \quad (5.2)$$

$[T_{th}]$ is independent on the amount of PdTPP, consequently also is τ . Thus doping PFO with PdTPP does not lead to the reduction of the triplet lifetime. In this respect PdTPP *does not perturb* the triplet population in PFO. Our findings are in agreement with studies reporting that the triplet lifetime in PFO is insensitive to the presence of Pt-coordinated porphyrins, which have similar phosphorescence decay time to PdTPP.^[23,24]

The non-perturbing triplet detection can be further understood by comparing the lifetimes of the excited states. The phosphorescence decay time of PdTPP is 0.9 ms, as we measured in PFO matrix. The triplet lifetime of PFO is estimated from the dependence of the intensity of the PIA band on the modulation frequency and fitted with the equation

$$-\Delta T / T \propto \frac{1}{\sqrt{1 + (2\pi\tau f)^2}} , \quad (5.3)$$

where f is the chopper frequency and τ is the triplet lifetime. At room temperature with excitation density of 500 mW/mm² it is equal to ~0.1 ms, which is one order of magnitude smaller than that of the phosphorescence decay time of PdTPP. Thus under continuous wave excitation it takes at least 10 lifetimes/generations of triplets in PFO between possible energy transfer events to a PdTPP molecule. Consequently the triplet's population is not perturbed by the presence of PdTPP.

Triplet excitons can be easily detected by PdTPP under experimental conditions that are particularly challenging for photoinduced absorption measurements, namely ultrathin films, room temperature and low excitation powers. The phosphorescence spectrum of the PdTPP-PFO heterostructure in Figure 5.1, shows a strong emission at 700 nm, which we accordingly assign to detected triplets in the 10 nm thick PFO layer under excitation of 50 mW/mm², that is well below the triplet-triplet annihilation threshold. Thus the proposed detection method is applicable to study triplet-triplet annihilation and other diffusion related processes in configurations appealing for practical applications.

5.6 Conclusions

In summary, we showed highly sensitive triplet detection in ultrathin films of polyfluorene under low excitation densities and at room temperature. Under these conditions conventional method of triplet exciton detection, photoinduced absorption, is extremely challenging. Because the triplet lifetime in PFO is constant upon blending with PdTPP, the detection is nearly non-perturbing for the continuously generated triplet population. The developed method can be applied to study important processes for lightening and solar cells in organic semiconductors such as triplet-triplet annihilation, fission of singlet excitons, and triplet diffusion.

5.7 Methods

Poly(9,9-di-n-octylfluorene) (PFO) was synthesized by the Netherlands Organization for Applied Scientific Research (TNO); meso-tetratolylporphyrin-Pd (PdTPP) was purchased from Porphyrin Systems; poly(methyl methacrylate) (PMMA) and polystyrene (PS) were acquired from Aldrich. The materials have been used without further purification. All sample fabrication steps including preparation of solutions, filtering, drop-casting and spin-coating were done under nitrogen atmosphere in a glove box. Drop-casting technique has been used to prepare PdTPP blends with PFO, PMMA and PS as well as to prepare ~1-2 μm PFO film for photoinduced absorption experiments. 10 nm films of PFO and PMMA have been spin-coated at 2000 rpm. The sublimation of PdTPP was performed in high vacuum with pressure lower than 2×10^{-7} mbar, at a deposition rate of 0.04 $\text{\AA}/\text{s}$. Samples for spectroscopic measurements were

mounted in an optical cryostat and kept under vacuum of 5×10^{-5} mbar. Absorption spectra were measured by a Perkin-Elmer spectrometer under ambient conditions. Polymer thickness was measured by Dektak profilometer and atomic force microscope.

The set-up for photoinduced absorption (PIA) experiments consists of an Argon laser operating at 466 nm, a Tungsten lamp, a monochromator and a low noise Silicon photodetector. A mechanical chopper was used to modulate the pump laser. The signal was further amplified using a phase sensitive detector. The dependence of the triplet PIA band intensity on the modulation frequency was measured with a Hamamatsu photomultiplier tube (PMT) loaded with a small resistance to ensure fast response in the modulation range of 40-2000 Hz.

The photoluminescence/phosphorescence spectra were recorded by the PMT in combination with a monochromator. As for PIA experiments the laser excitation at 466 nm was modulated by a mechanical chopper and the signal was enhanced by a lock-in amplifier. The phosphorescence decay time of PdTPP was measured with PMT directly linked to a digital oscilloscope.

The laser power was controlled by a circular variable neutral density filter and a power meter, which was connected with a computer to record the light intensity directly during the measurements. Each power dependence measurement has been swept from the highest to the lowest excitation power, followed by the back scan from the lowest to the highest. The back scan did not show notable degradation of the signal in all reported experiments. The incident power density was determined by dividing the total laser intensity over the circular area of the Gaussian beam waist radius. The beam waist was measured using pin holes of various sizes and found to be about 55 μm for the used experimental set up.

5.8 References

- [1] A. Köhler, H. Bässler, *Mater. Sci. Eng., R* **2009**, *66*, 71-109.
- [2] S. Reineke, F. Lindner, G. Schwartz, N. Seidler, K. Walzer, B. Lussem, K. Leo, *Nature* **2009**, *459*, 234-238.
- [3] G. Schwartz, S. Reineke, T. C. Rosenow, K. Walzer, K. Higley, *Adv. Funct. Mater.* **2009**, *19*, 1319-1333.
- [4] Y. Sun, N. C. Giebink, H. Kanno, B. Ma, M. E. Thompson, S. R. Forrest, *Nature* **2006**, *440*, 908-912.
- [5] D. Y. Kondakov, T. D. Pawlik, T. K. Hatwar, J. P. Spindler, *J. Appl. Phys.* **2009**, *106*, 124510-7.
- [6] W. A. Luhman, R. J. Holmes, *Appl. Phys. Lett.* **2009**, *94*, 153304-3.
- [7] B. P. Rand, S. Schols, D. Cheyns, H. Gommans, C. Girotto, J. Genoe, P. Heremans, J. Poortmans, *Org. Electron.* **2009**, *10*, 1015-1019.
- [8] S. T. Roberts, C. W. Schlenker, V. Barlier, R. E. McAnally, Y. Zhang, J. N. Mastron, M. E. Thompson, S. E. Bradforth, *J. Phys. Chem. Lett.* **2011**, *2*, 48-54.
- [9] C.-L. Lee, I.-W. Hwang, C. C. Byeon, B. H. Kim, N. C. Greenham, *Adv. Funct. Mater.* **2010**, *20*, 2945-2950.
- [10] J. C. Johnson, A. J. Nozik, J. Michl, *J. Am. Chem. Soc.* **2010**, *132*, 16302-16303.
- [11] A. Rao, M. W. B. Wilson, J. M. Hodgkiss, S. Albert-Seifried, H. Bässler, R. H. Friend, *J. Am. Chem. Soc.* **2010**, *132*, 12698-12703.
- [12] A. J. Cadby, P. A. Lane, H. Mellor, S. J. Martin, M. Grell, C. Giebeler, D. D. C. Bradley, M. Wohlgenannt, C. An, Z. V. Vardeny, *Phys. Rev. B* **2000**, *62*, 15604.
- [13] C. Rothe, A. P. Monkman, *Phys. Rev. B* **2003**, *68*, 075208.
- [14] V. Jankus, C. Winscom, A. P. Monkman, *J. Phys.: Condens. Matter* **2010**, *22*, 185802.
- [15] R. Österbacka, M. Wohlgenannt, D. Chinn, Z. V. Vardeny, *Phys. Rev. B* **1999**, *60*, R11253.
- [16] V. Cleave, G. Yahioglu, P. L. Barny, R. H. Friend, N. Tessler, *Adv. Mater.* **1999**, *11*, 285-288.
- [17] V. Cleave, G. Yahioglu, P. Le Barny, D. H. Hwang, A. B. Holmes, R. H. Friend, N. Tessler, *Adv. Mater.* **2001**, *13*, 44-47.
- [18] N. C. Giebink, Y. Sun, S. R. Forrest, *Org. Electron.* **2006**, *7*, 375-386.
- [19] D. L. Dexter, *J. Chem. Phys.* **1953**, *21*, 836.
- [20] N. Tian, Y. V. Aulin, D. Lenkeit, S. Pelz, O. V. Mikhnenko, P. W. M. Blom, M. A. Loi, E. Holder, *Dalton Trans.* **2010**, *39*, 8613.
- [21] J. Gao, H. You, J. Fang, D. Ma, L. Wang, X. Jing, F. Wang, *Synth. Met.* **2005**, *155*, 168-171.
- [22] J. Kalinowski, W. Stampor, M. Cocchi, D. Virgili, V. Fattori, P. Di Marco, *Chem. Phys.* **2004**, *297*, 39-48.
- [23] S. A. Chen, H. H. Lu, C. W. Huang, *Adv. Polym. Sci.* **2008**, *212*, 49-84.
- [24] A. Monkman, C. Rothe, S. King, F. Dias, in *Polyfluorenes*, Springer Berlin / Heidelberg, **2008**, pp. 187-225.
- [25] A. P. Monkman, H. D. Burrows, L. J. Hartwell, L. E. Horsburgh, I. Hamblett, S. Navaratnam, *Phys. Rev. Lett.* **2001**, *86*, 1358.
- [26] C. E. Swenberg, *J. Chem. Phys.* **1969**, *51*, 1753.

- [27] R. G. Kepler, J. C. Caris, P. Avakian, E. Abramson, *Phys. Rev. Lett.* **1963**, *10*, 400-402.
- [28] A. Suna, *Phys. Rev. B* **1970**, *1*, 1716-1739.
- [29] V. Dyakonov, G. Rösler, M. Schwoerer, E. L. Frankevich, *Phys. Rev. B* **1997**, *56*, 3852-3862.
- [30] J. Partee, E. L. Frankevich, B. Uhlhorn, J. Shinar, Y. Ding, T. J. Barton, *Phys. Rev. Lett.* **1999**, *82*, 3673-3676.
- [31] R. E. Merrifield, *Pure Appl. Chem.* **1971**, *27*, 481-498.

Chapter 6

Direct Measurement of the Triplet Exciton Diffusion Length

We present a new method to measure the triplet exciton diffusion length in organic semiconductors. N,N'-di-[(1-naphthyl)-N,N'-diphenyl]-1,1'-biphenyl-4,4'-diamine (NPD) has been used as a model system. Triplet excitons are injected into a thin film of NPD by a phosphorescent thin film, which is optically excited and forms a sharp interface with the NPD layer. The penetration profile of the triplet excitons density is recorded by measuring the emission intensity of another phosphorescent material (detector), which is doped into the NPD film at variable distances from the injecting interface. From the obtained triplet penetration profile we extracted a triplet exciton diffusion length of 87 ± 2.7 nm. For excitation power densities >1 mW/mm² triplet-triplet annihilation processes can significantly limit the triplet penetration depth into organic semiconductor.*

*O.V. Mikhnenko, R. Ruiter, P.W.M. Blom, M. A. Loi,
submitted for publication

6.1 Introduction

Both singlet and triplet excitons undergo incoherent hopping that can be described in terms of diffusion. Singlet exciton diffusion is due to electromagnetic dipole-dipole interactions according to Förster theory.^[1] The hopping of triplet excitons between organic molecules requires spatial overlap of the molecular orbitals since the actual exchange of electrons is needed. The theory describing this process was formalized by Dexter.^[2] Due to the long triplet lifetime, the average triplet diffusion distance is expected to be longer than that of singlet excitons. In organic solar cells long diffusion distances are beneficial to reach the interface where excitons dissociate into free charges that can be extracted as photocurrent.^[3–13] For efficient LEDs short singlet and long triplet diffusion lengths are needed to enable selective harvesting of triplet excitons by phosphorescent dopants at certain distance from the electron-hole recombination region.^[14–19] Thus, it is important to measure and control the exciton diffusion length in order to design efficient optoelectronic devices.

In many organic semiconductors the singlet exciton diffusion length is of the order of 10 nm,^[20–23] while the triplet diffusion length has been reported in a wide range from 10 to 5000 nm.^[7,9,11,12,23–39] The triplet diffusion length can be measured in a multilayer LED, in which electron-hole recombination is spatially confined within an interfacial region of a few nanometers thickness. Triplets are then detected at a variable distance from this electron-hole recombination region using a phosphorescent dopant. With this method triplet diffusion lengths varying in between 10 to 140 nm are obtained in common organic semiconductors.^[24–30] Triplet-polaron interactions are neglected in the modeling and it is difficult to evaluate the effect of triplet-triplet annihilation on the resulting values.^[19] Other methods include photocurrent modeling,^[8,9,31] remote triplet detection in bi-layer structures,^[32,33] variation of exciton profile due to the light penetration depth,^[23,34] triplet quenching,^[35] etc. In all these methods the effect of triplet-triplet annihilation is often neglected.

Even for the same materials quite different triplet diffusion lengths have been published. For instance, in *N,N'*-di-[(1-naphthyl)-*N,N'*-diphenyl]-1,1'-biphenyl)-4,4'-diamine (NPD) values of **12** and **87** nm have been measured (Ref. ^[9] and this paper); in *N,N'*-di-1-naphthalenyl-*N,N'*-diphenyl-[1,1':4',1'':4'',1''':4''']-4,4''-diamine (4P-NPD) of **11** and **54** nm (Ref. ^[25] and ^[27]); in 4,4'-bis(*N*-carbazolyl)biphenyl (CBP) of **16**, **25** and **250** nm (Ref ^[26], ^[32] and ^[31]). Thus the large spread of values for the triplet exciton diffusion length can not only be justified with the different nature of the molecules studied but also with the different measurement technique employed.

Here we developed a new direct method to accurately measure triplet exciton diffusion lengths in organic semiconductors. Triplets are injected into an organic thin film by a phosphorescent material, which is excited by a laser. Triplets are detected as

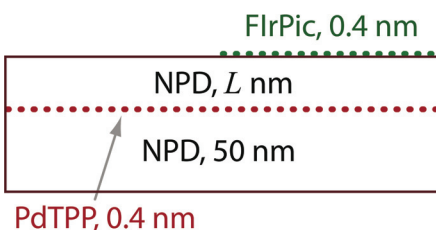


Figure 6.1: Sample structure for triplet exciton diffusion length measurements.

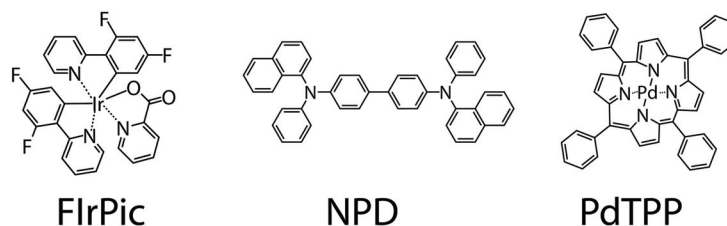


Figure 6.2: Chemical structures of Iridium(III)bis(2-(4,6-difluorophenyl)pyridinato-N,C²) (**FlrPic**), N,N'-di-[(1-naphthyl)-N,N'-diphenyl]-1,1'-biphenyl-4,4'-diamine (**NPD**), and meso-tetratolylporphyrin-Pd (**PdTPP**).

emission from a phosphorescent dopant-detector that is implemented into the organic film at variable distance from the triplet injecting interface. In this way the triplet penetration profile into the thin film of organic semiconductor is recorded and data are modeled using a 1D diffusion equation. Modeling of the experimental data yields a triplet diffusion length of 86.8 ± 2.7 nm for the prototypical semiconductor NPD. Furthermore, we demonstrate that triplet-triplet annihilation can significantly reduce the triplet penetration depth down to 24 nm and thus may be responsible for the variations of the reported values of diffusion length in the literature.

6.2 Sample Structure

Figure 6.1 schematically illustrates the sample structure that we use to measure the triplet exciton diffusion length. An NPD layer of variable thickness L is sandwiched between small amounts of phosphorescent molecules FlrPic and PdTPP; for full names and chemical structures we refer to **Figure 6.2**. This 3 layer heterostructure is placed on top of a 50 nm NPD layer that was deposited on a quartz substrate. Accordingly, the NPD-substrate interface does not influence the triplet population in the vicinity of the PdTPP layer. Both phosphorescent materials are sublimed by setting the thickness to 0.4 nm in the vacuum deposition system. The top layer of FlrPic was applied to only half of the sample area using a shadow mask. We will refer

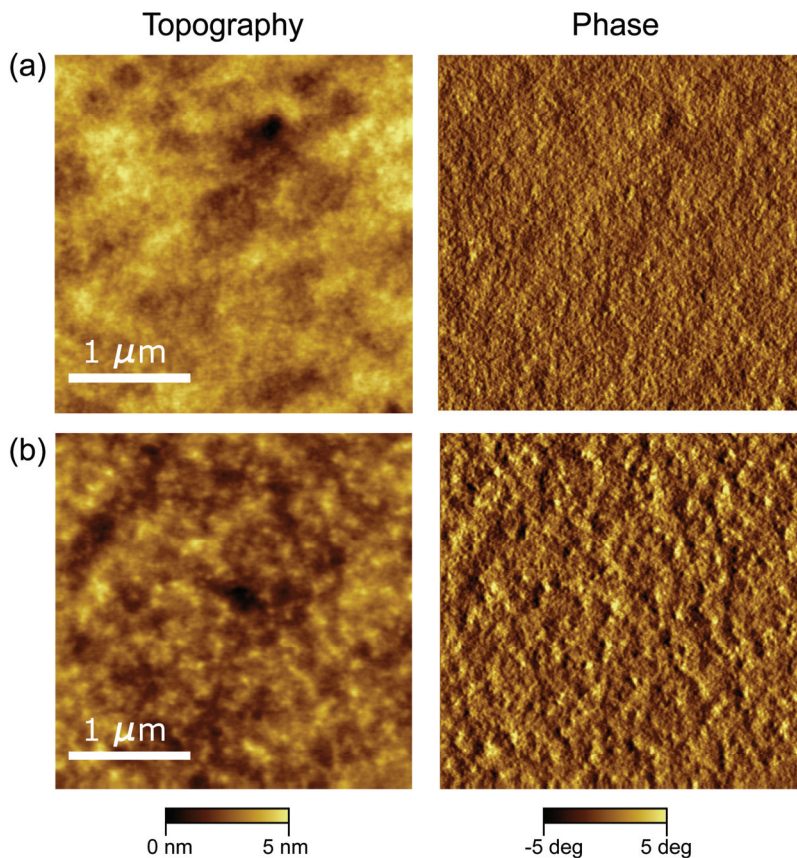


Figure 6.3: (a) Atomic force microgram of surface of neat NPD film. (b) 0.4 nm layer of FIrPic deposited on top of NPD.

to the two halves of a sample as “*FIrPic*” and “*Reference*” sides, indicating whether that side has the FIrPic layer or not.

Figure 6.3a shows topography and phase images of NPD that were acquired by an atomic force microscope operating in the tapping mode. **Figure 6.3b** shows the surface of the 0.4 nm layer of FIrPic deposited on top of the NPD layer. These images demonstrate that deposited FIrPic does not form a closed layer, but instead small islands of ~ 1 nm in height and about few tens of nanometers wide. It is important to note that the 0.4 nm thick layer of PdTPP has identical morphology when deposited on NPD.

Figure 6.4 shows the triplet energy levels of FIrPic (Ref. [40]), NPD (Ref. [27]) and PdTPP (deduced from the phosphorescence spectrum). The triplet energy level of NPD is in between that of FIrPic and PdTPP. Therefore it is energetically favorable that triplet excitons get transferred from FIrPic to NPD and subsequently from NPD to PdTPP. As a result optically excited triplets in the FIrPic can be injected into the NPD layer with thickness L , followed by their diffusion through this layer toward the

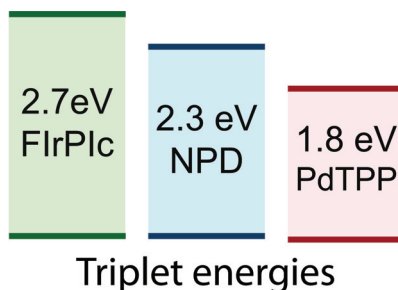


Figure 6.4: Energy levels of triplet excited states.

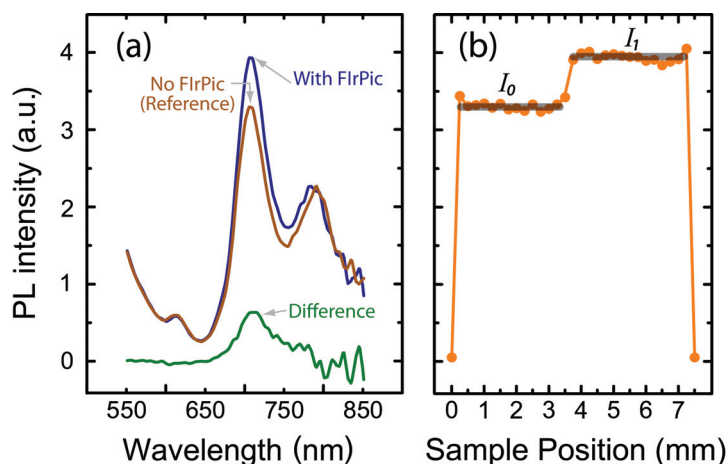


Figure 6.5: (a) Solid lines are photoluminescence spectra of *Reference* and *FIrPic* sides of a typical sample used for triplet exciton diffusion measurements. The arithmetical difference between these spectra is also presented. (b) Typical dependence of the phosphorescence emission of PdTPP (detected at 700 nm) depending on the sample spatial position. The average intensities of I_0 and I_1 correspond to the *Reference* and *FIrPic* sides of the sample, respectively.

PdTPP layer, where they are transferred to PdTPP leading to phosphorescent emission.

6.3 Injection of Triplet Excitons

The PL spectra of the *Reference* and *FIrPic* sides of a typical sample are presented in **Figure 6.5a**. Both spectra feature emission of PdTPP that is identified as pronounced prompt photoluminescence at 620 nm and strong phosphorescence at ~ 700 and at ~ 800 nm. The emission at shorter wavelengths is associated with the photoluminescence of NPD. The phosphorescence of the FIrPic layer is too weak to be detected with these measurements. The phosphorescence emission at ~ 700 nm of the *FIrPic* side appears to be considerably stronger than that of the *Reference* side of the

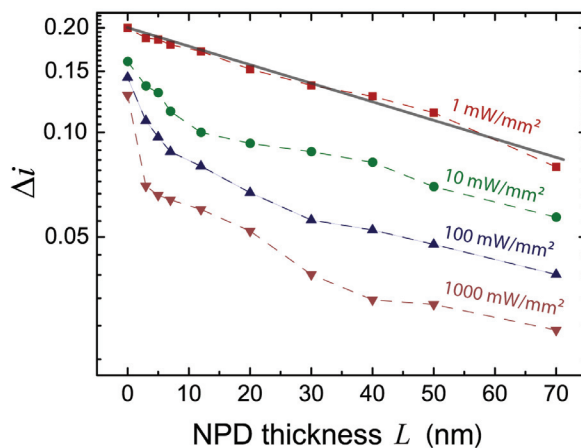


Figure 6.6: Normalized variation of the phosphorescence intensity at 700 nm (Δi) vs. NPD layer thickness L . Samples were excited at 466 nm; various excitation power densities are presented. The dashed lines serve as guides to the eye; the solid line is a fit with equation (6.4).

sample. The arithmetical difference between these spectra reveals a peak at ~ 700 nm. The noisy signal at above 750 nm is due to the limitation of the sensitivity range of the photomultiplier tube.

The phosphorescence intensity measured at 700 nm of the *Reference* and *FIRPic* sides of a typical sample is shown in **Figure 6.5b**. This spatially resolved data were recorded by scanning through the sample in the direction that is normal to the FIRPic – no FIRPic boundary. The average intensities of I_0 and I_1 correspond to the *Reference* and *FIRPic* sides of the sample, respectively. The constancy of this signal demonstrates the homogeneity of the sample. Generally the light outcoupling efficiency of PdTPP emission depends on the NPD layer thickness L . Therefore in order to compare different samples it is convenient to consider the normalized intensity variation:

$$\Delta i = \frac{I_1 - I_0}{I_0}. \quad (6.1)$$

Figure 6.6 shows the dependence of Δi on the NPD thickness L . At an excitation power density of 1 mW/mm² Δi shows a monoexponential decrease with NPD thickness, while at higher excitation densities the dependence is more complex.

We attribute the increase of the emission intensity Δi to the triplet excitons, which are injected into NPD by FIRPic, diffuse through the layer of thickness L , and are then detected by PdTPP. This increase of intensity cannot be due to the emission of FIRPic, because the two spectra are energetically well separated. Moreover, the small amount of applied FIRPic molecules cannot significantly modify the light

outcoupling efficiency or optical interference effects because the refractive indices of NPD and FIrPic are similar and FIrPic form islands of few nanometers that are much smaller than the emission wavelength. Additionally the intensity increase at 700 nm depends on the NPD thickness L that is consistent with the diffusion of triplet excitons through the NPD layer.

6.4 Detection of Triplet Excitons

In order to accurately model the process of triplet diffusion in our samples it is important to understand how PdTPP molecules influence the triplet density. In the previous chapter we have studied in detail the detection of triplet excitons using PdTPP as phosphorescent dopant in a material with a band gap similar to NPD.^[41] According to the energy gap law, materials of similar band gaps are expected to have a similar triplet lifetime, which is about 0.1 ms for compounds such as NPD at room temperature.^[41–44] The phosphorescence decay time of PdTPP is 0.9 ms (Ref. ^[41]), thus it takes at least 10 generations of triplet excitons between possible energy transfer events to a PdTPP molecule under continuous wave excitation. Therefore we and others^[45,46] did not detect reduction of triplet lifetime in the host material when doping with PdTPP and similar metal-coordinated porphyrins. Moreover, in our samples PdTPP does not even form a closed layer ensuring a minimal impact on the triplet population in NPD. In this respect PdTPP can be regarded as triplet detector that does not perturb the density of triplet excitons in the material under investigation.

Because PdTPP behaves as a non-perturbing triplet detector, triplet-triplet annihilation (TTA) can be observed by detecting the phosphorescence of PdTPP. TTA is the bimolecular recombination of two triplet excitons (T_1) that yields singlet ground (S_0) and singlet excited (S_1) states:



The efficiency of TTA is only significant if the probability that two triplet excitons meet each other during their lifetime is high. This probability becomes considerable when the triplet density overcomes a certain value. Since the TTA introduces an additional decay path for triplets, their density scales as square root of the generation rate at high excitation powers; while at low triplet generation rates the TTA is inefficient and the scaling is linear.^[14,47–52]

Figure 6.7 shows the dependence of the PdTPP phosphorescence emission intensity on the excitation power density (circles). In this case the 0.4 nm PdTPP layer was sandwiched between two 50 nm thick layers of NPD. The dependence shows slopes of 1 and 0.54 on the log-log scale at low and high excitation densities, respectively. In contrast, the prompt photoluminescence of NPD scales linearly within the whole studied range of the excitation densities (triangles). As a further check we

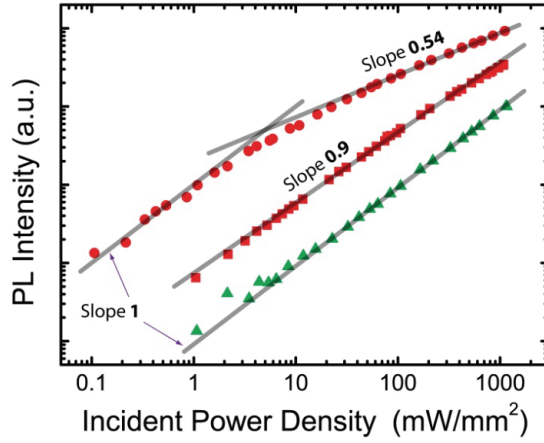


Figure 6.7: The dependence of the emission intensity on the incident power density in a NPD-PdTPP-NPD heterostructure at 700 nm (circles) and at 550 nm (triangles); in PdTPP-polystyrene blend at 700 nm (squares). Laser excitation was at 466 nm.

measured the phosphorescence emission of PdTPP molecules in the inert matrix of polystyrene and also this sample shows a nearly linear dependence on the excitation power (squares in Figure 6.7). Thus the sublinear growth with the scaling exponent of 0.54 measured at high excitation power is specific to the PdTPP-NPD heterojunction. In our previous work we associated such square root dependence to the detection^[41] of triplet excitons under TTA conditions. Consequently the phosphorescence emission of PdTPP is mainly determined by the triplet excitons, which were created via intersystem crossing in NPD layers and transferred to PdTPP.

6.5 Modeling the Triplet Penetration Profile

At the excitation power density of 1 mW/mm² the phosphorescence intensity at 700 nm is in the linear regime (Figure 6.7). Thus the TTA process is not efficient at this excitation power and diffusion of triplets that are injected by FIrPic can be modeled by a linear differential equation. Due to the sample symmetry, the density n of injected triplet excitons depends only on one spatial coordinate L that is the distance from the FIrPic-NPD interface:

$$\frac{\partial n}{\partial t} = D \frac{\partial^2 n}{\partial L^2} - \frac{n}{\tau}, \quad (6.3)$$

where $n \propto \Delta i$, D is the diffusion coefficient, and τ is the triplet lifetime. A continuous wave laser excitation can be described as a constant triplet generation rate G at the FIrPic-NPD interface $n(0, t) = G$. Then the thickness profile of the triplet

penetration into NPD layer is the steady state solution of equation (6.3) and can be easily found by setting $\partial n / \partial t = 0$:

$$n(L) = G e^{-L/L_D}, \quad (6.4)$$

where $L_D = \sqrt{\tau D}$ is the exciton diffusion length – the only fitting parameter. The solid line in Figure 6.6 is the fitting with Equation (6.4) that yields to the exciton diffusion length of 86.8 ± 2.7 nm; the error is the standard error of the fitting parameter. The triplet exciton diffusion coefficient D can be estimated by setting $\tau = 0.1$ ms resulting in the value of 7.5×10^{-7} cm²/s.

6.6 Discussion

Under intense laser excitation TTA becomes significant (see Figure 6.7) and the profile of triplet penetration cannot be described with equation (6.4). In order to compare the different profiles in Figure 6.6 we define the penetration depth λ as the distance from the FIRPic-NPD interface at which the concentration of injected triplets is attenuated by a value of e^{-1} . λ systematically decreases from 87 nm to 67; 39 and 24 nm when the excitation power densities is increased from 1 mW/mm² to 10; 100 and 1000 mW/mm² in accordance with TTA.^[32] Thus it is important to make sure that TTA is absent or it is taken into account in the measurement of triplet exciton diffusion length, because the penetration length λ can be mistakenly interpreted as the diffusion length L_D . Presumably, this may be the reason of the large spread in L_D values that were reported in the literature for the same materials; in those experiments the effect of TTA was usually neglected.^[9,25-27,31]

The proposed sample structure with distinct triplet injector and detector layers can be further developed to explore the spin degree of freedom of triplet excitons. In particular the influence of the magnetic field on the triplet diffusion length and triplet-triplet annihilation can be observed. The magnetic field may significantly decrease the efficiency of the triplet-triplet annihilation and consequently increase the triplet penetration depth at high excitation densities. New types of devices may emerge by using the spins of triplet excitons.

6.7 Conclusions

We presented a new direct method to accurately measure triplet exciton diffusion lengths in organic semiconductors. A triplet exciton diffusion length of 86.8 ± 2.7 nm was extracted for NPD. Our method can be applied to a wide selection of materials that are relevant for applications as OLEDs and solar cells. We have also shown that process of triplet-triplet annihilation can significantly reduce the penetration depth of

triplet excitons, being detrimental for the eventual use of triplet excitons in optoelectronic devices.

6.8 Methods

NPD, FIrPic and PdTPP were purchased from Sigma-Aldrich, American Dye Source and Porphyrin Systems, respectively. The materials were used without further purification. Multilayer heterostructures were prepared on quartz substrates by thermal sublimation in high vacuum of less than 2×10^{-7} mbar. The deposition rates of NPD and the metal-organic complexes were kept at ~ 1 Å/s and 0.04 Å/s, respectively. The film thickness was monitored during growth with a quartz microbalance, thickness and surface roughness were controlled after deposition by atomic force microscopy. The root mean square roughnesses of quartz substrates and deposited films were less than 1 nm on an area of $100 \mu\text{m}^2$. The samples were handled and stored in a nitrogen atmosphere.

The set-up for photoluminescence measurements consisted of an Argon ion laser operating at 466 nm, a monochromator and a photomultiplier tube. The signal was further amplified with a phase sensitive detector. The samples were mounted in a cryostat and kept under dynamic vacuum at a pressure of 5×10^{-5} mbar or less, at room temperature. The sample position was varied by shifting the cryostat relative to the optical path using a micrometer actuator. The dependence of the phosphorescence emission on the incident power density was measured using a circular variable neutral density filter and a power meter, which was connected with a computer to record the light intensity directly during the measurements. The Argon laser was detuned from the absorption bands of each material. For instance, the absorption coefficient of NPD is only $2.17 \times 10^{-3} \text{ nm}^{-1}$ at the excitation wavelength of 466 nm. Consequently, variations of the exciton density due to optical absorption can be safely neglected in the studied NPD thickness range up to 120 nm. Absorption spectra were measured by a Perkin-Elmer spectrometer under ambient conditions.

6.9 References

- [1] G. D. Scholes, *Annu. Rev. Phys. Chem.* **2003**, *54*, 57-87.
- [2] D. L. Dexter, *J. Chem. Phys.* **1953**, *21*, 836.
- [3] S. T. Roberts, C. W. Schlenker, V. Barlier, R. E. McAnally, Y. Zhang, J. N. Mastron, M. E. Thompson, S. E. Bradforth, *J. Phys. Chem. Lett.* **2011**, *2*, 48-54.
- [4] J. C. Johnson, A. J. Nozik, J. Michl, *J. Am. Chem. Soc.* **2010**, *132*, 16302-16303.
- [5] C.-L. Lee, I.-W. Hwang, C. C. Byeon, B. H. Kim, N. C. Greenham, *Adv. Funct. Mater.* **2010**, *20*, 2945-2950.
- [6] A. Rao, M. W. B. Wilson, J. M. Hodgkiss, S. Albert-Seifried, H. Bässler, R. H. Friend, *J. Am. Chem. Soc.* **2010**, *132*, 12698-12703.
- [7] B. P. Rand, C. Girotto, A. Mityashin, A. Hadipour, J. Genoe, P. Heremans, *Appl. Phys. Lett.* **2009**, *95*, 173304-3.
- [8] B. P. Rand, S. Schols, D. Cheyns, H. Gommans, C. Girotto, J. Genoe, P. Heremans, J. Poortmans, *Org. Electron.* **2009**, *10*, 1015-1019.
- [9] W. A. Luhman, R. J. Holmes, *Appl. Phys. Lett.* **2009**, *94*, 153304-3.
- [10] M. Arif, K. Yang, L. Li, P. Yu, S. Guha, S. Gangopadhyay, M. Forster, U. Scherf, *Appl. Phys. Lett.* **2009**, *94*, 063307-3.
- [11] Y. Shao, Y. Yang, *Adv. Mater.* **2005**, *17*, 2841-2844.
- [12] J. E. Kroeze, R. B. M. Koehorst, T. J. Savenije, *Adv. Funct. Mater.* **2004**, *14*, 992-998.
- [13] A. Köhler, H. F. Wittmann, R. H. Friend, M. S. Khan, J. Lewis, *Synth. Met.* **1994**, *67*, 245-249.
- [14] A. Köhler, H. Bässler, *Mater. Sci. Eng., R* **2009**, *66*, 71-109.
- [15] H. Kanno, Y. Sun, S. R. Forrest, *Appl. Phys. Lett.* **2006**, *89*, 143516-3.
- [16] Y. Sun, N. C. Giebink, H. Kanno, B. Ma, M. E. Thompson, S. R. Forrest, *Nature* **2006**, *440*, 908-912.
- [17] S. Reineke, F. Lindner, G. Schwartz, N. Seidler, K. Walzer, B. Lussem, K. Leo, *Nature* **2009**, *459*, 234-238.
- [18] D. E. Markov, P. W. M. Blom, *Appl. Phys. Lett.* **2005**, *87*, 233511-3.
- [19] N. C. Giebink, S. R. Forrest, *Phys. Rev. B* **2008**, *77*, 235215-9.
- [20] P. Peumans, A. Yakimov, S. R. Forrest, *J. Appl. Phys.* **2003**, *93*, 3693-3723.
- [21] O. V. Mikhnenko, F. Cordella, A. B. Sieval, J. C. Hummelen, P. W. M. Blom, M. A. Loi, *J. Phys. Chem. B* **2008**, *112*, 11601-11604.
- [22] P. E. Shaw, A. Ruseckas, I. D. W. Samuel, *Adv. Mater.* **2008**, *20*, 3516-3520.
- [23] R. R. Lunt, N. C. Giebink, A. A. Belak, J. B. Benziger, S. R. Forrest, *J. Appl. Phys.* **2009**, *105*, 053711-7.
- [24] W. Zhang, J. Yu, W. Wen, Y. Jiang, *J. Lumin.* **2011**, *131*, 1260-1263.
- [25] J. Wünsche, S. Reineke, B. Lüssem, K. Leo, *Phys. Rev. B* **2010**, *81*, 245201.
- [26] M. Lebental, H. Choukri, S. Chenais, S. Forget, A. Siove, B. Geffroy, E. Tutis, *Phys. Rev. B* **2009**, *79*, 165318-13.
- [27] G. Schwartz, S. Reineke, T. C. Rosenow, K. Walzer, K. Higley, *Adv. Funct. Mater.* **2009**, *19*, 1319-1333.
- [28] M. A. Baldo, S. R. Forrest, *Phys. Rev. B* **2000**, *62*, 10958.
- [29] M. A. Baldo, D. F. O'Brien, M. E. Thompson, S. R. Forrest, *Phys. Rev. B* **1999**, *60*, 14422.

- [30] C. Wu, P. I. Djurovich, M. E. Thompson, *Adv. Funct. Mater.* **2009**, *19*, 3157-3164.
- [31] N. Matsusue, S. Ikame, Y. Suzuki, H. Naito, *J. Appl. Phys.* **2005**, *97*, 123512-5.
- [32] N. C. Giebink, Y. Sun, S. R. Forrest, *Org. Electron.* **2006**, *7*, 375-386.
- [33] T. Fushimi, A. Oda, H. Ohkita, S. Ito, *J. Phys. Chem. B* **2004**, *108*, 18897-18902.
- [34] H. Najafov, B. Lee, Q. Zhou, L. C. Feldman, V. Podzorov, *Nat. Mater.* **2010**, *9*, 938-943.
- [35] M. Samiullah, D. Moghe, U. Scherf, S. Guha, *Phys. Rev. B* **2010**, *82*, 205211.
- [36] Y. Luo, H. Aziz, *J. Appl. Phys.* **2010**, *107*, 094510.
- [37] E. B. Namdas, A. Ruseckas, I. D. W. Samuel, S.-C. Lo, P. L. Burn, *Appl. Phys. Lett.* **2005**, *86*, 091104-3.
- [38] J. E. Kroeze, T. J. Savenije, L. P. Candeias, J. M. Warman, L. D. A. Siebbeles, *Sol. Energy Mater. Sol. Cells* **2005**, *85*, 189-203.
- [39] M. A. Baldo, C. Adachi, S. R. Forrest, *Phys. Rev. B* **2000**, *62*, 10967.
- [40] Q. Wang, J. Ding, D. Ma, Y. Cheng, L. Wang, X. Jing, F. Wang, *Adv. Funct. Mater.* **2009**, *19*, 84-95.
- [41] O. V. Mikhnenko, P. W. M. Blom, M. A. Loi, *Phys. Chem. Chem. Phys.* **2011**, *13*, 14453-14456.
- [42] J. S. Wilson, A. Kohler, R. H. Friend, M. K. Al-Suti, M. R. A. Al-Mandhary, M. S. Khan, P. R. Raithby, *J. Chem. Phys.* **2000**, *113*, 7627-7634.
- [43] C.-L. Lee, X. Yang, N. C. Greenham, *Phys. Rev. B* **2007**, *76*, 245201.
- [44] J. Kalinowski, W. Stampor, M. Cocchi, D. Virgili, V. Fattori, P. Di Marco, *Chem. Phys.* **2004**, *297*, 39-48.
- [45] D. F. O'Brien, C. Giebeler, R. B. Fletcher, A. J. Cadby, L. C. Palilis, D. G. Lidzey, P. A. Lane, D. D. C. Bradley, W. Blau, *Synth. Met.* **2001**, *116*, 379-383.
- [46] P. A. Lane, L. C. Palilis, D. F. O'Brien, C. Giebeler, A. J. Cadby, D. G. Lidzey, A. J. Campbell, W. Blau, D. D. C. Bradley, *Phys. Rev. B* **2001**, *63*, 235206.
- [47] R. G. Kepler, J. C. Caris, P. Avakian, E. Abramson, *Phys. Rev. Lett.* **1963**, *10*, 400-402.
- [48] C. E. Swenberg, *J. Chem. Phys.* **1969**, *51*, 1753.
- [49] A. Suna, *Phys. Rev. B* **1970**, *1*, 1716-1739.
- [50] R. E. Merrifield, *Pure Appl. Chem.* **1971**, *27*, 481-498.
- [51] V. Dyakonov, G. Rösler, M. Schwoerer, E. L. Frankevich, *Phys. Rev. B* **1997**, *56*, 3852-3862.
- [52] J. Partee, E. L. Frankevich, B. Uhlhorn, J. Shinar, Y. Ding, T. J. Barton, *Phys. Rev. Lett.* **1999**, *82*, 3673-3676.

Summary

Organic semiconductors open the door to new applications in electronics and optoelectronics where low costs, light weight, and biocompatibility are more important than durability and high performance. For instance, organic light-emitting diodes and solar cells can be integrated into clothing, newspapers, windows, etc. The working principle of these devices relies on the creation and recombination of excitons – nanometer-sized and electrically neutral quasiparticles that carry useful energy. Excitons in organic semiconductors can be viewed as strongly bound pairs of positive and negative elementary charges. In organic solar cells, the energy of absorbed light is transported by excitons to a specially designed interface, where they decompose into positive and negative charges leading to the generation of electrical current. Therefore, the motion of excitons – exciton diffusion – is a very important process. In particular, it is crucial to know how far excitons can diffuse for the design of solar cells. This thesis focuses on exciton diffusion in organic semiconductors and on related phenomena. The main achievements that are described here are twofold. (i) We have developed two new methods to measure the exciton diffusion parameters and (ii) we have used these tools to improve our understanding of excitonic processes in organic semiconductors.

Chapter 2 shows that excitons can be quenched in the “skin layer” of solution-processed polymer films. Such a “skin layer” is formed at the atmosphere-polymer interface as the solvent evaporates during spin-coating. This effect should be carefully taken into account in the measurement of the singlet exciton diffusion length using methods such as fluorescence quenching in bilayers. Exciton quenching in the “skin layer” is an additional complication in this conventional approach to study exciton diffusion. Therefore, in order to systematically study exciton diffusion in various materials, it is reasonable to seek more convenient methods.

A new method to obtain singlet exciton diffusion parameters is described in detail in **Chapter 3**. This method is based on modeling of the experimentally determined photoluminescence decays in blends of organic semiconductors with exciton quenching molecules. Our approach has numerous advantages compared to previous methods, including reliability and simplicity of execution. To illustrate the versatility of this method, we report the measurements of exciton diffusion parameters in several materials including three polymers and one small-molecule compound. In **Chapter 4** we show that our method can be easily applied to study the effect of thermal annealing – and similar treatments – on the exciton diffusion length. Thus, this tool enables us to conduct systematic studies, potentially allowing us to understand which physical parameters and structural features influence the exciton diffusion process.

Using the new method, we measured the exciton diffusion lengths for the first time in two narrow bandgap polymers, see **Chapter 3**. We show that a substitution of a carbon atom with a silicon atom in the polymeric backbone leads to a twofold reduction of the exciton diffusion coefficient, while the exciton diffusion length remains the same. Moreover, we show in **Chapter 4** that, in contrast to expectations, both exciton diffusion length and coefficient decrease upon thermal annealing of a thin film of a small-molecule organic semiconductor. Conversely, the performance of bulk heterojunction solar cells that are based on this material is significantly improved after the same thermal treatment. Therefore, we conclude that there is no straightforward correlation between the performance of bulk heterojunction solar cells and exciton diffusion length.

A reliable method to detect triplet excitons is necessary to measure their diffusion length. In **Chapter 5** we describe a highly sensitive detection method that is suitable for studying dynamics of triplet excitons. We blend a phosphorescent dopant, a Pd-coordinated porphyrin, with an organic semiconductor and demonstrate that the intensity of its phosphorescent emission is proportional to the triplet density in the host material. Although the detection mechanism relies on transferring the energy of triplet excitons to the porphyrin molecules, we demonstrate that the presence of the Pd-coordinated porphyrin does not reduce the average lifetime of triplet excitons in the host semiconductor. In this respect, the population of triplet excitons is not perturbed by the Pd-coordinated porphyrin. The capability of our method to detect a low triplet density in ultrathin films at room temperature is a feature that distinguishes our approach from standard techniques of triplet detection, such as photoinduced absorption.

Chapter 6 presents a new method to directly probe triplet diffusion in a prototypical organic semiconductor. We design a multilayer heterostructure that features designated triplet-injector and triplet-detector layers separated by an organic semiconductor layer of certain thickness. Upon optical excitation, triplet excitons diffuse through the organic semiconductor from the injector to detector layer. By varying the thickness of the organic semiconductor layer, we are able to record a triplet penetration profile, which directly yields the triplet diffusion length. In literature there are several papers that report different triplet exciton diffusion lengths in the range of 10-250 nm for the same materials. We show that triplet-triplet annihilation can significantly limit the spatial extent of the triplet exciton diffusion. This effect presumably is responsible for the large spread of the reported values of triplet exciton diffusion lengths in the mentioned studies.

Manipulation of triplet excitons may create possibilities for spin-based devices that operate with electrically neutral spins. Diffusion of triplet excitons may then serve as the transport mechanism for spins. Our multilayer structure with triplet injector and detector layers can be helpful to further study excitonic spin.

Samenvatting

Organische halfgeleiders openen de deur naar nieuwe toepassingen in de elektronica en optoelektronica waarin lage kosten, een laag gewicht en biocompatibiliteit belangrijker zijn dan duurzaamheid en hoge prestaties. Bijvoorbeeld kunnen organische lichtuitstralende diodes en zonnecellen worden geïntegreerd in kleding, kranten, ramen etc. Het grondbeginsel van operatie van deze schakelingen berust op de creatie en recombinatie van excitonen – nanometersgrote en elektrisch neutrale quasideeltjes die nuttige energie dragen. Excitonen in organische halfgeleiders kunnen worden gezien als sterk gebonden paren van positieve en negatieve elementaire ladingen. In organische zonnecellen wordt de energie van het geabsorbeerde licht door excitonen getransporteerd naar een speciaal ontworpen grensvlak, waar ze uiteenvallen in positieve en negatieve ladingen, die tot generatie van een elektrische stroom leiden. Daarom is de beweging van excitonen – excitondiffusie – een belangrijk proces. In het bijzonder is het cruciaal om te weten hoe ver excitonen kunnen diffunderen bij het ontwerpen van zonnecellen. Dit proefschrift richt zich op excitondiffusie in organische halfgeleiders en op gerelateerde verschijnselen. De voornaamste behaalde resultaten die hier worden beschreven zijn tweeledig. (i) We hebben twee nieuwe methodes ontwikkeld om de excitondiffusieparameters te meten (ii) we hebben deze middelen gebruikt om onze kennis over excitonische processen in organische halfgeleiders te verbeteren.

Hoofdstuk 2 laat zien dat excitonen kunnen worden uitgedoofd in de “huidlaag” van uit oplossing vervaardigde polymere dunne lagen. Zo een “huidlaag” wordt gevormd aan het atmosfeer-polymeer grensvlak gedurende het verdampen van het oplosmiddel tijdens het spincoaten. Met dit effect dient zorgvuldig rekening te worden gehouden wanneer de diffusielengte van het singlet exciton wordt gemeten doormiddel van bijvoorbeeld fluorescentie-uitdoving in bilagen. Uitdoving van excitonen in de “huidlaag” is een bijkomend probleem in deze gebruikelijke aanpak om excitondiffusie te bestuderen. Daarom is het redelijk om andere, meer geschikte methodes te zoeken om systematisch excitondiffusie in verschillende materialen te bestuderen.

Een nieuwe meetmethode om de parameters van singlet-excitondiffusie te verkrijgen wordt in detail beschreven in **Hoofdstuk 3**. Deze methode is gebaseerd op het modelleren van het experimenteel vastgestelde fotoluminescentieverval in mengsels van organische halfgeleiders en excitonuitdovende moleculen. Onze benadering heeft talrijke voordelen ten opzichte van eerder ontwikkelde methodes, zoals betrouwbaarheid en eenvoud van uitvoering. Om de veelzijdigheid van deze techniek te illustreren, rapporteren we hier metingen van excitondiffusieparameters in verscheidene materialen, waaronder drie polymeren en een klein molecuul. In

Hoofdstuk 4 laten we zien dat onze methode eenvoudig kan worden toegepast om het effect van het verhitten van de laag – en vergelijkbare behandelingen – op de excitondiffusielengte te bestuderen. Dientengevolge stelt deze techniek ons in staat om systematische studies uit te voeren, die in de toekomst kunnen leiden tot begrip over welke fysische parameters en structurele eigenschappen het excitondiffusieproces beïnvloeden.

Gebruikmakend van deze nieuwe methode hebben we voor de eerste keer de excitondiffusielengte gemeten in twee polymeren met een smalle energiebandkloof, zie **Hoofdstuk 3**. We laten zien dat vervanging van een koolstofatoom door een siliciumatoom in de polymeerketen leidt tot een halvering van de excitondiffusiecoëfficiënt, terwijl de excitondiffusielengte gelijk blijft. Bovendien laten we in **Hoofdstuk 4** zien dat, in tegenstelling tot de verwachting, zowel de excitondiffusielengte als -coëfficiënt kleiner worden als gevolg van het verhitten van een dunne laag van een klein-molecuul organische halfgeleider. Daarentegen nemen de prestaties van bulk heterojunctie zonnecellen gebaseerd op dit materiaal toe wanneer ze zijn blootgesteld aan dezelfde thermische behandeling. Derhalve concluderen wij dat er geen rechtlijnig verband is tussen de prestaties van bulk heterojunctie zonnecellen en de excitondiffusielengte.

Een betrouwbare methode om triplet excitonen te detecteren is noodzakelijk om hun diffusielengte te meten. In **Hoofdstuk 5** beschrijven we een zeer gevoelige detectiemethode die geschikt is om de dynamica van triplet excitonen te bestuderen. We mengen een fosforescerend molecuul, een Pd-gecoördineerde porfyriene, in een organische halfgeleider en tonen aan dat de intensiteit van de fosforescerende emissie evenredig is met de tripletdichtheid in het gastheermateriaal. Hoewel het detectiemechanisme berust op energieoverdracht van de triplet excitonen naar de porfyriene moleculen, laten we zien dat de aanwezigheid van Pd-gecoördineerde porfyrienes de gemiddelde levensduur van triplet excitonen in de halfgeleider niet reduceert. In dat opzicht wordt de populatie van triplet excitonen niet verstoord door de Pd-gecoördineerde porfyriene. Het vermogen van onze methode om een lage tripletdichtheid in ultradunne lagen op kamertemperatuur te kunnen detecteren is een eigenschap die onze benadering onderscheidt van standaardtechnieken voor tripletdetectie, zoals fotogeïnduceerde absorptie.

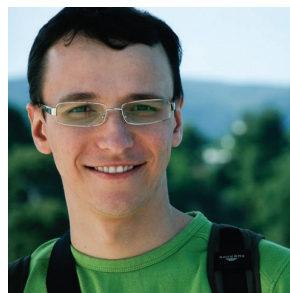
Hoofdstuk 6 toont een nieuwe methode om direct tripletdiffusie te meten in een prototypische organische halfgeleider. We ontwerpen een multilaagsheterostructuur met aangewezen tripletinjectie- en tripletdetectielagen, gescheiden door een organische halfgeleiderlaag van een zekere dikte. Na optische excitatie diffunderen triplet excitonen door de organische halfgeleider van de injectie naar de detectie laag. Door de dikte van de organische halfgeleiderlaag te variëren zijn we in staat om het tripletpenetratieprofiel vast te leggen, welke direct de tripletdiffusielengte oplevert. In de literatuur zijn er verscheidene artikelen te vinden die verschillende triplet-excitondiffusielengtes rapporteren over een bereik van 10-

250 nm voor dezelfde materialen. We laten zien dat triplet-triplet annihilatie het ruimtelijke bereik van triplet-excitondiffusie significant kan beperken. Dit effect is vermoedelijk verantwoordelijk voor de grote spreiding in de gerapporteerde waarden van triplet-excitondiffusie in de genoemde studies.

Manipulatie van triplet excitonen kan mogelijkheden scheppen voor spingebaseerde schakelingen die functioneren met elektrisch neutrale spins. Diffusie van triplet excitonen zou dan kunnen dienen als het transportmechanisme voor spins. Onze multilaagsstructuur met tripletinjectie- en tripletdetectielagen kunnen bruikbaar zijn om excitonische spin nader te bestuderen.

Translated to Dutch by Gert-Jan Wetzelaer

Curriculum Vitae



Oleksandr Mikhnenko

- February 24, 1984 Born in Brusyliv, Ukraine
- 1997-2000 Ukrainian Lyceum of Physics and Mathematics of
Taras Shevchenko National University of Kyiv
- 2000-2004 BSc in Applied Physics, *cum laude*
Taras Shevchenko National University of Kyiv
- 2004-2006 MSc in Applied Physics, *cum laude*
Taras Shevchenko National University of Kyiv
“Quantum Theory of Diffraction”
- 2005-2007 MSc in Nanoscience (Physics)
University of Groningen
“Low Temperature Study of The Exciton Diffusion in
Conjugated Polymers”
- 2007-2012 PhD in Physics
University of Groningen
“Dynamics of Singlet and Triplet Excitons in Organic
Semiconductors”
- Awards**
- 2011 Poster Prize at MRS meeting in San Francisco
- 2011 Poster Prize at Workshop "Materials for energy",
the Netherlands
- 2008 Poster Prize by Dutch Polymer Institute
- 2003 "Volunteer of the Year", the city of Kyiv

List of Publications

9. Direct Measurement of the Triplet Exciton Diffusion Length in Organic Semiconductors.

O. V. Mikhnenko, R. Ruiter, P. W. M. Blom, M. A. Loi, *submitted* **2011**.

8. Exciton Diffusion Length in Narrow Band Gap Polymers.

O. V. Mikhnenko, H. Azimi, M. Scharber, M. Morana, P. W. M. Blom, M. A. Loi, *submitted* **2011**.

7. Effect of Thermal Annealing on Exciton Diffusion in a Diketopyrrolopyrrole Derivative.

O. V. Mikhnenko, J. Lin, Shu, Y., J. E. Anthony, P. W. M. Blom, T.-Q. Nguyen, M. A. Loi, *submitted*. **2011**.

6. Exploring the origin of the temperature dependent behavior of PbS nanocrystal thin films and solar cells.

K. Szendrei, M. Speirs, W. Gomulya, D. Jarzab, M. Manca, **O. V. Mikhnenko**, M. Yarema, B. J. Kooi, W. Heiss, M. A. Loi, *Advanced Functional Materials*, **2011**, accepted.

5. Sensitive Triplet Exciton Detection in Polyfluorene Using Pd-coordinated Porphyrin.

O. V. Mikhnenko, P. W. M. Blom, M. A. Loi, *Phys. Chem. Chem. Phys.* **2011**, *13*, 14453-14456.

4. Cyclometalated Red Iridium(iii) Complexes Containing Carbazolyl-Acetylacetonate Ligands: Efficiency Enhancement in Polymer LED Devices.

N. Tian, Y. V. Aulin, D. Lenkeit, S. Pelz, **O. V. Mikhnenko**, P. W. M. Blom, M. A. Loi, E. Holder, *Dalton Trans.* **2010**, *39*, 8613.

3. Exciton Quenching Close to Polymer–Vacuum Interface of Spin-Coated Films of Poly(p-phenylenevinylene) Derivative.

O. V. Mikhnenko, F. Cordella, A. B. Sieval, J. C. Hummelen, P. W. M. Blom, M. A. Loi, *J. Phys. Chem. B* **2009**, *113*, 9104-9109.

2. Solution-Processable Near-IR Photodetectors Based on Electron Transfer from PbS Nanocrystals to Fullerene Derivatives.

K. Szendrei, F. Cordella, M. V. Kovalenko, M. Böberl, G. Hesser, M. Yarema, D. Jarzab, **O. V. Mikhnenko**, A. Gocalinska, M. Saba, F. Quochi, A. Mura, G. Bongiovanni, P. W. M. Blom, W. Heiss, M. A. Loi, *Adv. Mater.* **2009**, *21*, 683-687.

1. Temperature Dependence of Exciton Diffusion in Conjugated Polymers.

O. V. Mikhnenko, F. Cordella, A. B. Sieval, J. C. Hummelen, P. W. M. Blom, M. A. Loi, *J. Phys. Chem. B* **2008**, *112*, 11601-11604.

Acknowledgments

Great! This is the single word that describes my overall experience in Groningen. I feel like I matured a lot both personally and professionally during last few years. In that I am in debt to many people. It is my great pleasure to mention them here.

Maria Antonietta Loi, you introduced me to the world of spectroscopy and taught how to build an optical setup from scratch. In this way I learned from you invaluable experience how to set up a new optical lab. You did not like when I referred to you as “boss” in private conversations, because you put an effort to build our professional relationship as equal colleagues. I value that highly. I appreciate your guidance and the great amount of freedom that you granted me in the scientific research. Thank you for your patience with me.

Paul Blom, your lectures back in 2006 helped to make up my mind to start research in the field of organic semiconductors. I was greatly impressed by your style of teaching. I admire your abilities to bring pieces of puzzle together and see the big picture. Although you have permanently moved to Eindhoven to take a high level position in the Holst Center, you actively participated in many major decisions of my project. I am grateful for sharing with me your knowledge and experience. You certainly made an imprint on my approach for the scientific research.

Also I would like to thank Bert de Boer, who helped me a lot around the lab just when I started. Bert, your will be always remembered as a great colleague and supervisor.

I would like to express my gratitude to the members of the reading committee Vladimir Dyakonov, Peter Bobbert, and Kees Hummelen. Thank you very much for your time and effort in evaluating this thesis. Your valuable comments undoubtedly helped to improve the quality of my writing.

I am thankful to Dutch Polymer Institute (DPI) for providing funding for my PhD project. I enjoyed spending time with DPI community during the progress report meetings at various locations in the Netherlands. In particular, I am thankful to Frans de Schryver, John van Haare, Peter Bobbert, Rene Jansen, Reinder Coehoorn, and Marco Carvelli for their inputs into my research.

Renate Hekkema, you are the best secretary in the whole world! Your special calming charm transforms the bureaucratic procedures into pleasant encounters. We worked closely on organizing the group retreat at Texel, which was codenamed as a “workweek”. I really enjoyed planning that event with you and I learned quite some tips in dealing with people. I appreciate time talking with you about all kinds of things during numerous coffee breaks and social activities. Thank you!

Frans van der Horst, thank you very much for your great help in the lab. You always found ways to bend the rules and get things done just when we needed them.

Your sense of humor is unforgettable. You redefined the line between appropriate and inappropriate in your own way. I feel privileged to work with you just before your retirement, as you never hesitated to share the experience that you have collected through the years.

I would like to give thanks to our clean-room master, Jan Harkema. In the lab you are always extremely helpful and fast. It is a pleasure to step by your office and learn about your incredible adventures as a traveler, a motorcyclist, a sailor, an ice-skater or an actor. You are probably the most active person I've ever met. You always took an important part in organizing social events. Thank you!

Arjen Kamp joined our group only at my last year of PhD and I enjoyed a lot his company, sense of humor and sweet directness. Arjen, it is very easy to get things going with you. I wish we could work more together. In addition I would like to thank to Ben Hesp for helping around with optical setups, Jurrian Wildeman for advices in chemistry labs, Johan Holstein for keeping the NanoLab cleanroom in great shape, and Reinder Gooijaarts for the technical support around his labs.

During my PhD training, I was lucky to have multiple collaborations with great people. Alex Sieval and Kees Hummelen provided cross-linkable fullerenes that opened great possibilities in studding exciton diffusion in organic semiconductors. Kees, you are more than a collaborator, you are a teacher to me. I consider you lectures on organic electronics as one of the best I have ever attended. I admire your ability to look deep into the problem and put serious questions in a playful manner. Your great scientific talks inspired me to work on my own presentation skills.

I am grateful to Elisabeth Holder for providing highly performing phosphorescent molecules. Our collaboration is very special for me, as it was the first joint work that I initiated myself and delegated most of the work to a master student Yaroslav. It brought me great experience that resulted in a nice publication. I am also grateful to Markus Scharber and his co-workers from Konarka for providing narrow-bandgap polymers.

One of the highlights of my road trip in California 2011 was a visit to University of California in Santa Barbara, where I met charming Thuc-Quyen Nguyen. Quyen, I was impressed by your openness and clear thinking. We immediately found a way to collaborate. Thank you for sending Jason Lin to Groningen with materials that were synthesized in your group. You even offered me a post-doc position in your group, which I am happy to accept. My feeling is that I will have a very fruitful experience in your group.

Jason Lin, you were in Groningen only one month, and I consider that time as the most productive month throughout my whole PhD. We managed to measure exciton diffusion parameters in your materials with astonishing efficiency – one material per day. I still keep telling people that story about the front wheel of your bike, which was first stolen and then reappearing in the parking lot in front of

University. We made a great team and I am happy to continue working with you in Santa Barbara. Thank you. I would like also to thank Mananya Tantiwiwat for measuring the x-ray diffraction pattern that was used in this thesis.

We started collaboration with Martijn Kuik after this thesis was mostly ready. Thank you very much for explaining me the details of charge transport in organic semiconductors. It is a great fun not only to write a paper with you, but also spending time together during coffee breaks and at parties. Thank you!

I am grateful to talented students, that I was lucky to supervise. Nynke Vlietstra, Yaroslav Aulin, and Roald Ruiten, thank you very much for your contributions to my research projects. I enjoyed working with you guys. I believe that you will have a bright future independently of your choice of career path. In addition, very recently, I had a pleasure to work with Niels van der Kaap, who helped preparing samples for exciton diffusion length measurements. Niels, I am sure you will have great time as a PhD student in Groningen.

It was a pure pleasure to work in an international and open environment in the University of Groningen. I received many work- and life-related advices from senior colleagues. In particular I would like to thank Viktor Malyshev, Ton Schoot Uiterkamp, Petra Rudolf, Ryan Chiechi, Viktor Krashnikov, Jan Anton Koster, Dago de Leeuw, and Antoine van Oijen. Our short encounters made long-lasting imprints on me. Thank you!

It was a great fun to share the office with Dorota Jarzab. We started to work with Maria at about the same time. You found a great Italian boyfriend, Filippo, and it was fun to observe you transforming into an Italian person. I wish you success in future.

Jia Gao, your unique combination of pure honesty and directness makes your points in conversations particularly interesting. Our endless discussions absolutely helped to shape my decision making tree on future career. Thank you very much for your help in the optical lab. I wish you good luck in Princeton and I am sure you will reach all your goals.

Krisztina Szendrei brought a great tradition to our group. Kriszti, you started to bring chocolates each time you were coming back from a work trip or a vacation, and then others picked up that habit. You also treated us with great home baked cookies. It was also a pleasure to work with you in the lab. Thank you!

I would like to thank Artem Bakulin, with whom I spent a lot of time playing ping-pong, sailing, and talking about everything. We had a great fun driving around San Francisco after a conference.

Special thanks are addressed to Gert-Jan Wetzelaer for translating the summary of this thesis to Dutch and for the great fun we had at all the parties. In addition I am thankful to Jessica Sicard for proofreading parts of this thesis.

I would like to thank Hennie Valkenier for organizing the ice-skating events, helping me a lot with chemistry-related questions, and numerous conversations we

had about all kinds of things. I was truly amazed by your decision to spend one year as a science teacher at a charity hospital in Africa.

I would like to thank Marianna Manca, who introduced a cute chaos to our group. Your open and shining personality positively enriched my everyday life. Thank you very much for always being cheerful and understanding. I am very happy that you became my officemate and agreed to be my paranymp.

Marian Otter, we studied together as master students, we were teaching assistants for the solid state Physics course, and we even lived in the same house for a while. We always had a great time regardless of what we did. I am amazed by your positivity and ability to have everything done. You always managed to make enough of free time for a quality party. I am so happy that you agreed to be my paranymp.

I am particularly thankful to Fabrizio Cordella for teaching me spectroscopy, basic Italian, and cooking pasta; Simone Fabiano for being such a cool and funny colleague; Claudia Piliago for helping me finding contacts in California; Ilias Katsouras for nice photography trips; Deepak Prusty for helping around chemistry lab; Afshin Hadipour for great tips around the cleanroom; Hylke Akkerman for switching conversation to English during the coffee breaks; Johan Brondijk for geeky talks; Herman Nicolai for being a party master; Yuan Zhang for inviting me to Santa Barbara; Paul de Bruyn for sharing his music recordings; and Maksym Sladkov for letting me know about the opportunities of Master programs in Groningen.

In addition I would like to thank nearby working colleagues who created a great and friendly atmosphere in the lab: Anne-Marije Andringa, Kamal Asadi, Sartria Bisri, Irina Craciun, Vlad Derenskyi, Davide Fracasso, Andre Hof, Fatemeh Gholamrezaie, Widianta Gomulya, Auke Kronemeijer, Martijn Lenes, Mingtao Lu, Francesco Maddalena, Date Moet, Jolt Oostra, Parisa Pourhossein, Mark-Jan Spijkman, and Wenqiang Zou.

I am grateful for the quality time that we spent with friends outside the work: Antohin and Adrianka for being such a nice and positive people; Rudolph Wierda and Jessica Sicard for nice dinners; Giuseppe and Parisa for great adventures within the Couch Surfing community; Eva Magnuskova and Arnaud Maurer for teaching me a lot about Dutch culture, and Jacob and Marija Wubs for being the best landlords.

Many thanks are addressed to the Russian-speaking community in Groningen that helped me to make a smooth transition to the Dutch way of living. I am thankful to Alina Veligura and Csaba Jozsa, Sasha Fedorov and Natalya Dudkina, Carlijn Ubbens, Monika Lubomska, Dima Fishman, Maksym Sladkov, Ihor Shekarev, Dmitry Mazurenko, Andriy Kovalchuk, Ira Samarska, Sergii Denega and Katya Naumova, Sasha Zozulya, Dima Makogon, Oleg Antoniuk, Kedrov family, Vladimir Markov, Olya Kalmykova, Zhanna, Pavlo Gordiichuk, Sergii Yandyuk, Alex Nesterov, Alex Polyakov, Oleksii Ivashenko, and Vlad Pavelyev.

I would like to thank to Ihor Makarenko, who is being my mentor though many years. Ihor Petrovich, you always supported me in my big decisions with informed advices.

A word of thanks goes to my nearest family. In particular, I would like to thank for constant support my brother Misha, and his family, my parents in law Anatoliy and Lyuba, and my brother in law Slavik.

I am in great debt to my parents, Zoya and Viktor, who invested the best years of their lives into my education. When I was in junior school you spent countless hours teaching me to solve mathematical and chemistry problems. Your efforts created a solid knowledge basis, which led me to enter country's best boarding school in the age of 13. Then you struggled with enormously long salary delays back in the '90s to deliver necessary funds to keep up my further education. You always supported and trusted me. From the bottom of my heart I would like to express my sincere gratitude. My formal academic education is finalized by this thesis, which I am more than happy to devote to you.

Finally, I would like to thank my beloved wife Oksana. Your constant support helped me to accomplish this thesis. Your beautiful illustrations found a nice place at my posters, presentations and the cover of the thesis. It is incredible how different and yet similar we are. We have almost magical connection that synchronized our personal development in a very coherent way. Moreover, our endless discussions about selling vector graphics online inspired me to create the Monte Carlo simulation, which then became a basis for two chapters of this thesis. I am grateful for your great help and support and for teaching me the positive side of the world. It is never enough for us to spend time together. I love you.

I would like to express my apology to those, whom I forgot to mention here. I had so much help and support from many that now it is impossible to compose a full list. Thank you for understanding.

Oleksandr Mikhnenko
Groningen, December 2011

Preceding three paragraphs are translated into Ukrainian in the following.

Хочу висловити подяку моїм родичам, зокрема дякую за постійну підтримку моєму братові Міші та його родині, тестю Анатолію, тещі Любі, та моєму шурину Славіку.

Я у великому боргу перед моїми батьками Зоєю та Віктором, які вклали кращі роки свого життя в мою освіту. Дорогі Мамо і Батьку, коли я навчався в молодших класах, Ви витратили незліченну кількість годин навчаючи мене розв'язувати математичні та хімічні задачі. Ваші зусилля створили міцну основу знань, які допомогли мені поступити в найкращу спеціалізовану школу у віці 13 років. На той час, у 90-х роках, Ви боролися з надзвичайно тривалими затримками зарплатні, щоб забезпечити мою подальшу освіту. Ви завжди підтримували і довіряли мені. Від щирого серця я хотів би висловити мою подяку. Моя формальна освіта закінчується цією дисертацією, яку я присвячую Вам.

Я хочу також подякувати моїй коханій дружині Оксані, чия постійна підтримка допомогла мені написати цю дисертацію. Оксано, твої чудові ілюстрації знайшли собі місце на моїх постерах, презентаціях та прикрасили обкладинку цієї книги. Неймовірно, наскільки ми з тобою різні та водночас схожі. Між нами існує майже магічний зв'язок, який синхронізує наш особистий розвиток. Більше того, наші нескінченні дискусії про продаж векторної графіки онлайн надихнули мене на створення Монте Карло симуляції, котра стала основою для двох розділів цієї книги. Я вдячний за твою допомогу, підтримку та за те, що ти навчила мене завжди бачити позитивну сторону світу. Нам з тобою завжди хочеться проводити час разом. Я люблю тебе.

Нарешті, я хотів би вибачитись перед тими, кого я забув згадати на цих сторінках. Стільки людей допомагали мені за роки аспірантури, що зараз неможливо скласти повний список. Дякую за Ваше розуміння.

*Олександр Міхненко
Гронінген, грудень 2011*